Osaka University Knowledge Archive

Title	PHOTOLUMINESCENCE STUDY OF TRANSITION-METAL IMPURITIES IN GaAs
Author(s)	藤原, 康文
Citation	大阪大学, 1986, 博士論文
Version Type	VoR
URL	https://hdl.handle.net/11094/948
rights	
Note	

Osaka University Knowledge Archive : OUKA

https://ir.library.osaka-u.ac.jp/

Osaka University

PHOTOLUMINESCENCE STUDY OF TRANSITION-METAL IMPURITIES IN GaAs

Yasufumi FUJIWARA

June, 1986

Osaka University
Faculty of Engineering Science
Toyonaka, Osaka

PHOTOLUMINESCENCE STUDY OF TRANSITION-METAL IMPURITIES IN GaAs

Yasufumi FUJIWARA

Department of Electrical Engineering

Faculty of Engineering Science

Osaka University, Toyonaka, Osaka

June, 1986

ABSTRACT

A series of experimental investigations has been carried out on the photoluminescence associated with 3d-transition metal impurities in GaAs and its application to characterization of the material.

The luminescence due to the Cr deep acceptor in GaAs has been intensively studied with particular emphasis. Systematic studies on the luminescence for high-temperature thermal annealed GaAs:Cr have revealed that an arsenic vacancy (V_{As}) contributes to the well-known Cr-related sharp zero-phonon line at 0.8395 eV in GaAs:Cr. Effects of various donor impurities on the Cr-related luminescence have been investigated in GaAs, and new Cr-related zero-phonon lines associated with a Cr-Se complex have been observed for the first time in the 0.837 eV region. Effects of In-doping on the Cr-related luminescence have been also investigated in In, Cr-codoped GaAs and new Cr-related zero-phonon lines have been observed for the first time besides the

well-known Cr-V_{As} luminescence line. Based on a series of photoluminescence measurements, it has been found that these newly-observed Cr-related luminescence lines are originated from a Cr-V_{As}-In complex. In addition, the magnitude of local lattice strain induced by In-doping has been estimated from their peak positions. Furthermore, we have succeeded in developing a new characterization technique for arsenic vacancies in GaAs by monitoring the Cr-related characteristic luminescence lines.

The deep-level luminescence associated with a Ni acceptor has been investigated with various kinds of Ni-diffused GaAs. The in-depth profile measurements on the Ni-related luminescence intensities have indicated the builtup of S atoms in the vicinity of the surface region. Furthermore, time-resolved photoluminescence spectra associated with a V-related deep center have been measured with GaAs:V. From an analysis of the decay characteristics based on a configuration interaction model, the most probable origin for the V-related luminescence line has been identified.

A new technique by which the residual stress in GaAs:Cr can be sensitively characterized with the use of the 0.8395 eV Cr-related luminescence lines has been developed, and this technique has been successfully applied to the interface stress in ZnSe/GaAs:Cr heterostructures, the result implying the existence of anomalous stress in the GaAs substrate.

ACKNOWLEDGEMENT

The author would like to express his sincere thanks to Professor Y. Hamakawa for his useful advices and critical reading of this thesis. The author wishes to make his deep acknowledgement to Professors S. Namba, T. Sueta and S. Yamamoto for their kind guidance in the course of this study at Osaka University.

This work has been done at Semiconductor Laboratory, Faculty of Engineering Science, Osaka University, Toyonaka, Osaka under the direction of Professors Y. Hamakawa and T. Nishino. In particular, the author is much indebted to Professor Y. Hamakawa for his valuable and kind teaching, advice and encouragement throughout the course of this work. The author also wants to express his greatest thanks to Professor T. Nishino for his constant teaching, advice and encouragement throughout the course of this study and for the critical reading of this thesis. Professor T. Nishino kindly pointed out the importance of studies for deep impurities in gallium arsenide and suggested the significance of material characterization by photoluminescence techniques.

The author wishes to thank Dr. F. Yajima, Mr. E. Nishihara and Mr. N. Nishimoto of Mitsubishi Monsant Chemicals Corporation, Dr. Kashiwayanagi and Dr. K. Wagatsuma of Furukawa Electric Company, and Dr. K. Hoshikawa and Mr. T. Kobayashi of Nippon Telegraph and Telephone Corporation for supplying several GaAs wafers. Thanks are also due to Dr. M. Akiyama of Oki Electric Industry Company for his supplying of MOCVD-grown V-doped GaAs samples. In addition, the

author wants to express his thanks to Professor S. Fujita of Kyoto University for his supply of ZnSe samples and useful discussion on this thesis work.

The author is much indebted to Professors T. Kobayashi and M. Okuyama, Dr. H. Takakura, Dr. H. Okamoto and Mr. C. Sada for their useful advice and discussion throughout the course of this study and also to seniors, Dr. Y. Yamazoe, Dr. K. Okamoto, Dr. Y. Matsui, Dr. S. Nonomura, Mr. Y. Sasai, Mr. K. Ohnishi, Mr. K. Otsuka and Mr. J. Katsura for their kind advice and encouragement during this thesis work. Thanks are also due to Professor M. Umeno, Dr. H. Nakata, Dr. H. Nakayama and Dr. K. Yasutake of Osaka University for their kind teaching and discussion on this thesis work.

Valuable and enjoyable discussions with his colleagues, especially, Mr. S. Shirakata, Mr. H. Kida, Mr. D. Kruangam and Mr. K. Inoue are much appreciated by the author.

The author wishes to express his gratitude to his co-workers, Mr. M. Yasu, Mr. T. Yagi, Mr. A. Kojima, Mr. Y. Kita and Mr. Y. Tonami for their skillful technical helps on this thesis work.

Finally, the author would like to thank his parents and wife, and all his family for their endless encouragement and support.

TABLE OF CONTENTS

Chapter I. INTRODUCTION 1

1-1. Historical background 1

1-2. Purpose of this work 3

Chapter II. TRANSITION-METAL IMPURITIES IN GaAs 9

2-1. Introduction 9

2-2. 3d-electrons in crystal with T_d symmetry 10

2-3. Transition-metal impurities in GaAs 16

2-4. Luminescence associated with transition-metal impurities in GaAs 20

2-5. Summary 29

Chapter III. LUMINESCENCE IN GaAs:Cr 34

3-1. Introduction 34

3-2. Experiment apparatus for luminescence measurements 35

3-3. Effects of thermal-annealing 38

3-3-1. Cr-related luminescence 38

3-3-2. Model for Cr-related luminescence center 41

3-3-3. Interpretation of thermal-annealing temperature and time dependences 45

3-4. Doping effects of various donor impurities 47

3-4-1. New luminescence lines associated with Cr-Se complex 48

3-4-2. Trigonal field by group-VI donor species 53

3-5. Doping effects of In 56
3-5-1. In, Cr-related luminescence 56
3-5-2. In, Cr-related luminescence center 62
3-5-3. Interpretation of In-concentration dependence 64
3-5-4. Estimation of local lattice strain in GaAs:In 69
3-6. Characterization of arsenic vacancy by Cr-related luminescence 72
3-6-1. In-depth profiles of Cr-related luminescence intensities 72
3-6-2. Estimation of diffusion coefficient for arsenic vacancy 80
3-7. Summary 83

Chapter IV. LUMINESCENCE IN GaAs DOPED WITH Ni OR V 89
4-1. Introduction 89
4-2. Ni-related luminescence 90
4-2-1. Donor-species dependence 90
4-2-2. In-depth profiles of donor impurities 92
4-3. V-related luminescence 96
4-3-1. Time-resolved PL measurements 96
4-3-2. Identification of charge state 99
4-4. Summary 105

Chapter V. CHARACTERIZATION OF RESIDUAL STRESS IN GaAs 109
5-1. Introduction 109
5-2. Residual stress in plastically-bent GaAs:Cr 111
5-2-1. Sample preparation 111

5-2-2. Cr-related luminescence spectra in bent specimens .. 112

5-2-3. Effects of stress along [111] bending axis 115

5-2-4. Effects of compressive stress along
[110] and [001] bending axes 119

5-3. Application to ZnSe/GaAs:Cr heterostructure 125

5-3-1. Sample preparation 125

5-3-2. Interface stress due to lattice mismatch 126

5-3-3. Cr-related luminescence spectra
from GaAs substrates 127

5-3-4. Model for anomalous stress at ZnSe/GaAs interface .. 135

5-4. Summary 137

Chapter VI. CONCLUSIONS 140

I. INTRODUCTION

1-1. Historical background

GaAs crystals have been widely utilized as materials for optoelectronic devices such as light emitting diode (LED) and laser diode, since GaAs shows direct-type band gap, implying that electron-hole pairs radiatively recombine with high efficiency. Recently, GaAs metal-semiconductor field effect transistors (MESFETs) have received increasing attention over the past decade for applications beyond the 1-2-GHz operating range of silicon devices[1) because of high mobility with large saturation velocity compared with that in silicon and also its availability as a semi-insulating (SI) substrate. This technology has now progressed towards monolithic integration of many high-frequency circuit functions[2)], since the advent of monolithic GaAs integrated circuits (ICs) is expected to have a broad impact on the way in which microwave detection, signal processing and power amplification will be carried out in the future. Significant advances have already been demonstrated in the fabrication of monolithic GaAs amplifiers for low-noise figures (as low as 2.8 dB at 18 GHz) or high rf power outputs (exceeding 5 W at 12 GHz) at X-band frequencies and beyond, as well as in very high-speed GaAs digital logic ICs for "front-end" data processing.[3)]

Historically, GaAs MESFET technology has been strongly affected by the quality of the underlying SI substrate and, over the years, an epitaxial growth technology has been developed to circumvent the

unpredicted and often undesirable effects of the substrate. In contract to discrete FETs, however, the present trend in monolithic GaAs circuit fabrication strongly favors the use of direct-into-substrate implantation techniques.[4) This follows from a major flexibility that selective direct ion implantation enables active device regions to be confined to selected areas on a SI substrate without resorting to the mesa-etch isolation techniques of epitaxial structures. Significant progress is currently being made towards developing a viable planar ion-implantation technology[5,6)], but it is widely recognized that direct implantation imposes severe demands on the quality of SI GaAs substrates[7,8)]. In the past, the inferior properties of commercially-available SI substrates have been major limitations to obtaining uniform and predictable device characteristics by implantation. For example, the formation of a conductive p-type surface layer following post-implantation annealing[9)] adversely affects the implant profile and activation, and results in poor control of full-channel current and pinch-off voltage in directly implanted FET structures. Therefore, it is inevitable to establish some key techniques to grow high-quality GaAs crystals and to characterize with confidence in order to realize the full potential of direct ion implantation as a reliable, cost-effective fabrication technology of high-performance GaAs MESFET devices and integrated circuits.

Bulk SI GaAs is usually grown by two techniques, i.e., horizontal Bridgeman (HB) and liquid-encapsulated Czochralski (LEC) techniques. Residual electrically-active impurities (Si, S, C, Cu etc.) and point defects (Ga-vacancy, As-vacancy etc.) are always present in GaAs grown by these techniques. In general, in order to compensate them and to

enhance the resistivity of the material, special impurities such as Cr[10] or O[11,12] are intentionally introduced in HB crystals and native defects such as EL 2 are empirically incorporated with control of the melt stoichiometry in LEC crystals[13,14], which are expected to form deep levels and pin the Fermi level in the middle of the band gap. Therefore, the control and characterization of these compensating impurities and defects are particularly important and indispensable in growing high-quality GaAs materials.

1-2. Purpose of this work

3d-transition metal impurities in GaAs have been intensively studied so far, because some of them are usually used as compensators to obtain SI materials. Much efforts have been made to investigate the electrical properties of these deep acceptor centers by electrical, especially capacitance transient techniques[15]. However, it is difficult to obtain the whole understanding of their electronic states by such techniques. The low-temperature (PL) spectra associated with 3d-transition metal impurities in GaAs exhibit characteristic emission lines in the near-infrared region.[16] It is well recognized that these PL lines are closely related to the environment of their deep impurities, such as atomic structure, symmetry and charge states, suggesting a possibility for the characterization by this PL technique. However, details in the origin of the characteristic PL lines are not completely understood. This is due to the following facts;

1) 3d-transition metal impurities can exist in different charge states with respect to the position of Fermi level.

2) they can easily form various types of complexes including another impurity or defect in GaAs.

3) our knowledge about deep impurities in semiconductors is limited in spite of recent extensive studies from both theoretical and experimental aspects.

From these points of view, the purpose of this thesis work is to investigate the luminescence associated with these 3d-transition metal impurities in GaAs and to apply the information to the characterization of GaAs crystals.

In chapter II, the 3d-states of a single electron in tetrahedral (T_d) symmetry is described from crystal-field approach. Secondly, a survey on 3d-transition metal impurities in GaAs, assessed by electrical and Electron Spin Resonance (ESR) measurements, is presented. Finally, the characteristic luminescence associated with these deep impurities in GaAs is classified with respect to the recombination mechanism and summarized.[17)]

In chapter III, following a brief description on the experimental apparatus used in this work, the identification of the atomic structure of the PL center from which the well-known Cr-related zero-phonon line is originated is presented based on systematic PL studies on high-temperature thermal annealing of GaAs:Cr.[18-21)] Secondly, first observation of new PL lines associated with a complex consisting of a Cr and a Se is described.[22)] In addition, effects of In-doping on the Cr-related PL spectrum are investigated in In, Cr-codoped GaAs.[23-25)] In the final section of this chapter, a new characterization technique for arsenic vacancies is discussed by use of the above-obtained information.[26)]

In chapter IV, the in-depth profiles of the luminescence associated with Ni deep acceptors in Ni-diffused GaAs are investigated and the distribution of donor impurities is characterized based on the results.[27] Secondly, PL spectra associated with V- and Cr-related deep centers in GaAs are studied by a time-resolved PL technique and the electronic lifetimes of their excited states are estimated. From analyses of the results based on a configuration interaction model, the PL center contributed to the V-related sharp zero-phonon line at 0.7388 eV is identified.[17]

In chapter V, the author describes a new characterization technique for the residual stress in GaAs by monitoring the well-known Cr-related zero-phonon line in GaAs:Cr. Firstly, the results of systematic measurements on the Cr-related PL line in a series of plastically-bent GaAs:Cr samples are presented.[28,29] Secondly, this PL technique is applied to the characterization of the interface stress of ZnSe/GaAs:Cr heterostructures and its effectiveness is discussed.[30]

Finally, some conclusions obtained in this thesis work are summarized in the final chapter VI.

References

1) R. P. Mandal: Solid State Technology 25 (1982) 94.

2) R. L. Van Tuyl: IEEE Tran. Electron Devices ED-28 (1981) 166.

3) R. N. Thomas, H. M. Hobgood, G. W. Eldridge, D. L. Barrett, T. T. Braggins, L. B. Ta and S. K. Wang: Semiconductors and Semimetals (Academic Press, London, 1984) vol. 20, chap. 1.

4) C. A. Stolte: Semiconductors and Semimetals (Academic Press, London, 1984) vol. 20, chap. 2.

5) B. M. Welch, F. H. Eisen and J. A. Higgins: J. Appl. Phys. 45 (1974) 3685.

6) R. N. Thomas, H. M. Hobgood, D. L. Barrett and G. W. Eldridge: Proc. Int. Conf. Semi-Insulating III-V Mater., Nottingham, 1980 (Shiva Publishing Limited, Orpington, 1980) p. 76.

7) R. D. Fairman, R. T. Chen, J. R. Oliver and D. R. Ch'en: IEEE Tran. Electron Devices ED-28 (1981) 135.

8) H. M. Hobgood, G. W. Eldridge, D. L. Barrett and R. N. Thomas: IEEE Tran. Electron Devices ED-28 (1981) 140.

9) W. Y. Lum and H. H. Wieder: Appl. Phys. Lett. 31 (1977) 213.

10) R. W. Haisty and G. R. Cronin: Proc. 7th Int. Conf. Physics of Semiconductors, Dunod Paris, 1964 (Academic Press, New York, 1964) p. 1161.

11) J. F. Woods and N. G. Ainslie: J. Appl. Phys. 34 (1963) 1469.

12) T. Shimada and S. I. Akai: Jpn. J. Appl. Phys. 8 (1969) 1352.

13) D. E. Holmes, R. T. Chen, K. R. Elliott and C. G. Kirkpatrick: Appl. Phys. Lett. 40 (1982) 46.

14) D. E. Holmes, R. T. Chen, K. R. Elliott, C. G. Kirkpatrick and P.

W. Yu: IEEE Tran. Electron Devices ED-29 (1982) 1045.

15) for example, G. L. Miller, D. V. Lang and L. C. Kimerling: Ann. Rev. Mater. Sci. (Annual Reviews Inc., 1977) p. 377.

16) U. Kaufmann and J. Schneider: Festkorperprobleme XX (1980) 87.

17) Y. Fujiwara, T. Nishino and Y. Hamakawa: Oyo butsuri 54 (1985) 1202. (in Japanese)

18) T. Nishino, Y. Fujiwara and Y. Hamakawa: Proc. Int. Symp. Gallium Arsenide & Related Compounds, New Mexico, 1982 (Inst. of Phys., London, 1983) p. 71.

19) Y. Fujiwara, T. Nishino and Y. Hamakawa: Jpn. J. Appl. Phys. 21 (1982) L727.

20) T. Nishino, Y. Fujiwara, A. Kojima and Y. Hamakawa: Proc. SPIE Symp. Spectroscopic Characterization Techniques for Semiconductor Technology, Massachusetts, 1983 (Soc. Photo-Optical Inst. Eng., Washington, 1984) p. 2.

21) Y. Fujiwara, A. Kojima, T. Nishino and Y. Hamakawa: J. Luminescence 31&32 (1984) 451.

22) Y. Fujiwara, Y. Kita, Y. Tonami, T. Nishino and Y. Hamakawa: submitted to J. Phys. Soc. Jpn.

23) Y. Fujiwara, Y. Kita, Y. Tonami, T. Nishino and Y. Hamakawa: Jpn. J. Appl. Phys. 25 (1986) L232.

24) Y. Fujiwara, Y. Kita, Y. Tonami, T. Nishino and Y. Hamakawa: submitted to Appl. Phys. Lett.

25) Y. Fujiwara, Y. Kita, Y. Tonami, T. Nishino and Y. Hamakawa: to be published in Proc. Int. Conf. Semi-Insulating III-V Mater., Hakone, 1986.

26) Y. Fujiwara, A. Kojima, T. Nishino and Y. Hamakawa: Jpn. J. Appl.

Phys. 24I (1985) 1479.

27) Y. Fujiwara, A. Kojima, T. Nishino and Y. Hamakawa: Jpn. J. Appl. Phys. 22I (1983) L476.

28) Y. Fujiwara, A. Kojima, T. Nishino, Y. Hamakawa, K. Yasutake, M. Umeno and H. Kawabe: Ext. Abst. 16th Int. Conf. Solid State Devices & Mater., Kobe, 1984 (Japan Business Center for Academic Societies, Tokyo, 1984) p. 177.

29) Y. Fujiwara, T. Nishino and Y. Hamakawa: submitted to Appl. Phys. A.

30) Y. Fujiwara, S. Shirakata, T. Nishino, Y. Hamakawa and S. Fujita: submitted to Jpn. J. Appl. Phys.

II. TRANSITION METAL IMPURITIES IN GaAs

2-1. Introduction

Some impurities and lattice defects form deep electronic states, and behave as trapping and recombination centers in III-V compound semiconductors.[1)] Systematic experimental studies on these deep centers started only during the last decade, although some important contributions already fall into the sixties. The investigations are motivated mainly by the following three reasons; the first is that deep centers deleteriously affect minority carrier properties in injection devices, e.g. LED, as well as majority carrier properties in unipolar devices, e.g. FET, which is a major factor limiting device performance and reliability. The second is that deep impurities are used as compensators to grow semi-insulating substrate material. The last is that a better physical understanding of deep defects is highly desired from a basic scientific point of view.

The 3d-transition metal impurities occupy preferentially the Ga site and form deep acceptor centers in GaAs crystals,[2)] some of which are used to compensate residual shallow donors and to enhance the resistivity of the material. The electrical properties, such as activation energies and capture cross sections, of these deep acceptor centers associated with the transition metal impurities have been relatively well investigated by some electrical, especially capacitance transient measurements.[3)] As regards optical measurements, the low-temperature photoluminescence (PL) spectra

exhibit some characteristic emission lines,[4] depending on the kind of the 3d-transition metal impurity in the near-infrared region. However, the complete understanding of their microscopic properties, such as atomic structure, symmetry and charge states, has been not yet obtained. This is essentially due to the fact that these transition metal impurities can exist in different charge states with respect to the position of Fermi level and easily form complexes with other impurities or native defects involved together in GaAs crystals.

In this chapter, the behaviors of 3d-electrons in a crystal with T_d symmetry are briefly postulated based on crystal-field theory. Secondly, a survey on 3d-transition metal impurities in GaAs, assessed by electrical and ESR measurements is presented. Finally, the luminescence associated with these impurities in GaAs is classified with respect to recombination mechanism and summarized.

2-2. 3d-electrons in crystal with T_d symmetry

The electronic properties of a 3d-transition metal impurity are characterized by the many-electron nature of the d-shell. The many-electron character of the electronic structure has been a major obstacle in developing a quantitative theory. Theories of transition-metal ions in crystal have been originated from the crystal-field approach developed for ionic systems and proved to be fundamentally justified by some experimental evidences.[5] In this section, the 3d states of a single electron at a substitutional site of tetragonal (T_d) symmetry is briefly described from crystal-field approach[6].

We consider a hydrogen atom surrounded by four point-charges, $-Ze$, as indicated in Fig. 2-1. Here, $Z > 0$ for the negative charge and $Z < 0$ for the positive charge. The position of each point-charge is denoted in the figure. In this case, the electron of the hydrogen atom is exposed to the field due to the point-charges in addition to the Coulomb field due to the hydrogen nucleus. The potential energy, V_c, of the electron due to the field of the point-charges is given as

$$V_c(r) = \sum_{i=1}^{4} Ze^2/|R_i - r|, \tag{2-1}$$

where r is the electron coordinate and R_i is the position vector of the ith point-charge. Then, the Schrodinger equation for the electron

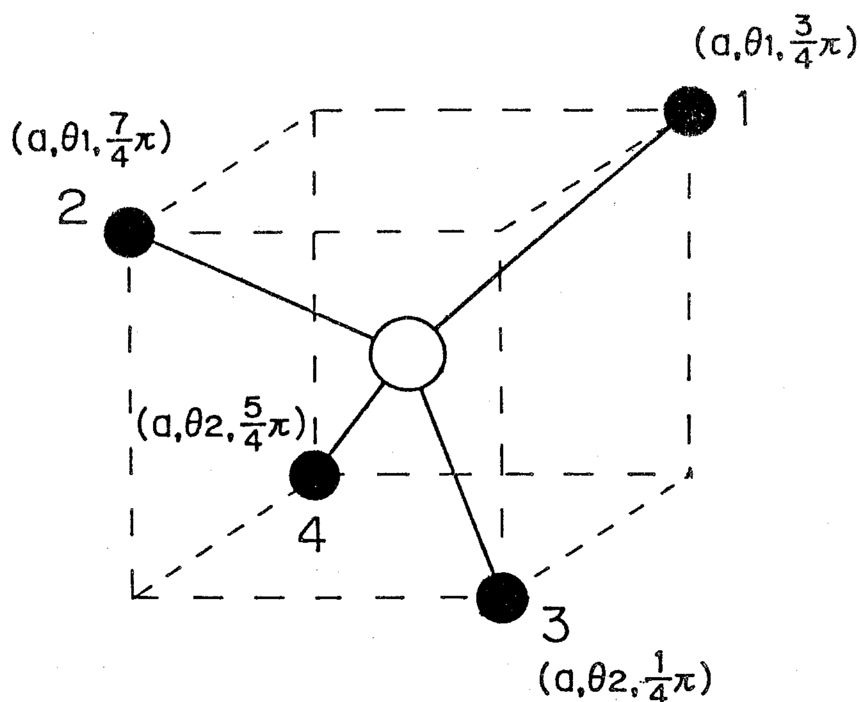

Fig. 2-1 Hydrogen atom surrounded by four point-charges; T_d symmetry. ●, $-Ze$ point-charge. O, hydrogen atom.

in this system is

$$[-(h^2/2m)\Delta + U(r) + V_c(r)]\Phi(r) = \varepsilon\Phi(r), \qquad (2\text{-}2)$$

where U(r) is the potential energy due to the hydrogen nucleus, $\phi(r)$ the wavefunction, and ε the energy eigenvalue.

In what follows, the perturbation method will be used to solve eq. (2-2) by assuming V_c to be a small perturbation on a free hydrogen atom. For this reason, considering that a is much larger than the radius of the hydrogen, it is convenient to expand V_c in terms of Legendre polynominals as follows;

$$V_c(r) = Ze^2\sum_{i=1}^{4}\sum_{k=0}^{\infty} a^{-1}\ (r/a)^k\ P_k(\cos\ \omega_i). \qquad (2\text{-}3)$$

Furthermore, the addition theorem for spherical harmonics shows

$$P_k(\cos\ \omega_i) = [4\pi/(2k+1)]\sum_{m=-k}^{k} Y_{km}(\theta,\phi)\ Y_{km}^*(\theta_i,\phi_i) \qquad (2\text{-}4)$$

where $Y_{km}(\theta,\phi)$ is the spherical harmonics, and (r,θ,ϕ) and (a,θ_i,ϕ_i) are the polar coordinates of r and R, respectively. Here $Y_{km}^*(\theta_i,\phi_i)$ is the complex conjugate of $Y_{km}(\theta_i,\phi_i)$. From eq. (2-3) and (2-4), V_c is given as a function of the electron coordinate r as follows;

$$V_c(r) = \sum_{k=0}^{\infty}\sum_{m=-k}^{k} r^k\ q_{km}\ C_m^{(k)}(\theta,\phi) \qquad (2\text{-}5)$$

where

$$q_{km} = [4\pi/(2k+1)]^{1/2}\ (Ze^2/a^{k+1})\ \sum_{i=1}^{4} Y_{km}^*(\theta_i,\phi_i) \qquad (2\text{-}6)$$

$$C_m^{(k)}(\theta,\phi) = [4\pi/(2k+1)]^{1/2} \, Y_{km}(\theta,\phi). \tag{2-7}$$

The q_{km}'s are given as

$$q_{km} = [2/(2k+1)]^{1/2} \, (2Ze^2/a^{k+1}) \, [R_{km}(\theta_1) \exp(-jm3\pi/4) + \Theta_{km}(\theta_2) \exp(-jm\pi/4)] \quad \text{(m: even)} \tag{2-8}$$

$$q_{km} = 0 \quad \text{(m: odd)} \tag{2-9}$$

in which Θ_{km} is defined by

$$Y_{km}(\theta,\phi) = (2\pi)^{-1/2} \, \Theta_{km}(\theta) \exp(jm\phi). \tag{2-10}$$

By inserting the explicit forms of Θ_{km} into the above equations, the explicit form $V_c(r)$ is obtained as follows;

$$\begin{aligned} V_c(r) = {} & 4Ze^2/a \\ & - (2\sqrt{10}/3) \, (Ze^2/a^4) \, j \, r \, [C_2^{(3)} - C_{-2}^{(3)}] \\ & - (14/9) \, (Ze^2/a^5) \, r^4 \, [C_0^{(4)} + (5/14)^{1/2} \, (C_4^{(4)} + C_{-4}^{(4)})] \\ & + (8/9) \, (Ze^2/a^7) \, r^6 \, [C_0^{(6)} - (7/2)^{1/2} \, (C_4^{(6)} + C_{-4}^{(6)})] \\ & + \text{------} \end{aligned} \tag{2-11}$$

The first term in eq. (2-11) represents the potential energy of the electron located at the position of the hydrogen nucleus and elevates all the energy levels of the hydrogen atom by the same amount, $4Ze^2/a$. The other terms split some of the degenerate energy levels as shown later.

Before discussing the details of the perturbation calculation, the matrix elements of V_c are calculated. Since the first term of V_c which is independent of the electron coordinate appears in all the diagonal matrix elements, we leave out the first term of V_c and shift the origin of the energy by $4Ze^2/a$. Therefore, V_c^0 is defined by the following equation;

$$V_c^0 = V_c - 4Ze^2/a. \qquad (2\text{-}12)$$

Now let us calculate the matrix elements of V_c^0 between the d-states. Considering that the wavefunction of the d-state, Φ_{n2m}, is denoted by

$$\Phi_{n2m} = R_{n2}(r)\ Y_{2m}(\theta,\phi), \qquad (2\text{-}13)$$

the nonvanishing matrix elements are given as follows;

$$\begin{aligned} \langle\Phi_{n2\pm2} \mid V_c^0 \mid \Phi_{n2\pm2}\rangle &= Dq \\ \langle\Phi_{n2\pm1} \mid V_c^0 \mid \Phi_{n2\pm1}\rangle &= -4Dq \\ \langle\Phi_{n2\,0} \mid V_c^0 \mid \Phi_{n2\,0}\rangle &= 6Dq \\ \langle\Phi_{n2\pm2} \mid V_c^0 \mid \Phi_{n2\mp2}\rangle &= 5Dq \end{aligned} \qquad (2\text{-}14)$$

where

$$Dq = -\ (2/27)\ (Ze^2/a^5)\ \langle r^4\rangle_{n2} \qquad (2\text{-}15)$$

$$\langle r^4\rangle_{n2} = \int dr\ r^6\ |R_{n2}(r)|^2. \qquad (2\text{-}16)$$

According to the perturbation theory, the perturbed energies of the 3d-level of the hydrogen atom due to the presence of the point-charges are given by solving the following secular equation;

$$\begin{vmatrix} \varepsilon_3^0+Dq-\varepsilon & 0 & 0 & 0 & 5Dq \\ 0 & \varepsilon_3^0-4Dq-\varepsilon & 0 & 0 & 0 \\ 0 & 0 & \varepsilon_3^0+6Dq-\varepsilon & 0 & 0 \\ 0 & 0 & 0 & \varepsilon_3^0-4Dq-\varepsilon & 0 \\ 5Dq & 0 & 0 & 0 & \varepsilon_3^0+Dq-\varepsilon \end{vmatrix} = 0, \qquad (2\text{-}17)$$

where

$$\varepsilon_3^0 = \varepsilon_3 + 4Ze^2/a \qquad (2\text{-}18)$$

and ε_3 is the energy of the 3d-state of the hydrostatic atom. As easily seen, eq. (2-17) splits into three one-dimensional and one two-dimensional determinantal equations and the energy eigenvalues are obtained as

$$\begin{aligned} \varepsilon^{(1)} &= \varepsilon_3^0 + 6Dq \\ \varepsilon^{(2)} &= \varepsilon_3^0 - 4Dq \end{aligned} \qquad (2\text{-}19)$$

where $\varepsilon^{(1)}$ and $\varepsilon^{(2)}$ are, respectively, doubly and triply degenerate. It is customary to call the states with energies $\varepsilon^{(1)}$ and $\varepsilon^{(2)}$, e_g and t_{2g} states, respectively, and to denote $\varepsilon^{(1)}$ and $\varepsilon^{(2)}$ as $\varepsilon(e_g)$ and $\varepsilon(t_{2g})$, respectively. The result in eq. (2-19) shows that the

3d-level of the hydrogen atom, which has fivefold degeneracy, is split into doubly and triply degenerate levels, as shown in Fig. 2-2.
In the case of 3d-transition metal ions with many d-shell electrons, the ground states can be essentially described by distribution of the electrons to these states.

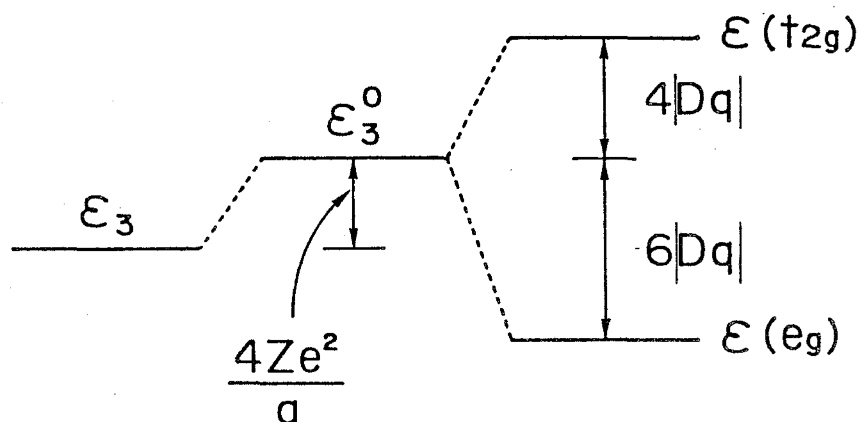

Fig. 2-2 Splitting of the 3d-level of a hydrogen atom in a tetragonal field.

2-3. Transition metal impurities in GaAs

The 3d-transition metal deep acceptor is a multivalent impurity with many d-shell electrons in the center and also holes are bound in the d-shell of the acceptor rather than bound hydrogenically in a simple acceptor such as the group IV element atom in GaAs. These 3d-transition metal impurities in GaAs have been studied so far, together with those in GaP and InP, but the complete understanding of the electronic states have been not yet achieved. This section briefly summarizes recent progress towards the understanding of

3d-transition metal impurities in GaAs by electrical and ESR measurements.

Titanium (Ti)

It has been reported that Ti introduces mid-gap levels in GaAs, suitable for creating semi-insulating (SI) materials. The Ti^{3+}/Ti^{2+} acceptor level is located at $E_c-0.28$ eV and the Ti^{4+}/Ti^{3+} donor level at $E_v+0.6$ eV.[7] The thermal stability of this new class of SI materials should be superior to that of Cr-doped or Fe-doped GaAs due to the low thermal diffusivity of Ti.

Vanadium (V)

V-doping of GaAs has been reported to give rise to an acceptor level very close to mid-gap and to enhance the resistivity of the material.[8] There has been some controversial discussion on the detailed assignment of the V-related center. Recent experimental evidences have shown the contribution of another impurity to the deep center.[9]

A characteristic ESR signal has been recently observed in SI GaAs:V.[10] Its g-factor, g = 1.957, and the ^{51}V hyperfine splitting, $A = 54 \times 10^{-4}$ cm^{-1}, are consistent with the assignment to a cubic V^{3+} center.

Chromium (Cr)

The deep Cr-related center at Ev+0.78 eV[11] is technologically important in GaAs because Cr-doping is the standard procedure to grow high-resistivity substrate material.

The ground state of the neutral Cr^{3+} acceptor in GaAs has been analyzed by ESR measurements.[12] It has been found that the ground state is formed by two Kramers doublets, separated by 7 cm^{-1}. Furthermore, a static orthorhombic Jahn-Teller distortion has been found to exist in the center. However, it has been not yet established whether the low symmetry of the center is due to an intrinsic distortion or to another nearby defect.

Upon tightly trapping an electron, the isolated Cr acceptor is converted to Cr^{2+}. Its ground state has been intensively studied by various spectroscopic techniques. By ESR measurements, it has been conclusively demonstrated that this state undergoes a static, tetragonal Jahn-Teller distortion in GaAs.[13] The direct confirmation that the reduced symmetry of Cr^{2+} is due to an intrinsic distortion via strong tetragonal Jahn-Teller coupling has been obtained from some experimental evidences.[14-16] The crystal-field absorption band of isolated Cr^{2+} in GaAs has been also identified.[17] Its zero-phonon structure bears all the characteristics expected for a ^5D ion in a tetragonally distorted, tetrahedral environment.[18]

An isotropic ESR line with g=1.993 has been observed in SI GaAs:Cr after in-situ optical excitation,[19] and originally thought to correspond to Cr^{+}. However, the recent observation of this line in p-type GaAs:Cr as a stable, light-insensitive signal has raised doubts about the above-mentioned assignment,[20] suggesting that the g=1.993 signal is due to Cr^{4+}.

Manganese (Mn)

The ionization energy of Mn in GaAs has been found to be smallest

among all the other 3d-acceptors and amount to 0.1 eV.[21] In this acceptor, a hole is energetically favoured in a more delocalized orbital because of the rather low ionization energy and the great stability of the $3d^5$ configuration, different from other 3d-transition metal impurities except for Cu. The experimental evidence has been obtained by analyzing the spectral response associated with the ionization of the neutral Mn acceptor in GaAs.[22]

Iron (Fe)

It is well-known that Fe forms a deep acceptor level at Ev+0.52 eV in GaAs[11] and is used as a compensator to obtain the high-resistivity materials. From the crystal-field approach, the ground state of Fe^{3+} in a cubic crystal-field is the spin-only sextet, $^6A_1$, all the other excited states being separated by more than 1 eV. The ESR signal has been reported for Fe^{3+} in GaAs.[23]

The crystal-field level scheme of Fe^{2+} in tetrahedral symmetry has been previously established to account for the infrared spectrum of Fe^{2+} in II-VI compound semiconductors.[24] In the level scheme, the tenfold degenerate ^5E ground state of Fe^{2+} is split by second-order spin-orbit interaction into five equidistant close-lying sublevels. Their energy separation has been estimated to be 15 cm^{-1} in GaAs.[25]

Cobalt (Co)

The ionization energy of the neutral Co acceptor in GaAs amounts to 0.16 eV.[21] By considering that the electronic configuration of Co^{3+} is $3d^6$, its electronic ground state is the same as that of Fe^{2+}.

The electronic ground state of Co^{2+}, ${}^4A_2$, is orbitally nondegenerate but has fourfold spin degeneracy. The ESR spectrum has been observed for Co^{2+} in GaAs.[26)]

Nickel (Ni)

The ionization energies reported for Ni in GaAs range from 0.20 eV[21)] to 0.42 eV[27)]. The ESR spectrum of the neutral acceptor state has been observed in GaAs.[28)] The electronic ground state of Ni^{3+} is the spin-only quartet, ${}^4A_2$, in analogy to Co^{2+}.

Copper (Cu)

In semiconductors, Cu diffuse rapidly interstitially. Several Cu-related defects have been reported in GaAs.[29,30)] Zeeman and piezospectroscopic studies have revealed that these centers have lower than cubic symmetry, indicating association with other defects. However, the chemical identity of the associated defects has been not definitely established.

2-4. Luminescence associated with transition metal impurities in GaAs[31)]

A number of characteristic sharp PL lines have been observed in the near-infrared region for GaAs doped with 3d-transition metal impurities. Based on the recombination mechanism, they can be classified as shown in Table 2-1. Intracenter transitions are characteristic of 3d-transition metal ions with unfilled d-shells and correspond to optical transitions between the energy levels of the

ions split by the crystal field of the GaAs lattice. The half-width of these PL lines is very narrow (about 0.1 meV) and the peak energy positions differ among transition metals. Furthermore, intracenter transitions are subdivided with respect to the microscopic structure of the luminescence centers. Although an isolated transition metal ion at a Ga site is subject to the perturbation of T_d symmetry, the symmetry of the suffered crystal field is lowered and the degenerate levels are split if another impurity or defect exists in the neighbor of the ion, which is referred to a complex hereafter. Therefore, in this case, new sharp PL lines are observed, different from those associated with the isolated ion, and their peak energy positions are dependent on the impurity or defect involving in the complex.

Table 2-1 Classification of the luminescence associated with 3d-transition metal impurities in GaAs.

A) Intracenter transition

microscopic structure

a) isolated ion --- V, Fe

b) complex involving another impurity

--- Cr, Ni

c) complex involving another defect

--- Cr

B) Donor-acceptor (D-A) pair transition

--- Mn, Cu

The Fe and V-related sharp zero-phonon lines observed in GaAs are attributed to intracenter transitions of isolated Fe and V ions, respectively. Figure 2-3 shows the Fe-related PL spectrum. Four characteristic sharp PL lines can be observed in the 0.37 eV region and are assigned as due to the $^5T_2$ - ^5E intracenter transitions of an isolated Fe^{2+}.[25,32,33] The V-related PL spectra are shown in Fig. 2-4. Zeeman spectroscopic studies have revealed that a sharp zero-phonon line at 0.7388 eV is originated from an isolated V ion under T_d symmetry.[10] However, the detailed assignment has been not yet obtained. As for the charge states of the ion, results of

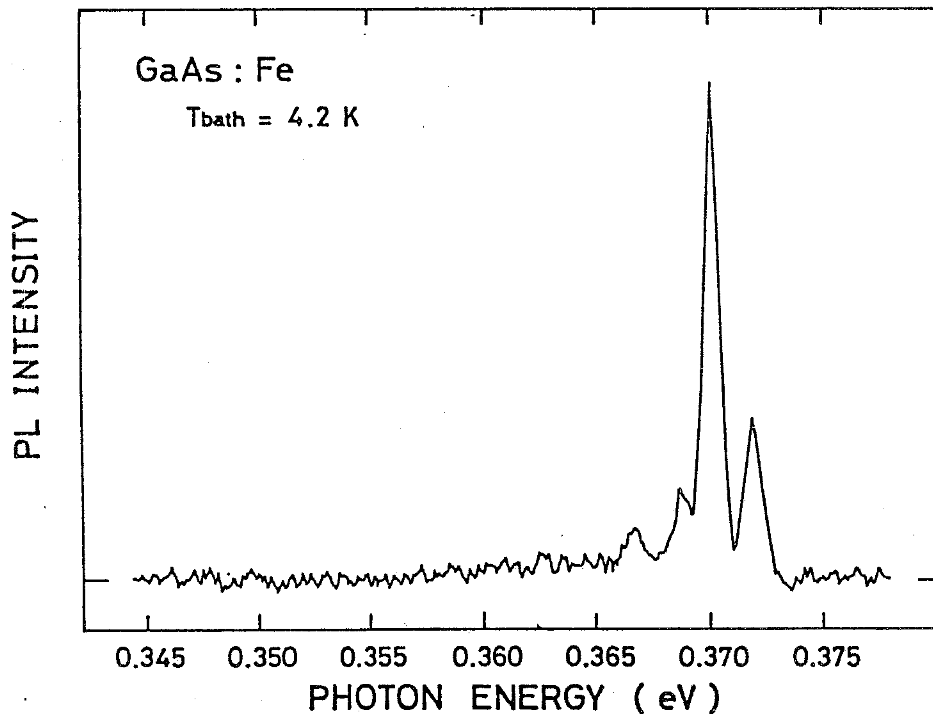

Fig. 2-3 Fe-related PL spectrum in GaAs:Fe. Four sharp zero-phonon lines in the 0.37 eV region are attributed to the $^5T_2$ - ^5E intracenter transitions of an isolated Fe^{2+}.

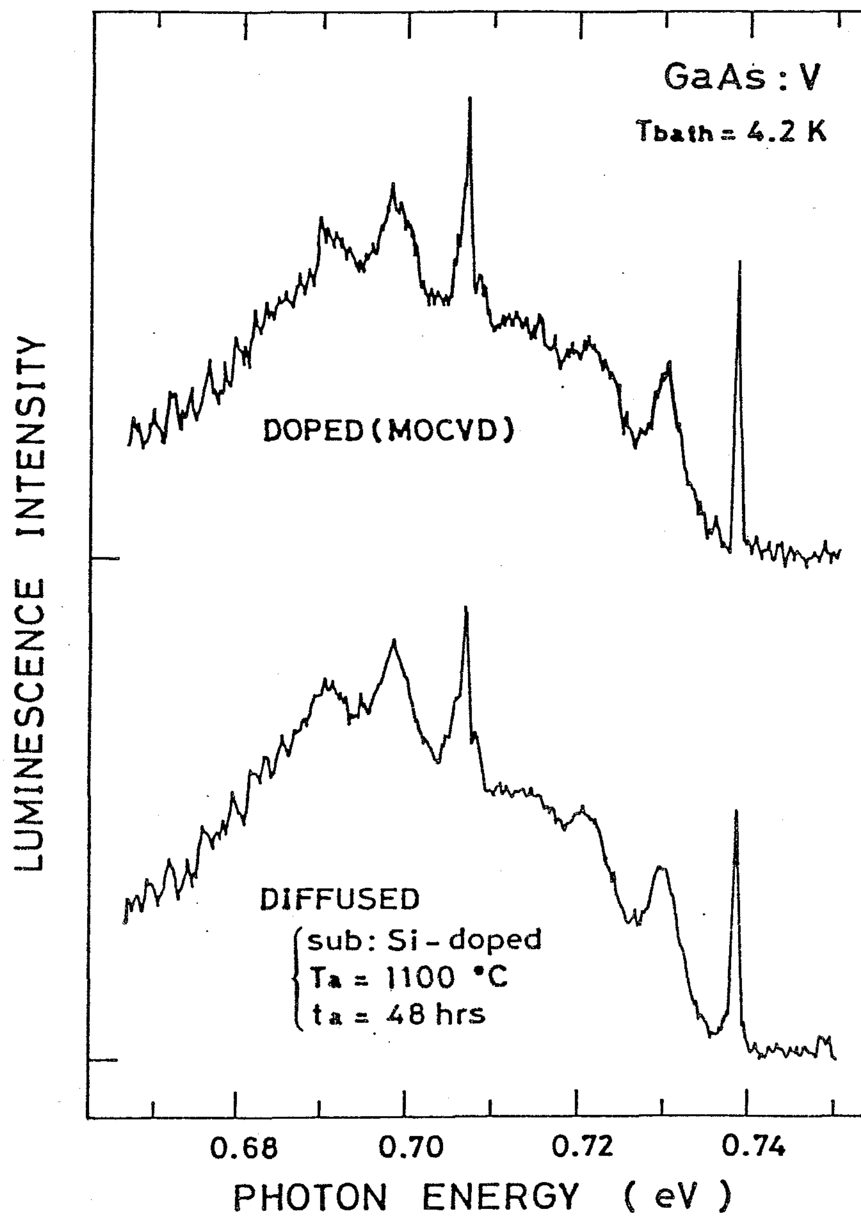

Fig. 2-4 V-related PL spectra in GaAs:V. A sharp zero-phonon line at 0.7388 eV is assigned as due to an intracenter transition of an isolated V ion.

time-resolved PL measurements have indicated that V^{3+} is the most probable candidate for the luminescence center, which will be fully described in section 4-3.

The PL spectrum associated with the Ni deep acceptor can be observed in the 0.5 eV region in GaAs. Some specific sharp PL lines appear in accordance with the chemical species of donor impurities involved in GaAs substrate.[34,35] Therefore, they are considered as due to intracenter transitions in Ni-shallow donor pairs, which will be in detail presented in section 4-2. Figure 2-5 shows the typical PL spectrum due to Ni-S pairs in GaAs. Similar associations with donor impurities have been reported for Cr in GaAs.[36-38] In Fig.

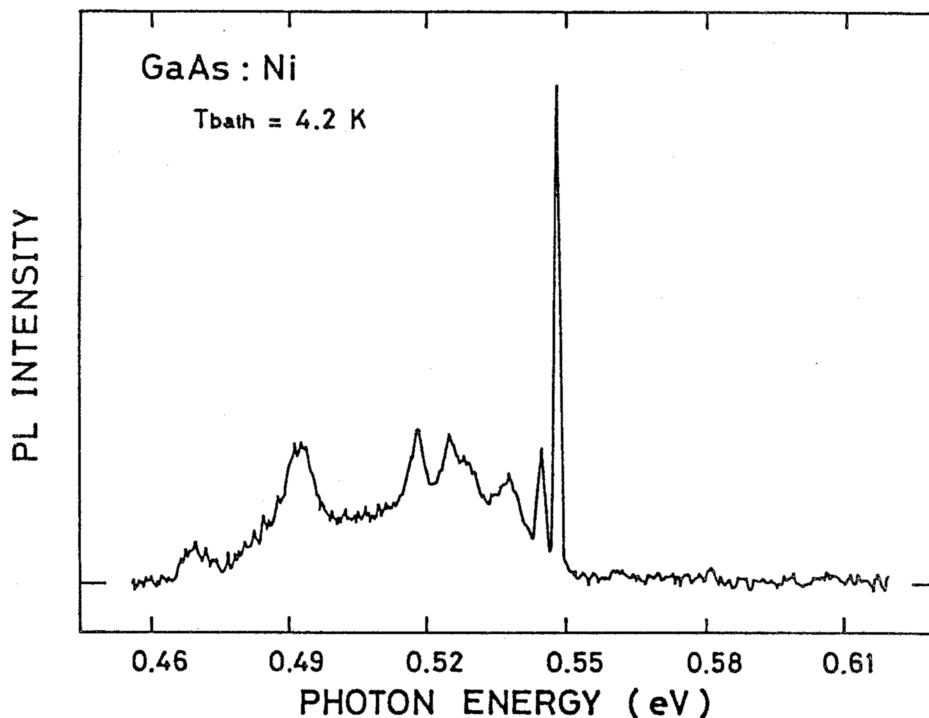

Fig. 2-5 Ni-related PL spectrum in GaAs:Ni. It is originated from a complex involving a Ni at a Ga site and a S in its nearest-neighbor.

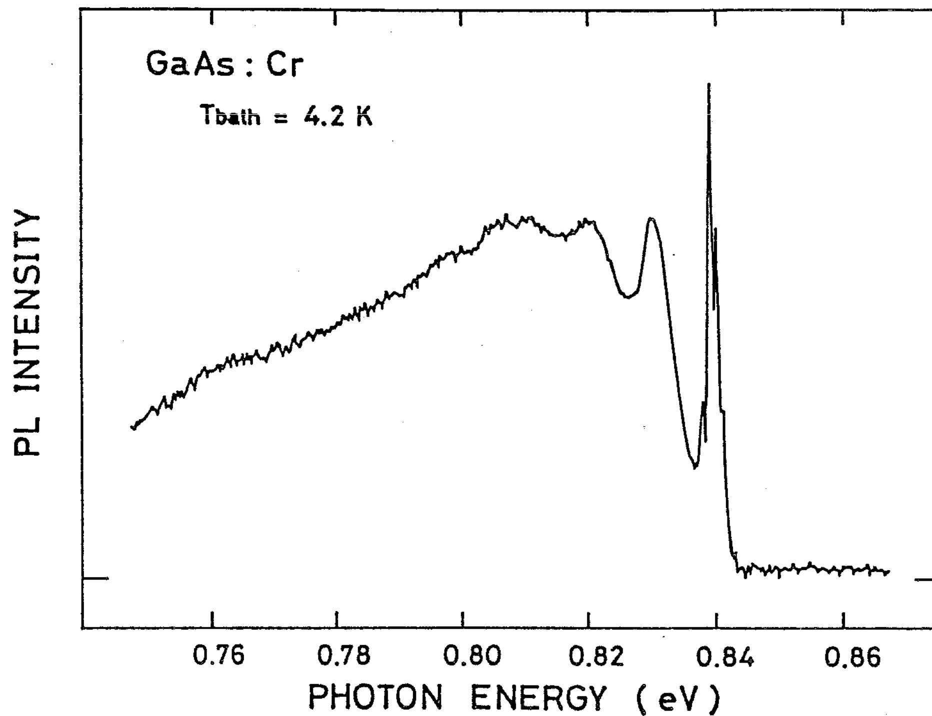

Fig. 2-6 Cr-related PL spectrum in GaAs:Cr. A series of sharp zero-phonon lines in the 0.839 eV region are originated from a complex involving a Cr at a Ga site and an arsenic vacancy in its nearest-neighbor.

2-6, the well-known Cr-related PL spectrum in GaAs is displayed. A series of sharp zero-phonon lines observed in the 0.839 eV region are attributed to the ^5E - $^5T_2$ intracenter transitions of the Cr^{2+} center, but recent detailed analyses of these lines have shown that the origin is due to a complex involving a Cr at a Ga site and an arsenic vacancy in its nearest-neighbor,[39-42] which will be demonstrated in section 3-3.

For GaAs doped with other 3d-transition metal impurities, Mn and Cu, no sharp zero-phonon lines due to intracenter transitions have been observed. These two 3d-transition metals easily form complicated

complexes involving other impurities or defects in GaAs and they act as relatively shallower acceptors, different from other 3d-transition metal impurities mentioned above. Therefore, the luminescence associated with these two acceptors is similar to those due to radiative recombination in band-to-acceptor and donor-to-acceptor pair transitions in semiconductors. In GaAs doped with Mn, a luminescence band accompanying with LO-phonon replica is observed at 1.412 eV,[43-48] as seen in the upper part of Fig. 2-7. The luminescence band is attributed to a donor-to-acceptor pair recombination involving a Mn acceptor. The non-occurrence of the $^4T_1$ - ^6A intracenter transitions of Mn in GaAs may indicate that the excited level lies above the conduction band edge. In the case of GaAs doped with Cu, the situation is similar to the case of GaAs doped with Mn, and Cu easily form complexes with other impurities or defects in GaAs. The PL spectrum of GaAs:Cu shows a strong luminescence band at 1.359 eV arising from a Cu-related complex,[49-51] which is displayed in the lower part of Fig. 2-7, and a variety of complexes involving Cu have been considered to interpret the origin of the luminescence band. According to recent piezospectroscopic investigation to this luminescence band, the Cu-related complex has been shown to have the C_{2v} rather than C_{3v} symmetry, but the chemical identification of this complex has not been established.[52] The dominant peak energy positions and the most probable assignments of the luminescence lines or bands associated with 3d-transition metal impurities in GaAs are summarized in Table 2-2.

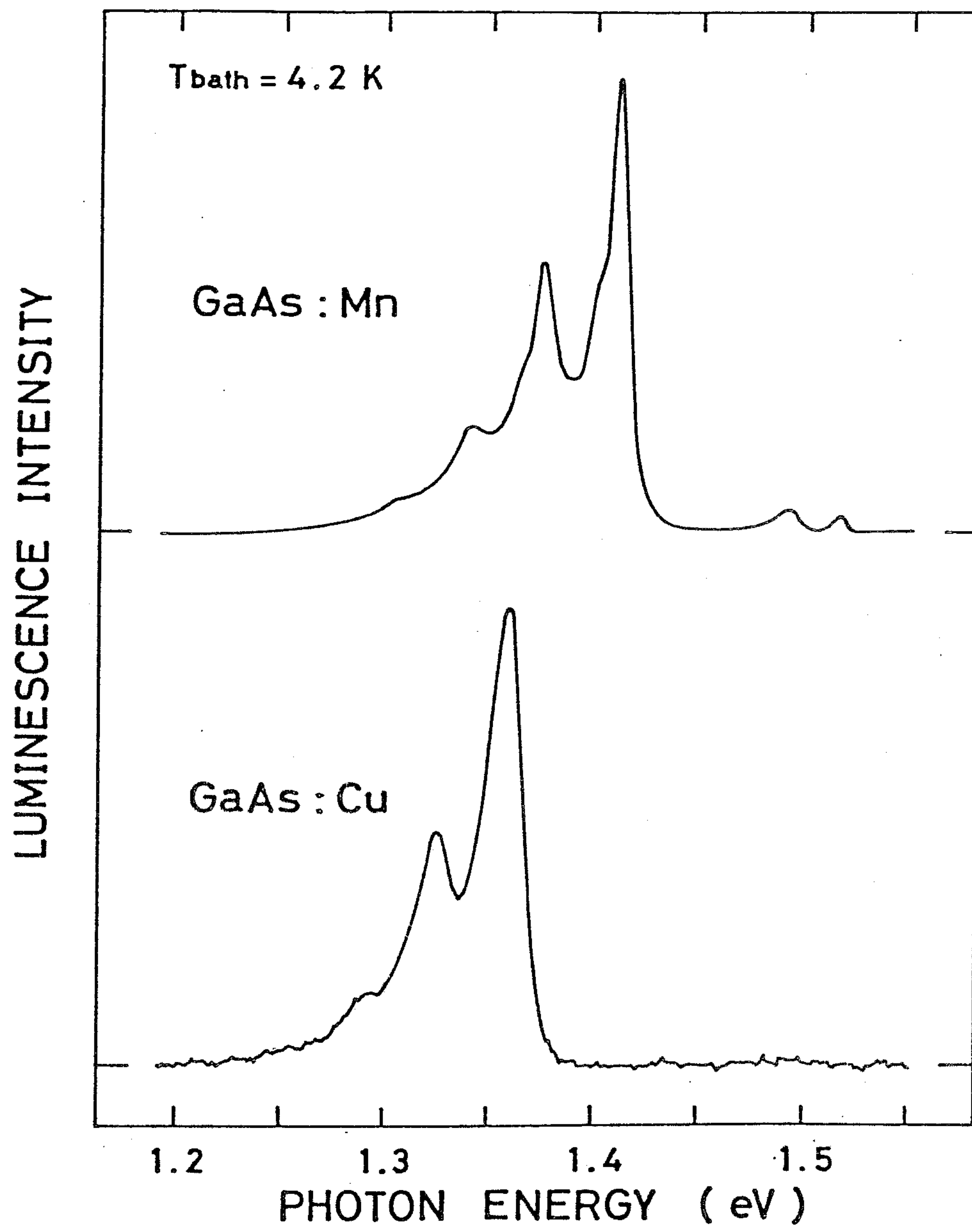

Fig. 2-7 Mn and Cu-related PL spectra in GaAs:Mn and GaAs:Cu, respectively. They are attributed to donor-to-acceptor pair recombinations involving Mn and Cu acceptors, respectively.

Table 2-2 Peak energy positions and the most probable assignments of the spectral lines due to 3d-transition metal impurities in GaAs.

3d transition metal	PL peak energy (eV)	assignment
V	0.7388	V^{3+},
Cr	0.8395	$Cr^{2+} - V_{As}$,
	0.8441	Cr^{2+} - Te,
Mn	1.412	Mn,
Fe	0.3705	Fe^{2+},
Co	0.5008*	Co^{2+},
Ni	0.5413	Ni^{+} - Te,
	0.5464	Ni^{+} - Se,
	0.5490	Ni^{+} - S,
	0.5727	Ni^{+} - Sn,
	0.5818	Ni^{+} - Si,
Cu	1.359	V_{As} - Cu - V_{As},

* absorption data (ref. 53)

2-5. Summary

The behaviors of 3d-electrons in a crystal with T_d symmetry have been briefly described from crystal-field approach. Secondly, recent progress towards understanding of 3d-transition metal impurities in GaAs by electrical and ESR measurements has been summarized. Finally, we have shown low-temperature PL spectra associated with 3d-transition metal impurities, V, Cr, Mn, Fe, Ni and Cu in GaAs. Several characteristic PL lines are successfully observed in the near-infrared region, the results of which can be utilized as a spectroscopic characterization technique for the identification of these impurities in GaAs. Furthermore, their PL lines have been classified to several groups, based on the recombination mechanism and the microscopic structure of the luminescence centers.

References

1) A. G. Milnes: Deep Impurities in Semiconductors (John Wiley & Sons, New York, 1973).

2) R. W. Haisty and G. R. Cronin: Proc. 7th Int. Conf. Physics of Semiconductors, Dunod Paris, 1964 (Academic Press, New York, 1964) p. 1161.

3) for example, G. L. Miller, D. V. Lang and L. C. Kimerling: Ann. Rev. Mater. Sci. (Annual Reviews Inc., 1977) p. 377.

4) U. Kaufmann and J. Schneider: Festkorperprobleme - Advances in Solid State Physics (Vieweg, Braunschwing, 1980) Vol. XX p. 87.

5) for example, J. S. Griffith: The Theory of Transition-Metal Ions (Cambridge University Press, New York, 1971).

6) S. Sugano, Y. Tanabe and H. Kamimura: Multiplets of Transition-Metal Ions in Crystals (Acadenic Press, New York & London, 1970).

7) G. Guillot, G. Bremond, A. Bencherifa, A. Nouailhat and W. Ulrici: to be published in Proc. Int. Conf. Semi-Insulating III-V Mater., Hakone, 1986.

8) A. V. Vasil'ev, G. K. Ippolitova, E. M. Omel'yanovskii and A. I. Ryskin: Sov. Phys. Semicond. 10 (1976) 341.

9) A. M. Hennel, C. D. Brandt, L. M. Pawlowicz and K. -Y. Ko: to be published in Proc. Int. Conf. Semi-Insulating III-V Mater., Hakane, 1986.

10) U. Kaufmann, H. Ennen, J. Schneider, R. Worner, J. Weber and F. Kohl: Phys. Rev. 25 (1982) 5598.

11) D. V. Lang and R. A. Logan: J. Electron Mater. 4 (1975) 1053.

12) J. J. Krebs and G. H. Stauss: Phys. Rev. B15 (1977) 17.

13) J. J. Krebs and G. H. Stauss: Phys. Rev. B16 (1977) 971.

14) J. J. Krebs and G. H. Stauss: Phys. Rev. B20 (1979) 795.

15) R. J. Wagner and A. M. White: Solid State Commun. 32 (1979) 399.

16) H. Tokumoto and T. Ishiguro: J. Phys. Soc. Japan 46 (1979) 84.

17) B. Clerjaud, A. M. Hennel and G. Martinez: Solid State Commun. 33 (1980) 983.

18) U. Kaufmann: Phys. Rev. B14 (1976) 1848.

19) U. Kaufmann and J. Schneider: Solid State Commun. 20 (1976) 143.

20) U. Kaufmann and J. Schneider: Appl. Phys. Lett. 36 (1980) 747.

21) W. J. Brown and J. S. Blakemore: J. Appl. Phys. 43 (1972) 2242.

22) R. A. Chapman and W. G. Hutchinson: Phys. Rev. Lett. 18 (1967) 443.

23) G. H. Stauss, J. J. Krebs and R. L. Henry: Phys. Rev. B16 (1977) 974.

24) G. A. Slack, F. S. Ham and R. M. Chrenko: Phys. Rev. 152 (1966) 376.

25) G. K. Ippolitova and E. M. Omel'yanovskii: Sov. Phys. Semicond. 9 (1975) 156.

26) M. Godlewski and A. M. Hennel: Phys. Stat. Sol. (b) 88 (1978) K11.

27) N. I. Suchkova, D. G. Andrianov, E. M. Omel'yanovskii, E. P. Rashevskaya and N. N. Solov'ev: Sov. Phys. Semicond. 9 (1975) 469.

28) M. DeWit and T. L. Estle: Bull Am. Phys. Soc. 7 (1962) 449.

29) E. F. Gross, V. I. Safarov, V. E. Sedov and V. A. Marushchack: Sov. Phys. Solid State 11 (1969) 277.

30) F. Willmann, D. Bimberg and M. Blatte: Phys. Rev. B7 (1973) 2473.

31) Y. Fujiwara, T. Nishino and Y. Hamakawa: Oyo Butsuri 54 (1985) 1202. (in Japanese)

32) V. A. Bykovskii, V. A. Vil'kotskii, D. S. Domanevskii and V. D. Tkachev: Sov. Phys. Semicond. 9 (1975) 1204.

33) A. V. Vasil'ev, G. K. Ippolitova, E. M. Omel'yanovskii and A. I. Ryskin: Sov. Phys. Semicond. 10 (1976) 713.

34) H. Ennen, U. Kaufmann and J. Schneider: Appl. Phys. Lett. 38 (1981) 355.

35) Y. Fujiwara, A. Kojima, T. Nishino and Y. Hamakawa: Jpn. J. Appl. Phys. 22 (1983) L476.

36) B. Deveaud, B. Lambart and G. Picoli: J. Appl. Phys. 55 (1984) 4356.

37) Y. Fujiwara, A. Kojima, T. Nishino and Y. Hamakawa: Jpn. J. Appl. Phys. 24 (1985) 1479.

38) Y. Fujiwara, Y. Kita, Y. Tonami, T. Nishino and Y. Hamakawa: submitted to J. Phys. Soc. Jpn.

39) M. S. Skolnick, M. R. Brozel and B. Tuck: Solid State Commun. 43 (1982) 379.

40) T. Nishino, Y. Fujiwara and Y. Hamakawa: Proc. Int. Symp. Gallium Arsenide & Related Compounds, New Mexico, 1982 (Inst. of Phys., London, 1983) p. 71.

41) Y. Fujiwara, T. Nishino and Y. Hamakawa: Jpn. J. Appl. Phys. 21 (1982) L727.

42) Y. Fujiwara, A. Kojima, T. Nishino and Y. Hamakawa: J. Luminescence 3132 (1984) 451.

43) T. C. Lee and W. W. Anderson: Solid State Commun. 2 (1964) 265.

44) W. Shairer and M. Schmidt: Phys. Rev. B10 (1974) 2501.

45) M. Ilegems, R. Dingle and L. W. Rupp, Jr.: J. Appl. Phys. 46 (1975) 3059.

46) M. Lin, K. Gamo, K. Masuda and S. Namba: Jpn. J. Appl. Phys. 15 (1976) 53.

47) P. W. Yu and Y. S. Park: J. Appl. Phys. 50 (1979) 1097.

48) S. H. Xin, C. E. C. Wood, D. DeSimone, S. Palmateer and L. F. Eastman: Electron. Lett. 18 (1982) 3.

49) H. J. Queisser and C. S. Fuller: J. Appl. Phys. 37 (1966) 4895.

50) C. J. Hwang: J. Appl. Phys. 39 (1968) 5347.

51) S. Y. Chiang and G. L. Pearson: J. Luminescence 10 (1975) 313.

52) N. S. Averkiev, T. K. Ashirov and A. A. Gutkin: Sov. Phys. Semicond. 15 (1981) 1145.

53) H. Ennen, U. Kaufmann and J. Schneider: Solid State Commun. 34 (1980) 603.

III. LUMINESCENCE IN GaAs:Cr

3-1. Introduction

Cr-doped semi-insulating (SI) GaAs is of current technological importance since this material is often used as a substrate for various GaAs-based devices. Cr-doped GaAs is, however, sensitive to heat treatment because it is compensated with mobile Cr ions. A high-resistive region is frequently formed at the interface between the epitaxial layer and the substrate during growth.[1] Ion-implantation also has some thermal conversion problems.[2] Some experimental evidences have pointed out that the annealing process causes redistribution or out-diffusion of Cr atoms, resulting in a conductive layer near the surface.[3,4] It is important to remove such an undesirable resistance change in the substrate for device fabrication. From these points of view, considerable efforts have been made to understand some electronic behaviors of Cr in GaAs.

The Cr-related centers have been intensively studied by optical, particularly photoluminescence (PL),[5-7] and EPR measurements[8-12] as well as electrical measurements[13]. The low-temperature PL spectrum associated with Cr in GaAs consists of a series of sharp zero-phonon lines around 0.839 eV and a broad band in their lower-energy side.[14-16] These Cr-related sharp PL lines were assigned as due to intracenter transitions between d-states in a divalent Cr ion in GaAs, but there was some controversy on the detailed assignment. Zeeman spectroscopic data on the dominant zero-phonon line revealed that the

luminescence center has [111] C_{3v} axial symmetry rather than T_d symmetry expected for an isolated Cr ion at a Ga site in GaAs crystal[17], suggesting the contribution of another impurity or defect to the Cr-related center. Effects of uniaxial stress on these Cr-related PL lines have been also studied in details to get further knowledge about the origin of this luminescent center and it has been illustrated that the results are well interpreted by the hypothesis of a substitutional divalent Cr ion at a Ga site subjected to the perturbation of C_{3v} symmetry.[18]

In this chapter, following the brief description on the experimental apparatus used in this work, the identification of the Cr-related luminescence center is presented based on systematic studies on high-temperature thermal annealing of GaAs:Cr. Secondly, first observation of new PL lines associated with a Cr-Se complex is described. In addition, effects of In-doping into GaAs are investigated by monitoring Cr-related PL lines. In the final section of this chapter, the author proposes a new characterization technique for arsenic vacancies utilizing the above-mentioned findings.

3-2. Experiment apparatus for luminescence measurements

Samples used in this work are divided into two groups; one is GaAs doped with Cr during growth in nominally undoped GaAs and another GaAs diffused with Cr by solid diffusion into various kinds of GaAs substrate.

Cr-doped GaAs wafers with (100) crystal orientation were cut from the ingots grown by a gradient freeze (GF) technique. Mirror-polished

samples cut from these wafers were degreased in organic solvents and etched slightly with Br_2-methanol mixture to remove the damaged layer.

In Cr-diffusion, a variety of GaAs crystals was used, which were doped with different majority donor impurities (Si, Sn, S, Se, Te), nominally undoped or In-doped. After pure Cr metal was evaporated under vacuum on the substrate surface, all the samples were immediately sealed in a quartz ampoule with a small amount of As at 10^{-6} Torr. The ampoule was heated in a diffusion furnace at 1100 °C for 24 hrs, and then cooled to room temperature. The diffusion was followed by etching off the surface layer of several microns.

The in-depth profiles of the Cr-related PL intensities in Cr-diffused GaAs were investigated in a series of layer stripping measurements by the chemical etching using a 10:1:1 mixture of H_2SO_4:H_2O_2:H_2O. The thickness of the removed layer was determined by weighing the sample before and after.

PL measurements were carried out with samples directly immersed in liquid He at 4.2 K. The photoexcitation source was a cw Ar^+ laser operating 514.5 nm with a beam diameter of about 1 mm. The photoexcitation power was changed by using neutral-density filters as well as by controlling the laser current.

The luminescence was taken from the irradiated surface, analyzed by a SPEX 1704 grating monochromator with a 600 grooves/mm grating blazed at 1.25 μm and detected by a NORTH-COAST Ge p-i-n photodiode cooled by liquid N_2. The detector output was fed to an EG&G 124A lock-in amplifier and processed with a computer-controlled signal-averaging system to improve the ratio of signal to noise. The block diagram of the averaging system is presented in Fig. 3-1.

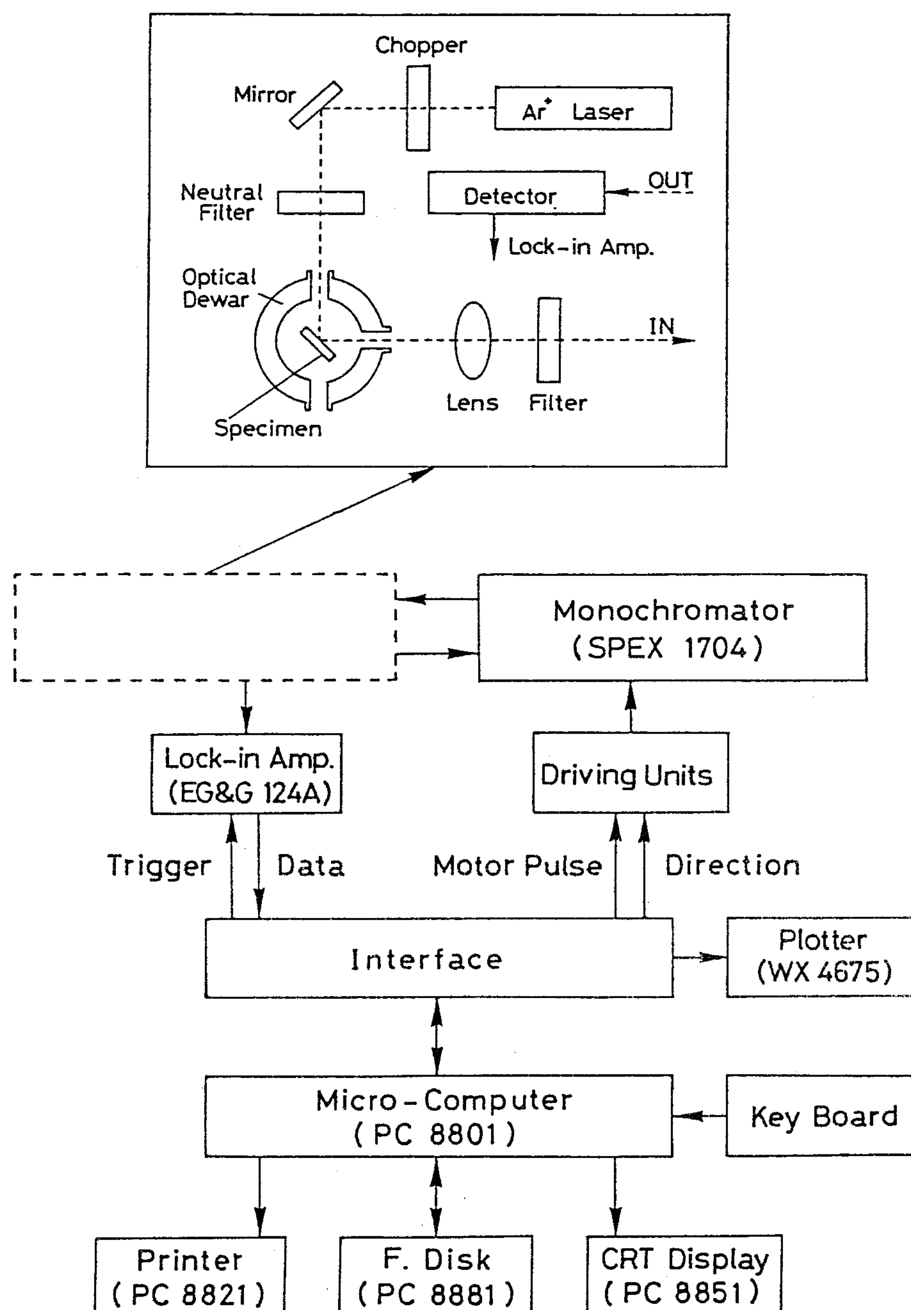

Fig. 3-1 Diagram of signal averaging system used in this work for photoluminescence measurements.

3-3. Effects of thermal annealing[19-22)]

3-3-1. Cr-related luminescence

Figure 3-2 shows a typical PL spectrum measured with Cr-doped GaAs at 4.2 K. A strong emission line with a LO-phonon replica is observed at 1.490 eV besides the near-edge emission line peaked at 1.513 eV. The 1.490 eV emission line is thought to be due to donor-acceptor pair recombination between shallow donors and residual carbon acceptors involved in GaAs crystals.[23)] On the other hand, two broad emission bands at 1.35 eV can be assigned as due to Cu-related complexes.[24)] In the lower energy region, the well-known Cr-related luminescence is observed, which is dominated by a sharp zero-phonon line at 0.8395 eV accompanying with a broad band in its lower-energy side. In Fig. 3-3, the high resolution fine structure in the 0.839 eV

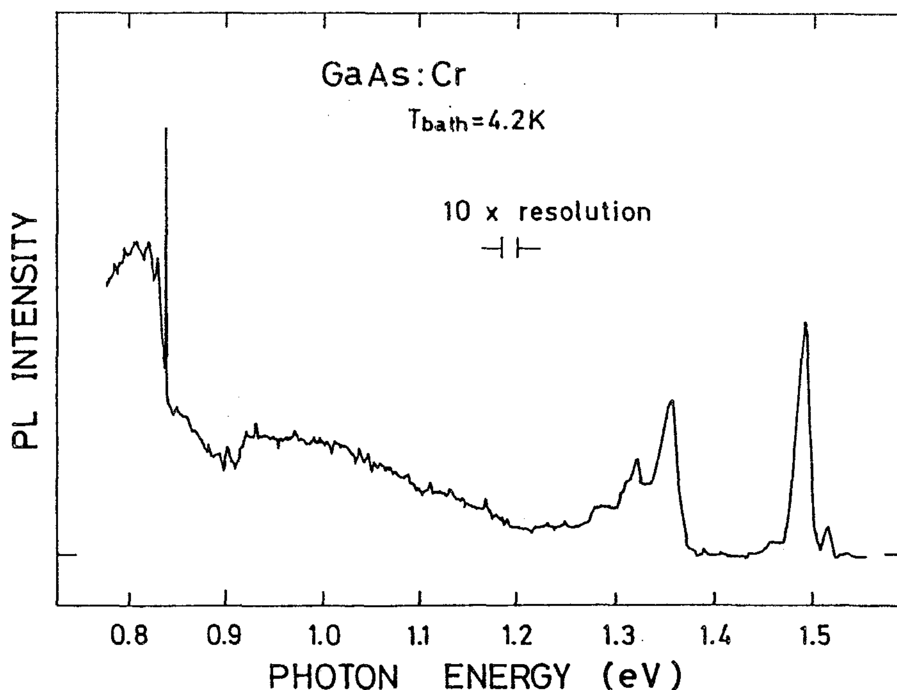

Fig. 3-2 Typical PL spectrum from Cr-doped GaAs.

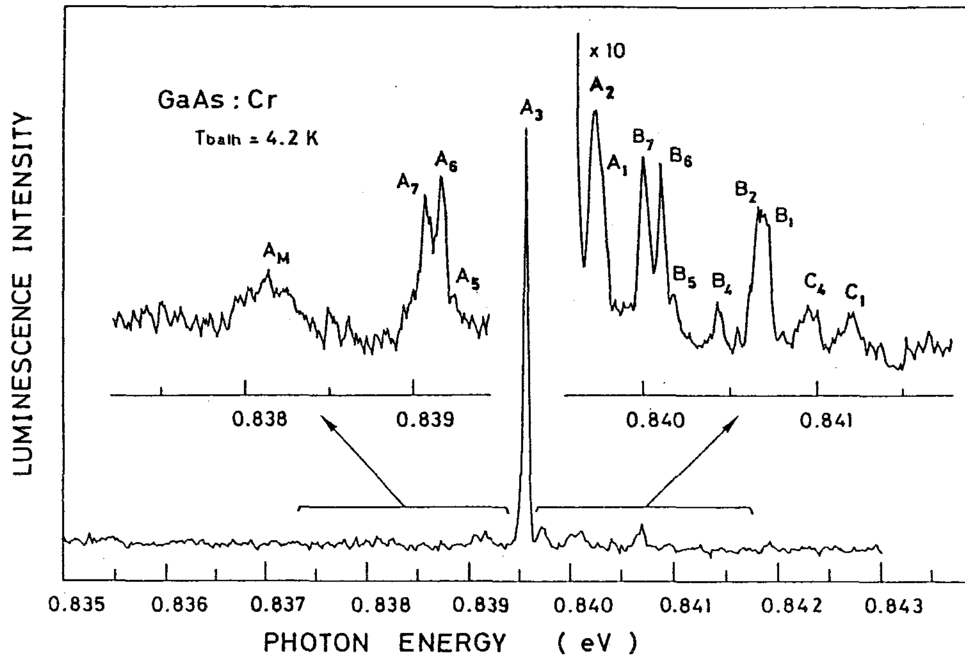

Fig. 3-3 Cr-related high-resolution fine-structure in the 0.839 eV region.

region is displayed. Many zero-phonon lines can be observed and each PL line is labelled in Barrou's nomenclature[16).

The Cr concentration dependence of the Cr-related PL spectra has been investigated. The result is shown in Fig. 3-4. The PL intensity increases with the Cr concentration, which was analyzed by secondary ion mass spectroscopy (SIMS), without change in the spectral shape. This result implies the probability of nondestructive estimation of the Cr concentration by PL measurements. The PL intensity versus the Cr concentration, however, is not straightforward, as can be seen in plots of the PL intensity of the 0.8395 eV Cr-related PL line with respect to the Cr concentration in Fig. 3-5. Similar tendency has been also observed in a series of Cr, O-codoped SI GaAs. Such a

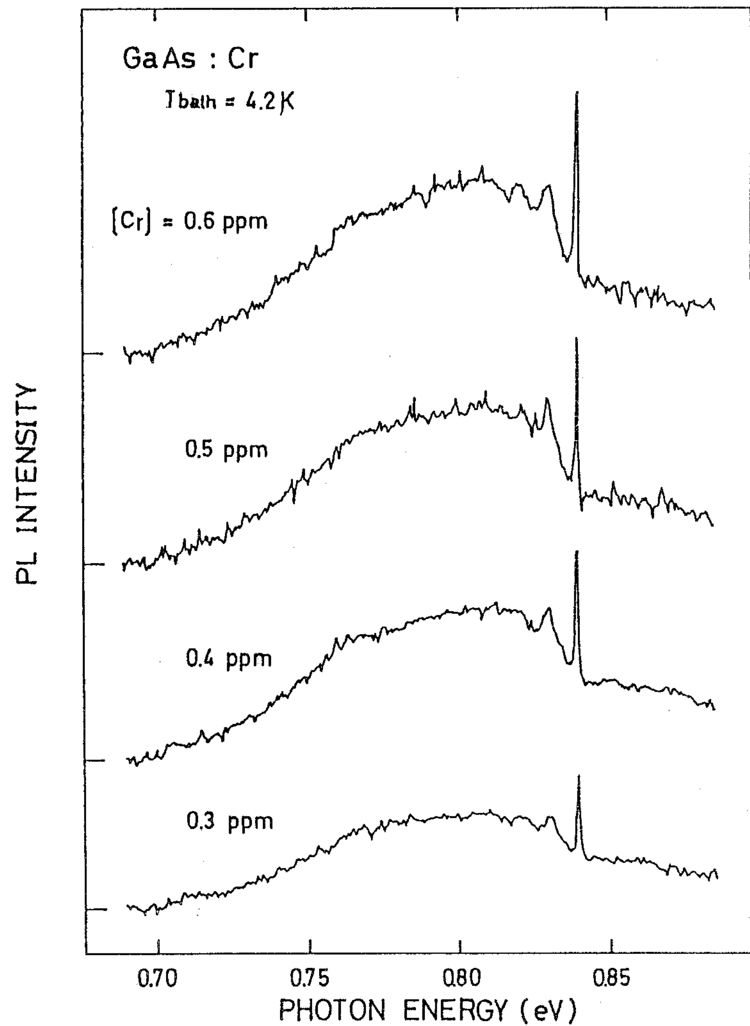

Fig. 3-4 Cr-related intracenter luminescence spectra measured for a series of GaAs doped with different Cr concentration.

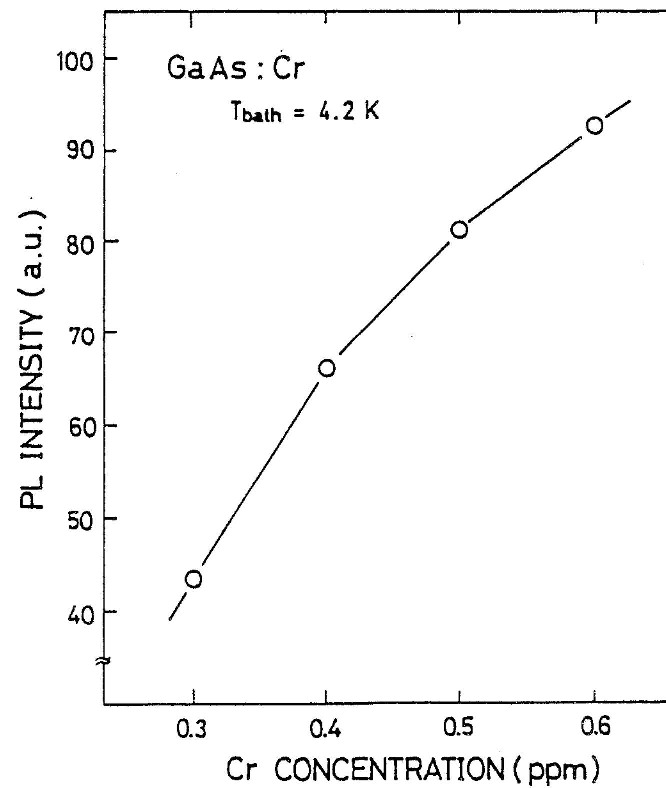

Fig. 3-5 Cr concentration dependence of the intensity of the Cr-related zero-phonon line at 0.8395 eV in Cr-doped GaAs.

behavior was also reported by Sckolnick et al.[25) These results support the recent assignment that a series of sharp zero-phonon lines observed in the 0.839 eV region in Cr-doped GaAs is originated from a complex involving Cr and another defect or impurity in the neighborhood of the Cr ion.

3-3-2. Model for Cr-related luminescence center

To clarify whether the partner of Cr in the complex is a defect or a impurity, the donor-type dependence of the 0.8395 eV zero-phonon line has been systematically investigated. As a result, it has been found that the sharp zero-phonon line is observed in all the samples, independent of the donor-type involved in the substrate crystals, though other Cr-related zero-phonon lines appear in Cr-diffused GaAs doped with Te or Se, the result of which will be in detail described in the next section. This result indicates that the partner of Cr in the complex responsible for the 0.8395 eV zero-phonon line is not a donor impurity.

The arsenic-pressure dependence of the 0.8395 eV Cr-related PL line has been also investigated. Samples used here were cut from Cr-doped SI GaAs wafers with the Cr concentration of 0.47 wt.ppm. Heat treatments of these samples were carried out in a horizontal two-zone furnace for 10 hrs. During the heat treatments, the temperature of samples was kept at 900 °C, and the ambient arsenic pressure was controlled by the temperature of arsenic source in the range of 400-600 °C. The arsenic pressure corresponding to a given arsenic source temperature was calculated according to the data

reported by Honig[26]. When the heat treatment was completed, the sample sealed ampoule was quenched into water to room temperature.

Figure 3-6 shows the excess arsenic pressure dependence of the 0.8395 eV Cr-related PL intensity and the well-known 1.49 eV C-related donor-acceptor pair PL intensity in annealed GaAs:Cr. Here each PL intensity is normalized by the Cu-related PL intensity observed at 1.35 eV in order to eliminate effects of difference in surface treatment and optical pass. In Fig. 3-6, one can see that the normalized 0.839 eV Cr-related PL intensity is proportional to $P_{As}^{-1/4}$ and the C-related PL intensity to $P_{As}^{-1/2}$, where P_{As} is the pressure of excess As_4 molecules, which are the dominant species at this temperature since that of As_2 molecules in the vapor phase is less than 10^{-2} Torr according to the vapor pressure data previously reported.[27,28] Therefore the intensity ratio of the 0.8395 eV Cr-related luminescence to the C-related luminescence is proportional to $P_{As}^{1/4}$.

This result has been analyzed based on mass-action equations for reactions involving several point defects in GaAs. The Cr-related PL intensity is clearly proportional to the concentration of the luminescence center, that is, the product of the concentration of Cr at a Ga site, $[Cr_{Ga}]$, and that of the partner of its nearest neighbor, [X]. Moreover, considering the chemical reactions of formation, $[Cr_{Ga}]$ is proportional to the product of Ga vacancy concentration, $[V_{Ga}]$, and interstitial Cr concentration, $[Cr_i]$. Here, supposing that the ratio of some charge states of a Cr ion is hardly affected by the introduction of impurities and defects during thermal annealing and that $[Cr_i]$ is not dependent upon excess arsenic pressure but upon

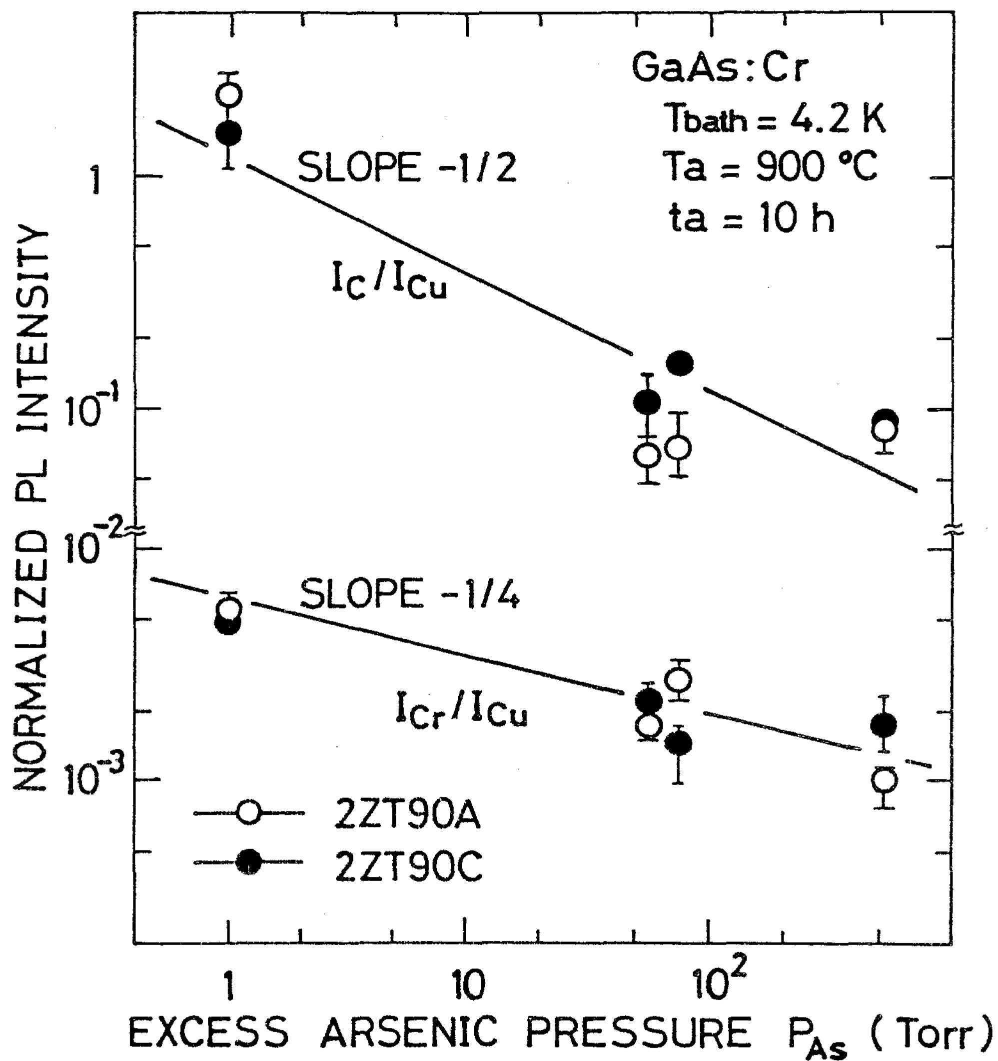

Fig. 3-6 Excess arsenic pressure dependence of the 0.8395 eV Cr-related PL intensity and the 1.49 eV C-related PL intensity in annealed GaAs:Cr. Here each PL intensity is normalized by the intensity of the Cu-related PL line at 1.35 eV.

annealing temperature, the 0.8395 eV Cr-related PL intensity is proportional to the product of $[V_{Ga}]$ and [X]. On the other hand, though the C-related PL intensity is similarly proportional to the product of As vacancy concentration, $[V_{As}]$, interstitial C concentration, $[C_i]$, and shallow donor concentration, [D], it has been obtained that its luminescence intensity has the excess arsenic pressure dependence of $P_{As}^{-1/4}$ within experimental error, which suggests that the product of $[C_i]$ and [D] is independent of the excess arsenic pressure during thermal annealing. Therefore, these results implies that [X] has the excess arsenic pressure dependence of $P_{As}^{-1/4}$, because $[V_{Ga}]$ increases with the excess arsenic pressure by the one-fourth power since As_4 molecules are the dominant species in the vapor phase at this temperature. Furthermore, considering the excess arsenic pressure dependence of various point defects in GaAs,

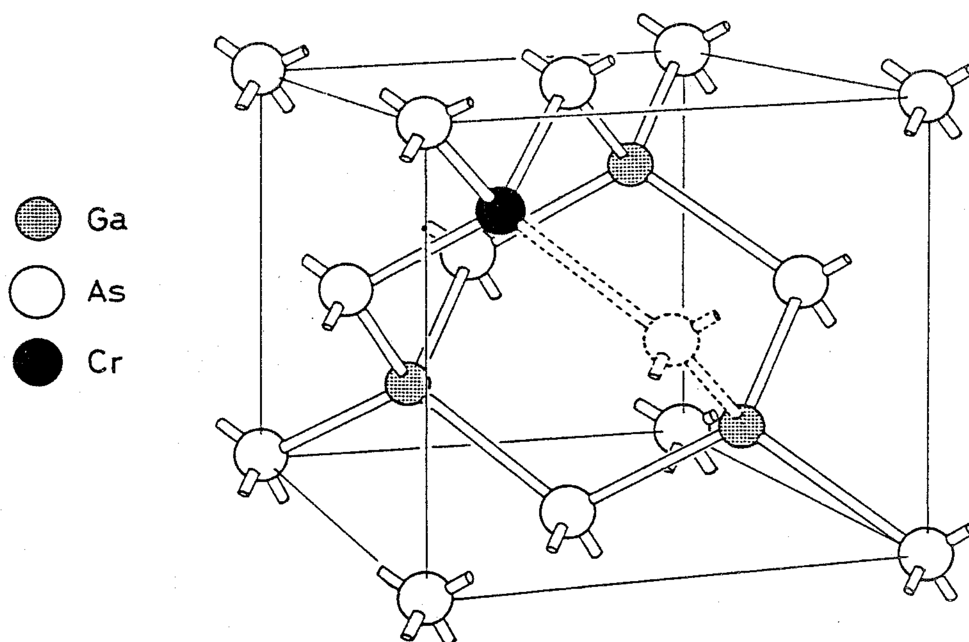

Fig. 3-7 A model of Cr-V_{As} complex center.

this analysis has led us to the conclusion that an arsenic vacancy contributes to the 0.8395 eV Cr-related luminescence center in GaAs:Cr and the luminescence is due to a complex involving a Cr impurity and an arsenic vacancy V_{As} in its nearest neighbor, i.e. a Cr-V_{As} complex, which is schematically shown in Fig. 3-7. This complex, of course, satisfies the C_{3v} symmetry of the center responsible for the 0.8395 eV Cr-related PL line in GaAs:Cr.

3-3-3. Interpretation of thermal annealing temperature and time dependences

Based on the above-mentioned model for the Cr-related luminescence center, the annealing temperature and time dependences of the 0.8395 eV Cr-related PL line in annealed GaAs:Cr can be well interpreted. In Figs. 3-8 and 3-9, the in-depth profiles of the PL intensities of the 0.8395 eV Cr-related zero-phonon line are shown with the parameters of annealing temperature and time, respectively. All the samples showed similar behaviors to those in these figures. The intensity of the 0.8395 eV PL line decreases with increasing annealing temperature and time, as can be seen in the figures. These decreases in the Cr-related PL intensity are probably due to the dissociation of the Cr-V_{As} complex in GaAs after high-temperature thermal annealing. However, in the surface region of several microns from the front surface, the Cr-related PL intensity exhibits very complicated in-depth profiles. At annealing temperatures below 900 °C, the PL intensity decreases at several microns in depth. Such decrease in the near-surface region can be also seen for short time annealing even at 900 °C, as shown in Fig. 3-9. At annealing

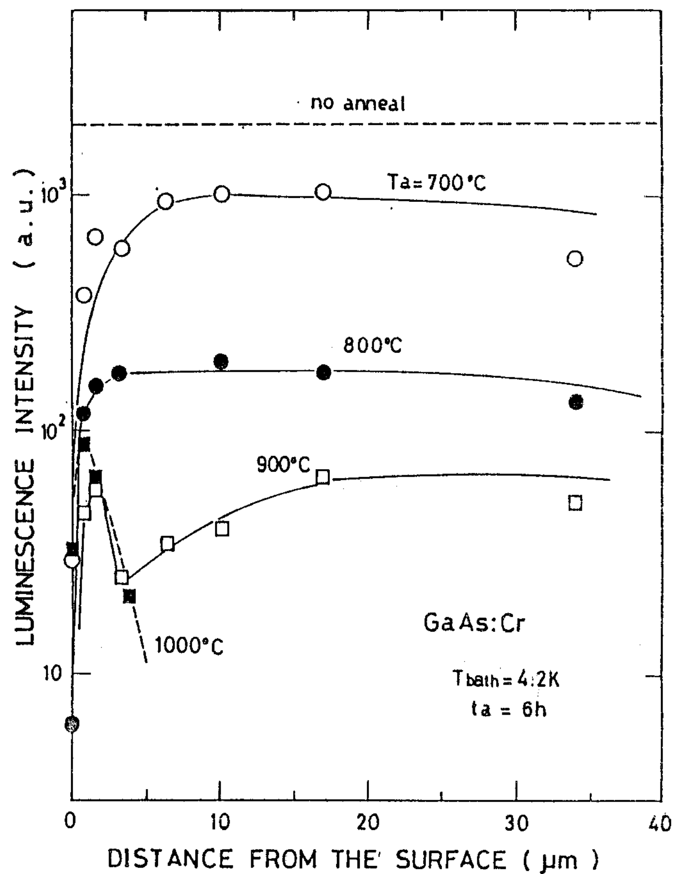

Fig. 3-8 In-depth profiles of the Cr-related PL line intensity in annealed GaAs:Cr as a function of annealing temperature.

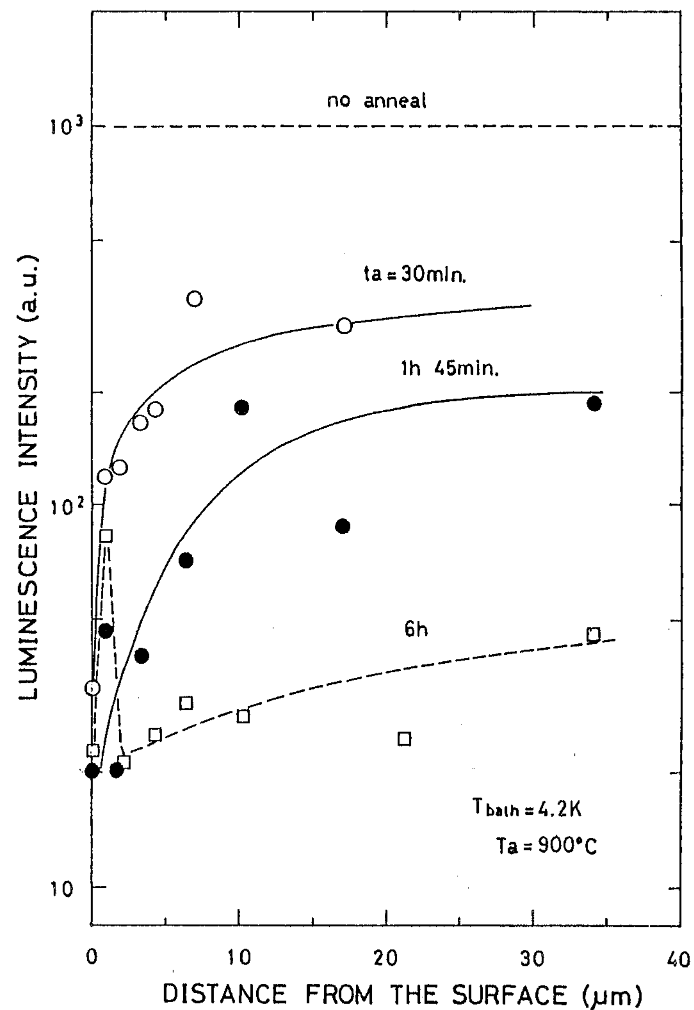

Fig. 3-9 In-depth profiles of the Cr-related PL line intensity in annealed GaAs:Cr as a function of annealing time.

temperatures above 900 °C, the Cr-related PL line appears in the near-surface region with relatively strong intensity. The intensity decrease in the surface region seems to be related to the Cr vaporization from the surface which was experimentally confirmed in connection with the well-known thermal conversion problem in SI GaAs crystals[29,30]. It should be noted here that the in-depth profiles in the near-surface region in the case of high-temperature annealing, for example 1000 °C in Fig. 3-8, can be approximately fitted to the theoretical curve of an arsenic vacancy introduced into GaAs. This result suggests that an arsenic vacancy is introduced into GaAs from the surface and a Cr-V_{As} complex considered as the luminescence center is formed after such high-temperature annealing. In order to understand these complicated in-depth profiles of the Cr-related PL intensity of annealed GaAs:Cr, it is necessary to know in detail how Cr ions and their partners redistribute in GaAs after high-temperature annealing. At the present stage, however, it is probably reasonable to consider that both the introduction of an arsenic vacancy from the surface and the dissociation of a Cr-V_{As} complex occur in GaAs after annealing and that these in-depth profiles of the Cr-related 0.8395 eV PL line reflect the redistribution of Cr and its partner, i.e. arsenic vacancy, in annealed GaAs:Cr.

3-4. Doping effects of various donor impurities[31]

In PL measurements, some complexes involving a transition metal and another impurity have been found in GaAs. Ennen et al. has firstly reported PL lines due to Ni-S, Ni-Se, Ni-Te, Ni-Si and Ni-Sn

complexes in Ni-diffused GaAs.[32] As for Cr-related complexes, the PL lines related to a Cr-Te complex have been observed at 0.844 eV in Cr, Te-codoped GaAs by Deveaud et al.[33] Furthermore, a series of characteristic PL lines has been found in Cr, In-codoped GaAs by Fujiwara et al.[34-36] and assigned to be due to a Cr-V_{As}-In complex, which will be in detail described in the next section. In this section, effects of various donor impurities on the Cr-related PL spectra in GaAs have been investigated.

3-4-1. New luminescence lines associated with Cr-Se complex

Figure 3-10 shows Cr-related PL spectra for Cr-diffused GaAs doped with S, Se and Te which are group VI elements occupying As sites, together with that for a commercially-available HB-grown SI GaAs:Cr. In SI GaAs:Cr without intentional doping of other impurities, the well-known Cr-V_{As} PL line can be observed at 0.8395 eV. In Cr-diffused GaAs doped with S, the observed PL spectrum is the same as that of SI GaAs:Cr and any new PL lines can be never observed. This suggests that the axial field induced by a S impurity in the nearest neighborhood of the Cr ion is not so strong enough to bring out the isolated Cr excited states embedded into the conduction band and to induce new Cr-related PL lines. On the other hand, as seen in this figure, a sharp PL line can be observed at 0.8441 eV in addition to the dominant Cr-V_{As} PL line in Cr, Te-codoped GaAs, which is assigned to be due to a Cr-Te complex by Deveaud et al.[33] and called Cr-Te PL line hereafter. In Cr, Se-codoped GaAs, a new zero-phonon line has been observed, for the first time, at 0.8371 eV, which is shown by an arrow. The details of the PL line measured with higher

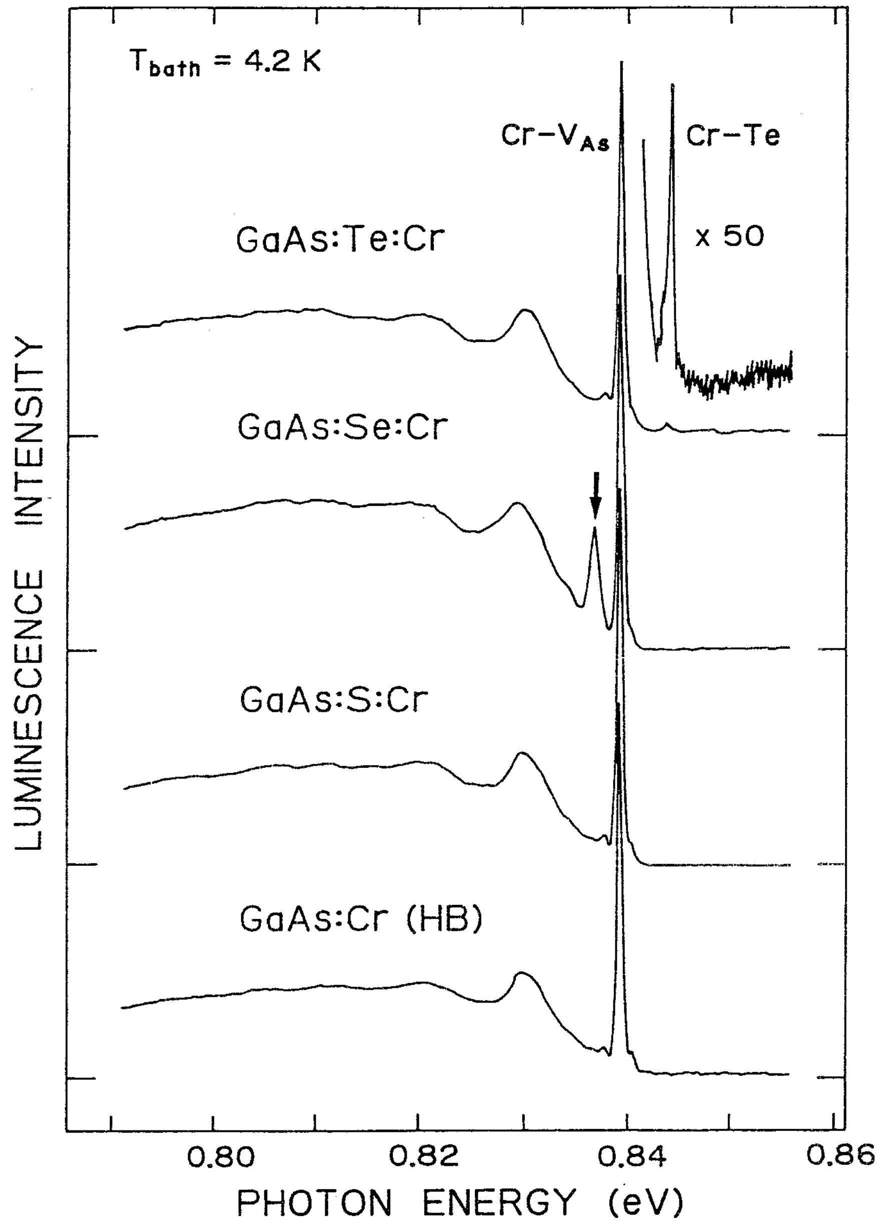

Fig. 3-10 Cr-related PL spectra for Cr-diffused GaAs doped with S, Se and Te, respectively, together with that for HB-grown GaAs:Cr.

resolution are shown in Fig. 3-11. In the higher-energy side of the spectrum, a series of PL lines associated with a Cr-V_{As} complex can be observed. In Lightowlers' nomenclature[15)], the PL lines correspond in order from high energy to line C, line E, line F, line G, line H and line I. Cr, Se-related PL spectrum involve six zero-phonon lines, which are denoted by a-f in the figure. The exact peak positions of these PL lines are listed in Table 3-1.

Temperature dependence of the PL intensities has been investigated. As a result, it has been found that the intensities of all Cr, Se-related PL lines gradually decrease with the increase of temperature, which indicates that they are cold lines.

Similar experiments have been performed for Cr-diffused GaAs doped with Si and Sn which are group IV elements occupying Ga sites. In both cases, any new Cr-related PL lines can be never observed, suggesting that the field induced by a Si or Sn impurity in the second-nearest neighborhood of the Cr ion is also not so strong.

The in-depth profiles of the intensities of the Cr-V_{As} and Cr, Se-related PL lines have been measured in Cr-diffused GaAs doped with Se. Figure 3-12 shows the typical result of the Cr-related PL spectra for a variety of thickness, d, of the surface layer successively etched off. In the region near the surface, the observed PL spectrum is dominated by the Cr-V_{As} PL line, as shown in the figure. The intensities of both PL lines gradually decrease with the increase of the distance from the surface. However, their behaviors differ considerably. That is, the intensity of the Cr-V_{As} PL line decreases more rapidly than that of the Cr, Se-related PL line and consequently the PL spectrum is dominated by the Cr, Se-related PL line in the

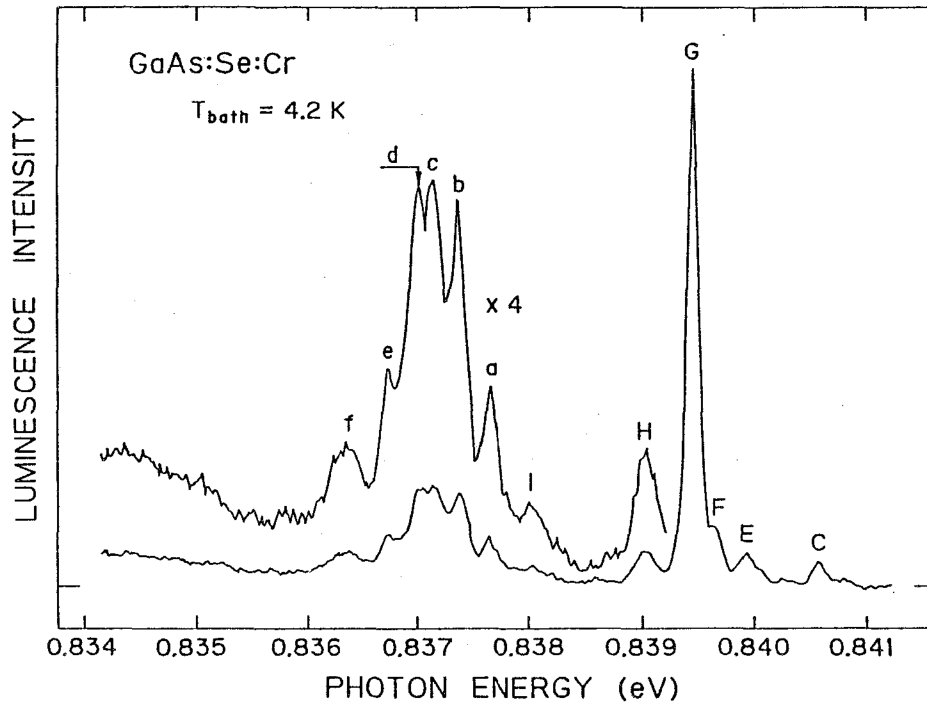

Fig. 3-11 Details of the Cr-related PL spectrum for Cr, Se-codoped GaAs.

Table 3-1 Peak positions of new PL lines observed in Cr, Se-codoped GaAs.

energy	(meV)
a	837.65
b	837.37
c	837.14
d	837.02
e	836.75
f	836.33

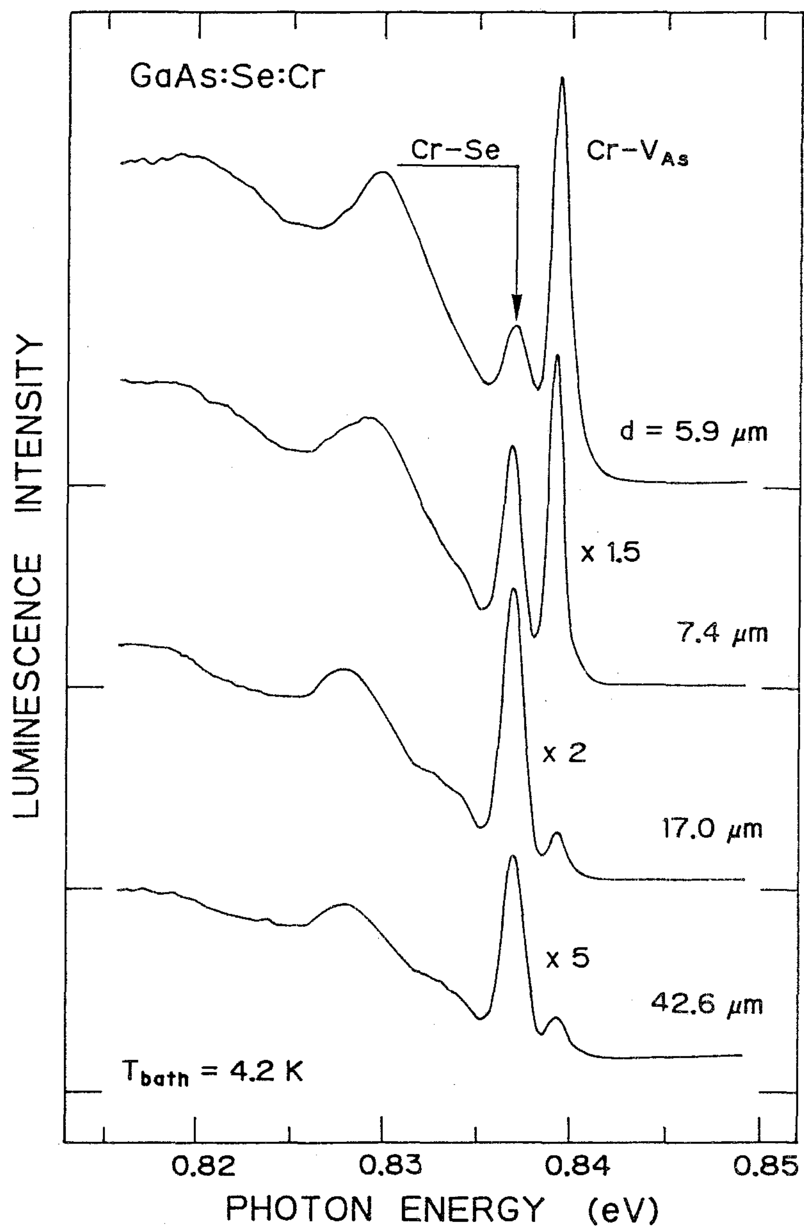

Fig. 3-12 Spectral change of the Cr-related PL spectrum for Cr-diffused GaAs doped with Se with the depth from the sample surface.

region far from the surface. These profiles can be well fitted by a complementary error function, assuming a constant supply of the diffusion source at the surface.[37] Based on the fitting of the calculated diffusion profiles to the measured points, it has been found that the diffusion coefficient is 6×10^{-11} cm^2/s for the Cr, Se-related PL center. Here, it should be noticed that this diffusion coefficient is well comparable to the value for Cr impurity reported by Tuck et al., 9×10^{-11} cm^2/s at 1100 °C[38]. Considering that the diffusion coefficient for Se impurity in GaAs is small, 2×10^{-12} cm^2/s at 1100 °C[39], i.e., that the redistribution of Se impurities is negligible during Cr-diffusion, this result suggests that the PL center is a complex involving a Cr impurity and a Se impurity. So it is called Cr-Se PL line in this section.

3-3-2. Trigonal field by group-VI donor species

The trigonal field at the Cr-Se complex has been considered by analyzing the peak position of the Cr-Se PL line together with those of the Cr-Te and Cr-V_{As} PL lines. The peak position for the zero-phonon line E_{ZPL} is concerned with the fact that the crystal-field splitting Δ increases by an amount of the trigonal field contribution ΔC_{3v} and the Jahn-Teller energy in the ground states $E_{JT}(^5T_2)$ decreases with the increase of the trigonal field W. E_{ZPL} can be, in general, expressed as follows[33];

$$E_{ZPL} = \Delta + \Delta C_{3v} + W/3 + E_{JT}(^5T_2) - E_{JT}(^5E) \qquad (3\text{-}1)$$

where $E_{JT}(^5E)$ represents the Jahn-Teller energy in the excited states. Δ, $E_{JT}(^5T_2)$ and $E_{JT}(^5E)$ for the isolated divalent Cr ion are estimated to 5970 cm^{-1}, 700 cm^{-1} and 50 cm^{-1}, respectively, by Deveaud et al.[33] $E_{JT}(^5T_2)$ and ΔC_{3v} for the Cr-Te complex are also estimated to 600 cm^{-1} and 156 cm^{-1}, assuming that the trigonal field is 400 cm^{-1}. Furthermore, $E_{JT}(^5T_2)$ for the Cr-V_{As} complex is estimated to 200 cm^{-1}.

The trigonal field at the Cr-Se complex can be estimated with two assumptions as a first approximation; the first is that ΔC_{3v} increases almost linearly with the trigonal field, i.e., that it can be represented by multiplying those for the Cr-Te complex by a constant A which is defined as a trigonal field parameter in this thesis. The second assumption is that though the change in $E_{JT}(^5E)$ is negligible, $E_{JT}(^5T_2)$ can be represented by the following equation;

$$E_{JT}(^5T_2) = 700 - 1.1 \times A - 98.9 \times A^2 \quad cm^{-1}. \qquad (3\text{-}2)$$

This is obtained by fitting to the above-mentioned values, which is shown by a dotted line in Fig. 3-13, considering that the trigonal field at the Cr-Te complex is stronger than that at the Cr-V_{As} complex[33]. Therefore, eq. (3-1) can be rewritten by the trigonal field parameter, which is shown by a solid line in the figure, as follows;

$$E_{ZPL} = 6619 + 288 \times A - 98.9 \times A^2 \quad cm^{-1}. \qquad (3\text{-}3)$$

Based on the results that the trigonal field increases when going from S to Se and to Te for nickel-donor complexes in GaAs[32], the

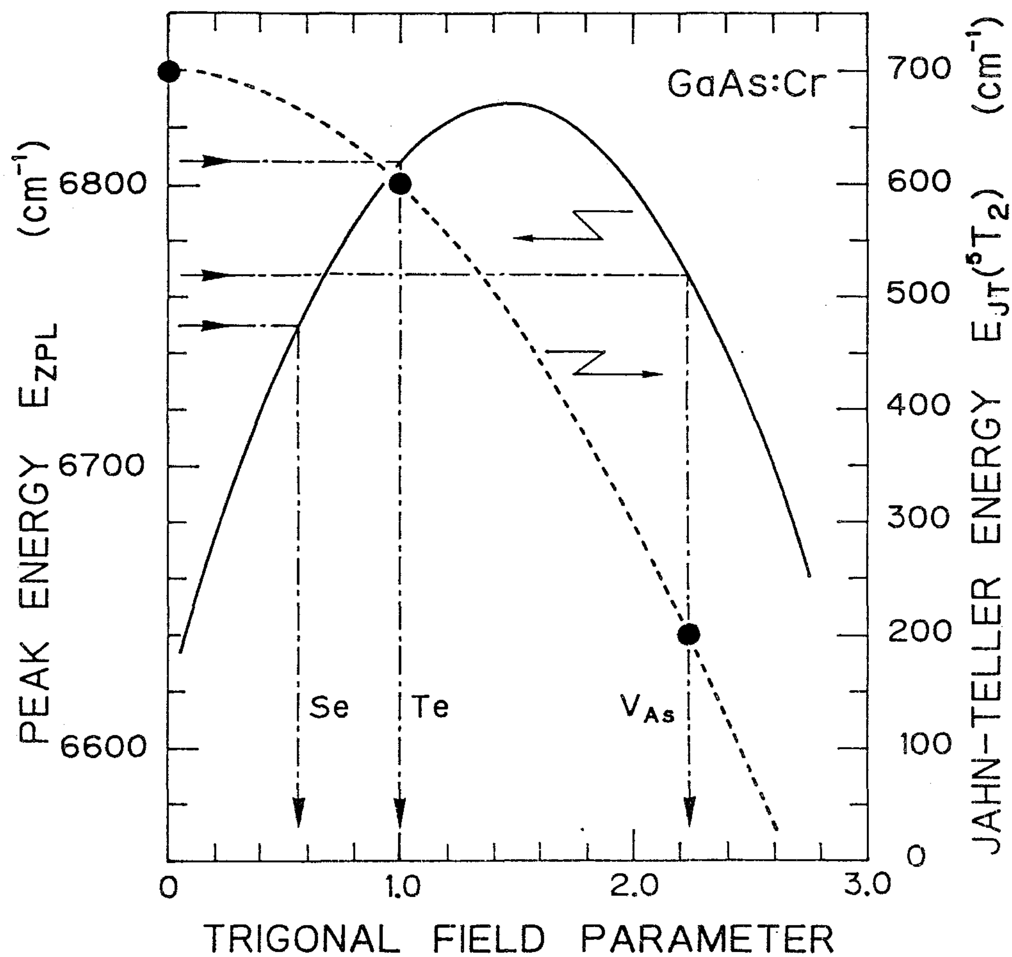

Fig. 3-13 Trigonal field parameter dependence of the peak position of the zero-phonon line (solid line) and the Jahn-Teller energy in the ground states (dotted line) for the Cr-related center. The closed circles represent the previously-reported values of the Jahn-Teller energy in the ground states for various Cr-related PL centers.

trigonal field parameter can be estimated to 0.55 from the peak position of the Cr-Se PL line (0.837 eV = 6750 cm^{-1}). Furthermore, the trigonal field parameter for the Cr-V_{As} complex is 2.25. These results imply that the trigonal field at the Cr-Se complex is about two times weaker than that at the Cr-Te complex and about four times than that at the Cr-V_{As} complex.

3-5. Doping effects of In[34-36]

In-doped SI GaAs grown by the liquid-encapsulated Czochralski (LEC) method is a promising material as the substrate for GaAs large-scale integrated circuits. The addition of a few percent In to GaAs grown from the melt reduces the dislocation density by several orders of magnitude without degrading its high resistivity.[40-42] Recent experimental evidence indicates that an array of field-effect transistors fabricated by direct ion implantation on a LEC-grown In-doped SI GaAs wafer exhibits greater uniformity of threshold voltage than such an array similarly processed on a conventional LEC-grown SI GaAs wafer.[43] In this section, the Cr-related PL lines have been investigated in this technologically important In-doped SI GaAs.

3-5-1. In, Cr-related luminescence

Samples used here are In, Cr-codoped LEC GaAs and In-doped LEC GaAs into which Cr was diffused. For comparison, Al-doped LEC GaAs into which Cr was diffused was also used. The In concentration was in

range from 4.0 x 10^{18} cm^{-3} to 1.2 x 10^{21} cm^{-3}, which were measured by inductively-coupled plasma emission spectrometry (ICP).

Figure 3-14 shows typical Cr-related PL spectrum observed for GaAs:In:Cr, together with that for HB-grown Cr-doped GaAs. The In concentration was 1.3 x 10^{20} cm^{-3}. In conventional Cr-doped GaAs, the well-known Cr-V_{As} PL line is observed at 0.8395 eV accompanied by the TA-phonon replica and 2TA-phonon replica in its lower-energy side, as shown at the lower part of Fig. 3-14. In GaAs:In:Cr we have observed, for the first time, new Cr-related PL lines besides the Cr-V_{As} PL line, as seen at the upper part of Fig. 3-14. It seems that the observed new PL lines at 0.8730 eV and 0.8564 eV are zero-phonon lines, because the half widths are almost the same as that of the Cr-V_{As} PL line, and two other PL lines observed at 0.8645 eV and 0.846 eV are a little broader than these zero-phonon lines; hereafter we refer to these zero-phonon lines as lines A and B, respectively. The latter broad PL lines can be easily assigned, based on the energy separation from lines A and B, as being due to the TA-phonon replica of lines A and B. The peak position of the Cr-V_{As} PL line shifts about 1 meV towards the lower-energy side and the half width is about five times broader than in GaAs:Cr without In.

PL excitation-power dependence of these Cr-related PL lines observed in GaAs:In:Cr has been investigated. In Fig. 3-15, the result is compared with the result for the Cr-V_{As} PL line observed in GaAs:Cr. The intensities of all these Cr-related PL lines increase similarly with PL excitation-power, suggesting that the excitation mechanism is the same for all these PL lines.

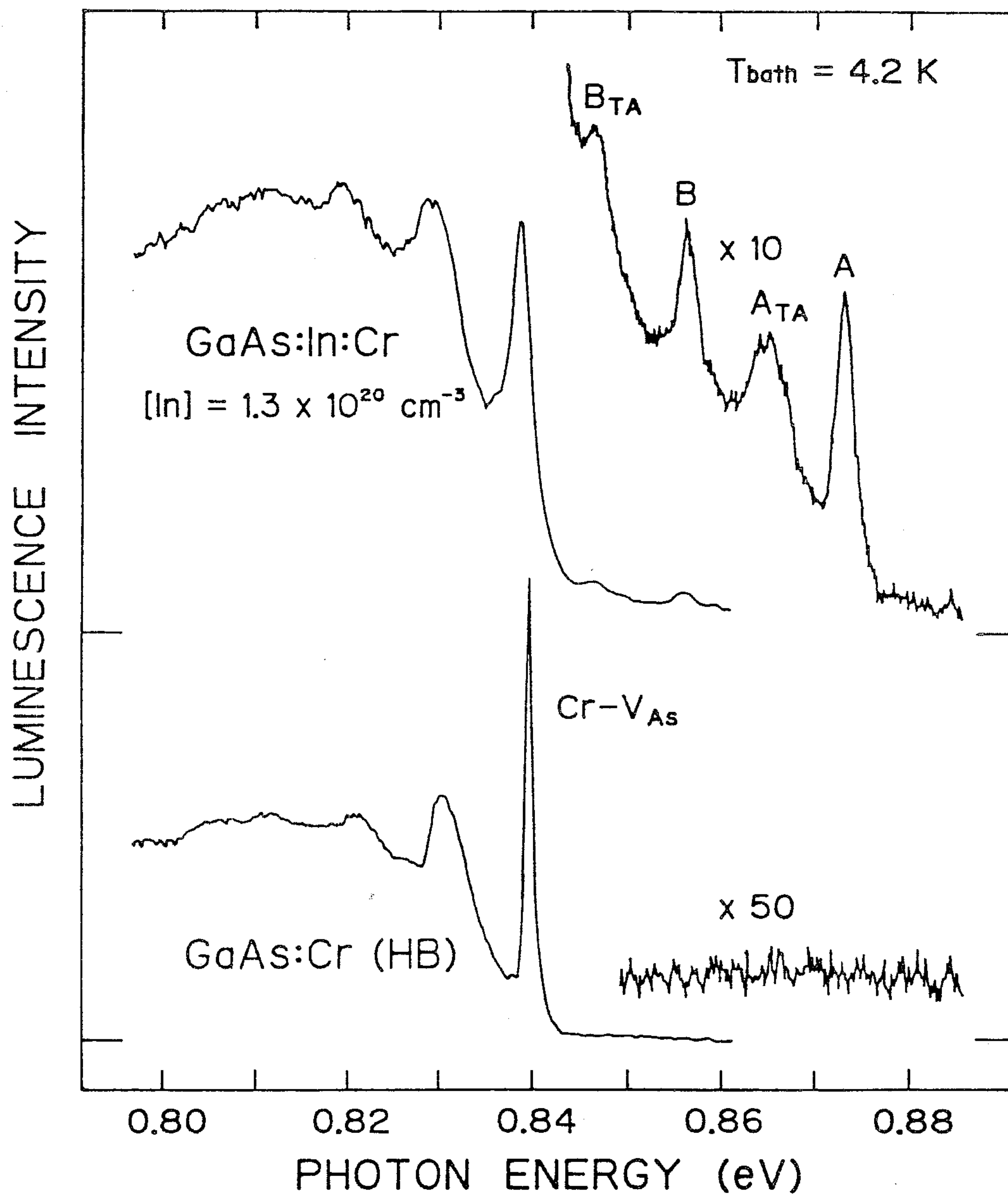

Fig. 3-14 Cr-related PL spectra for LEC-grown GaAs:In:Cr and HB-grown GaAs:Cr.

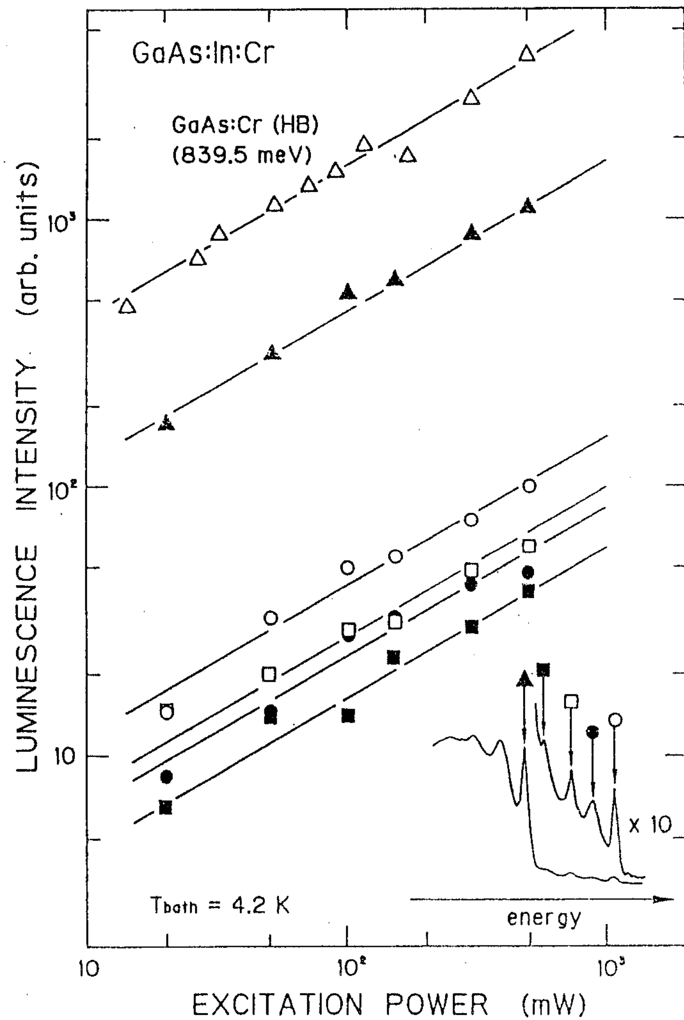

Fig. 3-15 Excitation-power dependence of the Cr-related PL intensities for GaAs:In:Cr, and that for HB GaAs:Cr for comparison.

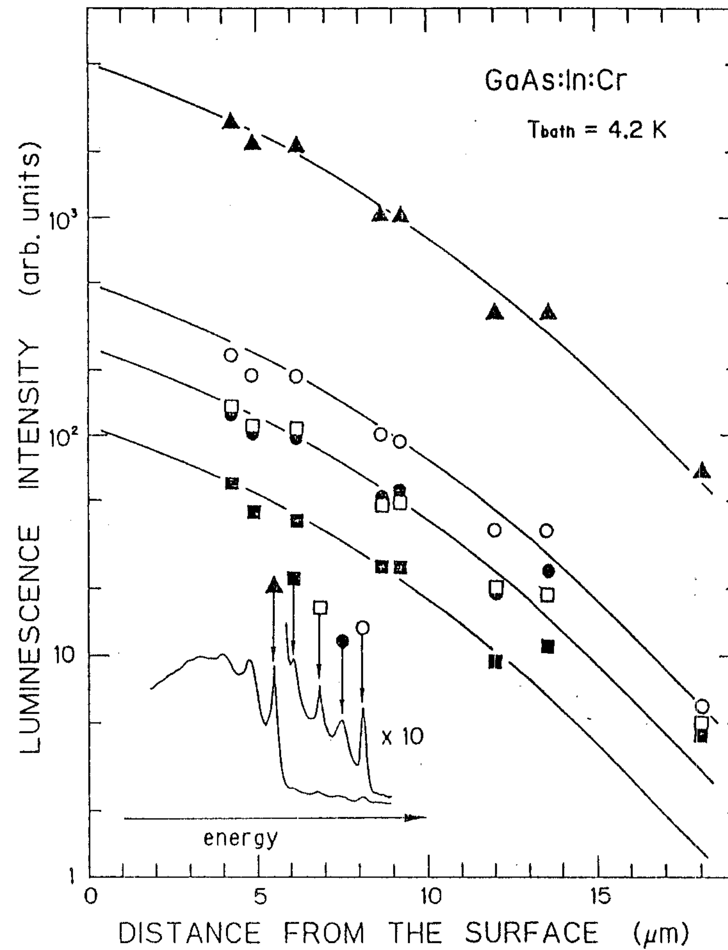

Fig. 3-16 In-depth profiles of the Cr-related PL intensities for Cr-diffused GaAs:In.

Temperature dependence of the Cr-related PL lines observed in GaAs:In:Cr has also been investigated. As a result, the peak position of each Cr-related luminescence line was nearly independent of temperature until about 80 K. Furthermore, the intensities of all these PL lines gradually decrease with the increase of temperature and suddenly drop around 80 K, this result indicating that these are cold lines. Such temperature dependence is similar to that of the Cr-V_{As} line observed in conventional GaAs:Cr and characteristic of the luminescence related to intracenter transitions in a localized center, differing from transitions associated with bands or shallow impurities.

Figure 3-16 shows the in-depth profiles of the intensities of these Cr-related PL lines observed in GaAs:In diffused with Cr. The intensities of all these PL lines decrease similarly with the increase in distance from the surface. These in-depth profiles could be well fitted by a complementary error function. The solid lines in Fig. 3-18 show such best fitted curves, which were calculated with the same diffusion coefficient of 4×10^{-12} cm^2/s. This value of diffusion coefficient is comparable to the previously-reported value for the Cr-V_{As} center in GaAs:Cr without In[37), which will be fully discussed in next section. This result implies that these Cr-related PL lines are originated from the same luminescence center involving an arsenic vacancy.

The Cr-related PL spectra of GaAs doped with Al, which is the same group III element as In have been also measured. In these GaAs crystals, B was unintentionally involved together with Al. In Fig. 3-17, the Cr-related PL spectra in GaAs:Al:Cr are shown together with

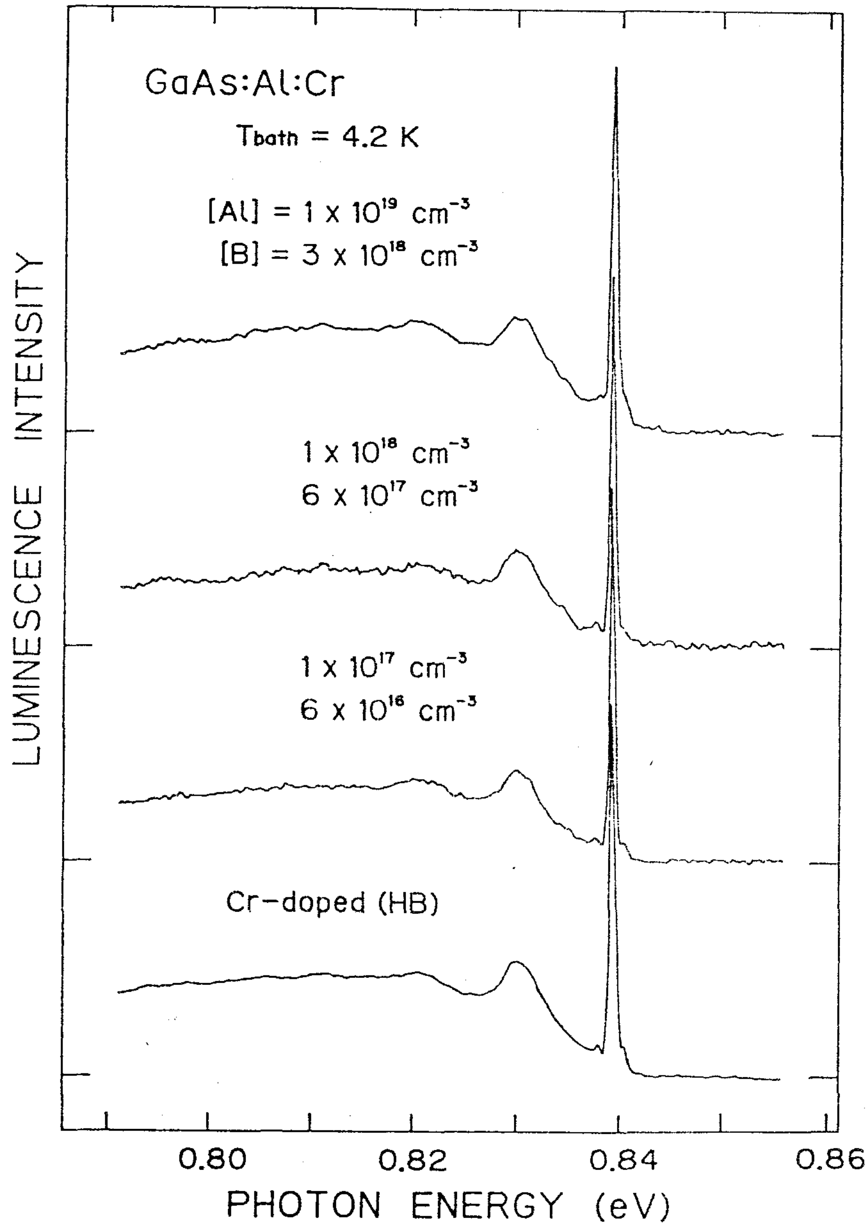

Fig. 3-17 Cr-related PL spectra for LEC-grown GaAs:Al:Cr and HB-grown GaAs:Cr.

the normal Cr-related PL spectrum. As shown, the Cr-related PL spectra were independent of the concentration of Al in GaAs and also almost the same as in GaAs:Cr without Al. The new Cr-related PL lines seen in GaAs:In:Cr could be never observed. This result is probably due to the fact that the covalent radius of Al is almost equal to that of Ga,[44] and hence the substitutional Cr ion is hardly influenced by the existence of Al in its second-nearest neighbor.

3-5-2. In, Cr-related luminescence center

The probability for existence of In atoms in the second-nearest neighbor of a Cr atom has been calculated by using a bimodal distribution. The results are shown in Fig. 3-18. As can be seen in

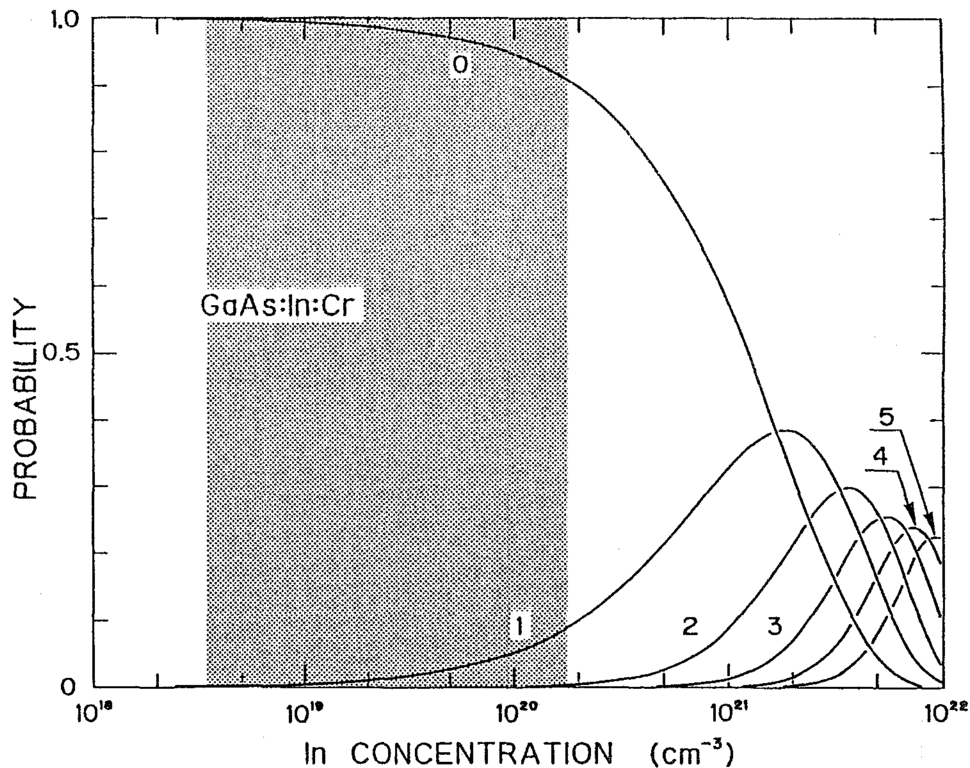

Fig. 3-18 Calculation for the existence probability of In atoms in the second-nearest neighbor of a Cr atom.

the figure, it has been found that the probability for absence of In atoms in the second-nearest neighbor gradually decreases with the increase of the In concentration and becomes about 0.55 at the In concentration of 10^{21} cm^{-3}, though it is almost unity for the In concentrations below 10^{19} cm^{-3}. The existence probability of only one In atom gradually increases with the In concentration, and has a peak at the In concentration of 2 x 10^{21} cm^{-3}. The maximum probability is about 0.4. The existence probability of more In atoms in the second-nearest neighbor of the Cr atom is negligible in range of the In concentration in which lines A and B can be clearly observed, which is shown by the shaded region.

Based on the above results, it can be speculated that the newly-observed lines A and B are originated from a complex involving a

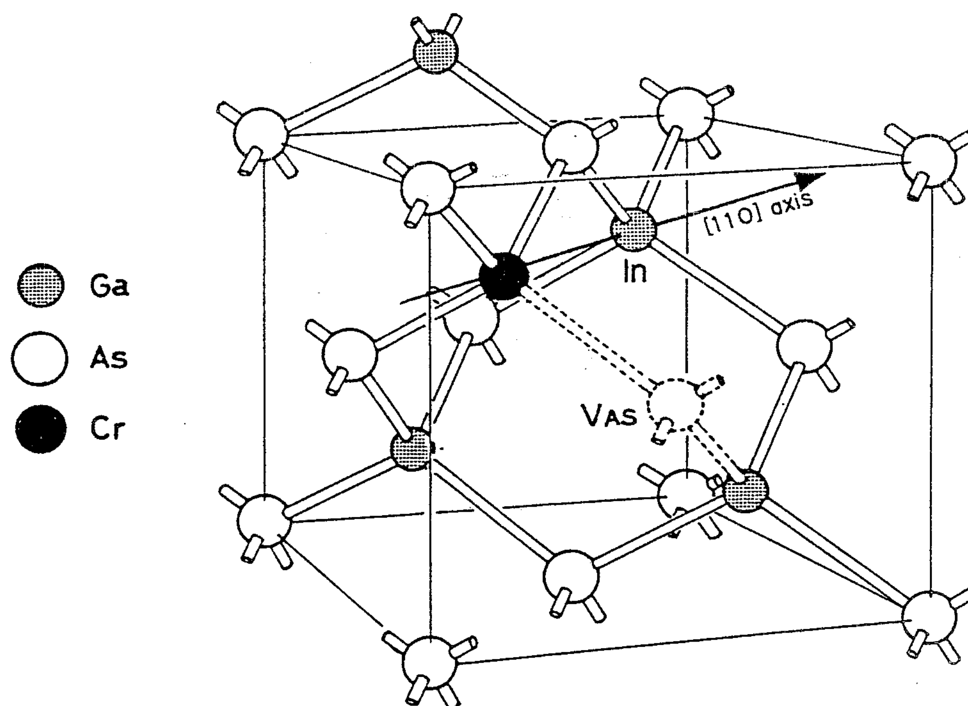

Fig. 3-19 A model for new Cr-V_{As}-In complex center

Cr-V_{As} pair influenced by the existence of an In atom in the second-nearest neighbor of the Cr atom in GaAs, which is schematically shown in Fig. 3-19.

3-5-3. Interpretation of In concentration dependence

The In concentration dependence of these In, Cr-related PL lines has been systematically investigated in order to obtain further information about the luminescence center. Figure 3-20 shows the In concentration dependence of the Cr-related PL spectra in GaAs:In,Cr. As seen in the figure, with the increase of the In concentration, the peak positions of lines A and B similarly shift together with the Cr-V_{As} PL line towards the lower-energy side and their half widths become large. In GaAs:In,Cr with the In concentration over 10^{21} cm^{-3}, all the Cr-related PL lines completely disappear. Here, it should be noticed that the relative peak positions of lines A and B with respect to that of the Cr-V_{As} PL line are invariable, independent of the In concentration. Furthermore, the ratio of the intensity of line A I_A to that of the Cr-V_{As} PL line I_0 increases with the In concentration, which is shown in Fig. 3-21. Similar result is obtained for line B.

Based on the above-mentioned model for the newly-observed Cr-related luminescence center, the increase of the intensity ratio of line A to the Cr-V_{As} PL line with the In concentration has been considered. Here, the following assumptions have been made; the first is that line A is originated from a complex involving a Cr-V_{As} pair influenced by the existence of an In atom in the second-nearest neighbor of the Cr atom while the Cr-V_{As} PL line from a complex involving only a Cr-V_{As} pair not subjected to perturbation by In

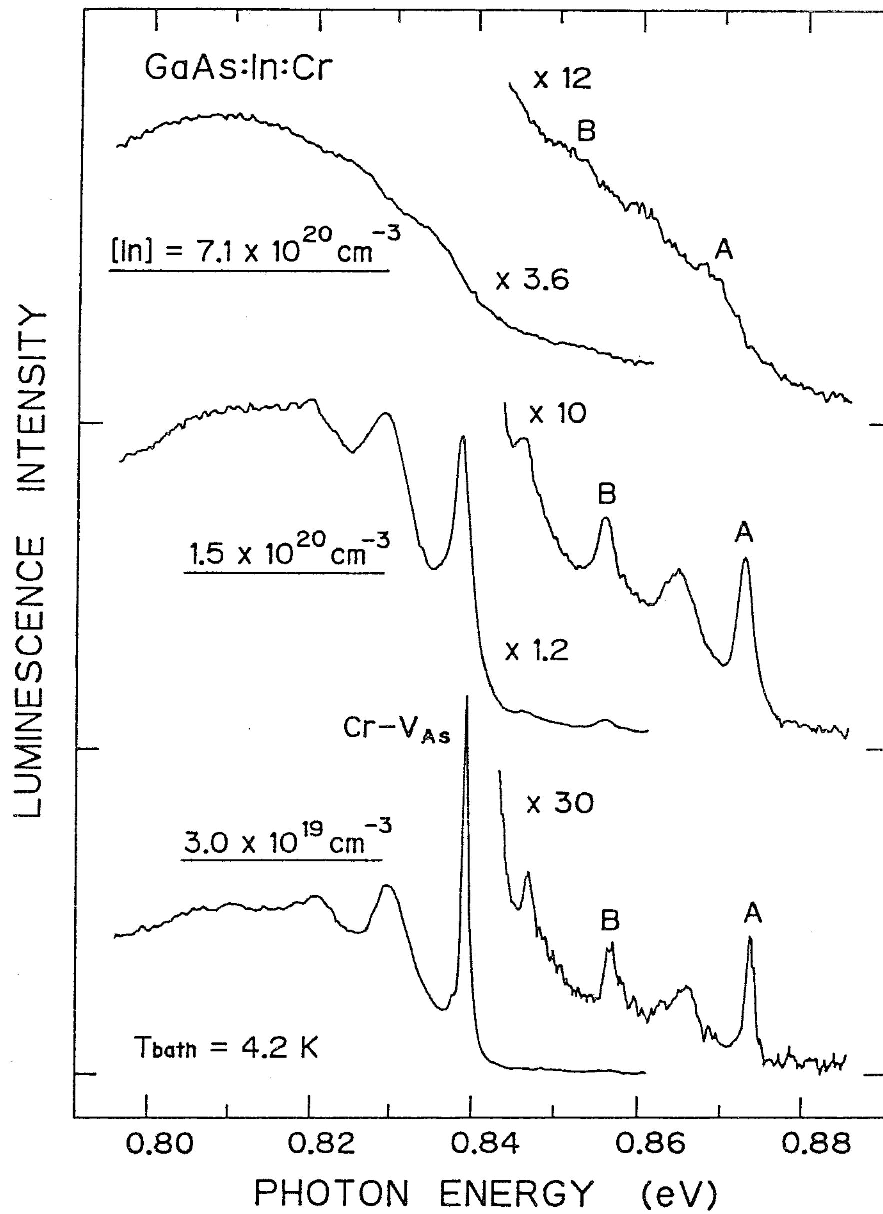

Fig. 3-20 In concentration dependence of the Cr-related PL spectra in GaAs:In:Cr.

atoms. The second assumption is that the PL intensity is proportional to the concentration of the luminescence center. These assumptions lead us to the conclusion that the intensity ratio I_A/I_0 of line A to the Cr-V_{As} PL line varies with the In concentration n as follows;

$$I_A/I_0 = 12 \times (n / (N-n)) \qquad (3-4)$$

where N represents the density of Ga sites in GaAs, which is equal to 2.21×10^{22} cm^{-3}. The calculated curve is indicated by a solid line in Fig. 3-21. As seen in the figure, the calculated curve well fits

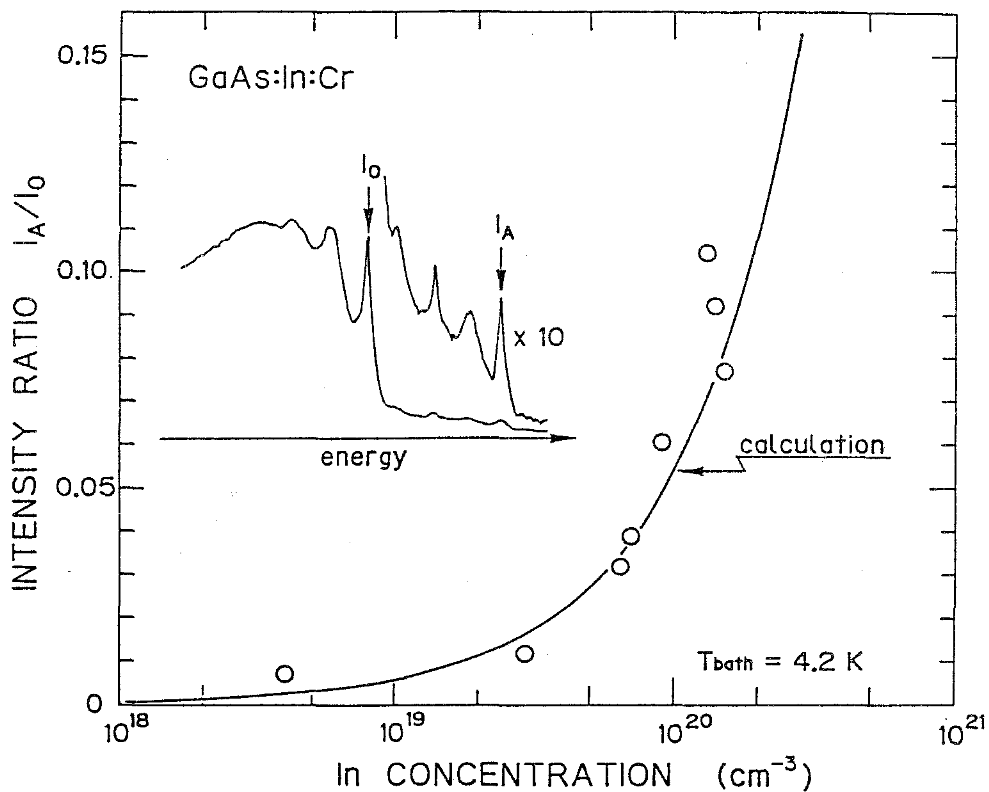

Fig. 3-21 In concentration dependence of the intensity ratio of line A to the Cr-V_{As} PL line in GaAs:In:Cr. Solid line represents a calculated curve.

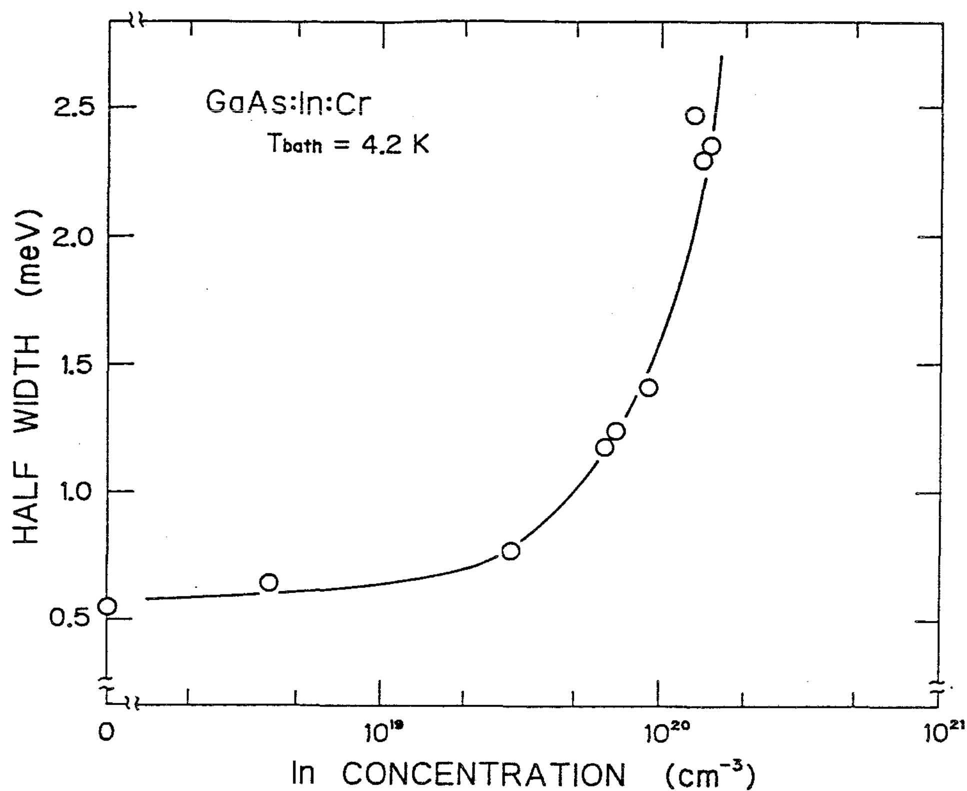

Fig. 3-22 In concentration dependence of the half width of the $Cr-V_{As}$ PL line in GaAs:In:Cr.

to the measured points. Similar result is also obtained for line B, attesting that the luminescence center for lines A and B is the above-proposed complex of $Cr-V_{As}-In$. Although the cause of the increase in half widths for all the Cr-related PL lines with the In concentration, as indicated in Fig. 3-22, is not clear at present, it is probably due to the local fluctuation of the In distribution in GaAs.

Nextly, the reason why the peak positions of all the Cr-related PL lines similarly shift towards the lower-energy side with the increase of the In concentration, which is shown in Fig. 3-23, has been considered. Based on crystal-field theory, in general, the

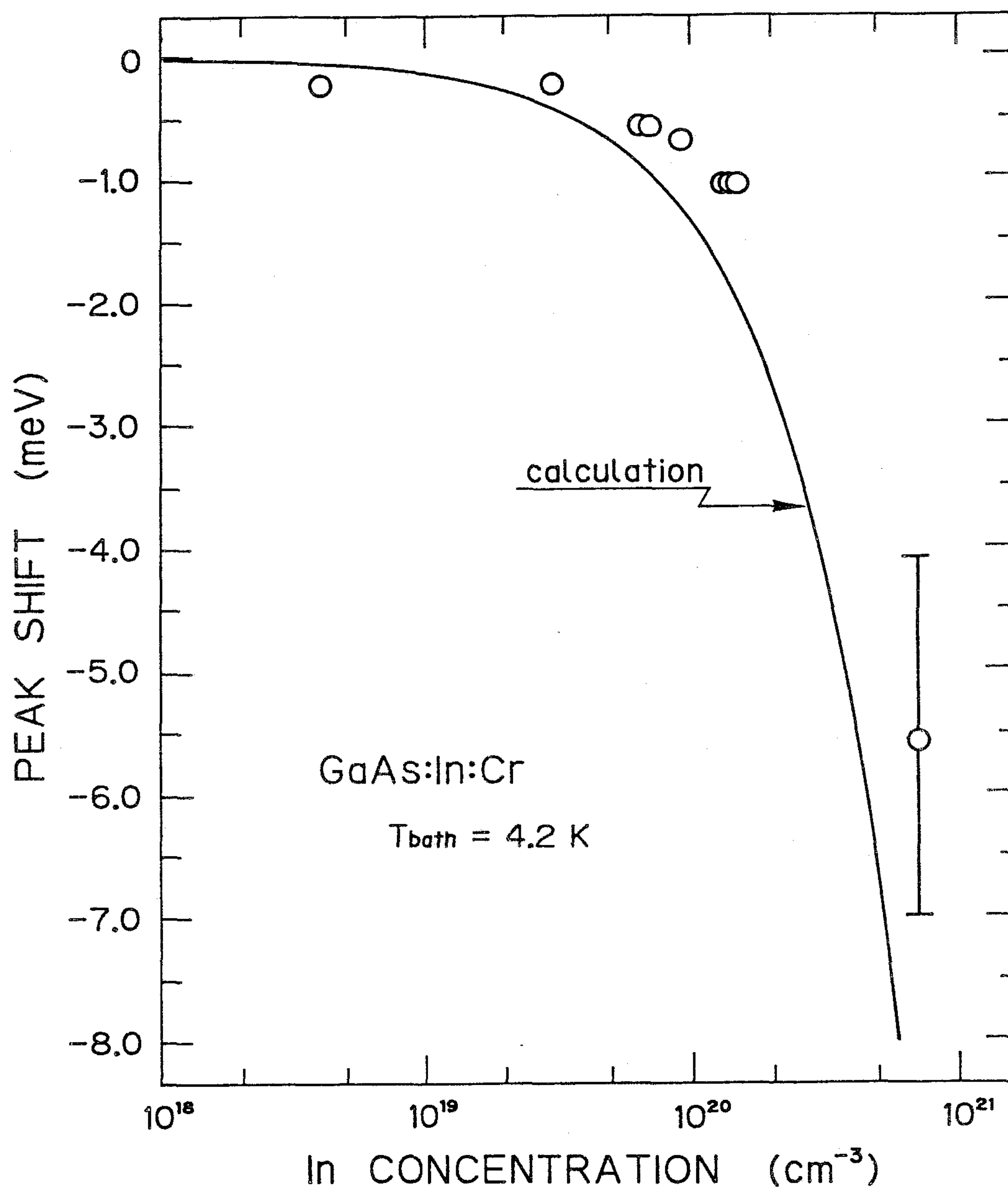

Fig. 3-23 In concentration dependence of the peak position of the Cr-V_{As} PL line in GaAs:In:Cr. Solid line represents a calculated curve.

magnitude of the crystal-field splitting between ground and excited states of the ion is inversely proportional to the fifth power of the lattice constant of a host material. In addition, it has been confirmed by X-ray diffraction measurements that the lattice constant in GaAs:In macroscopically obeys Vegard's law, i.e., it linearly varies between the lattice constant of GaAs and that of InAs, depending on the In concentration.[45] Therefore, the change E in magnitude of the crystal-field splitting between ground and excited states of the Cr ion in GaAs has been estimated by using the following equation;

$$E = E_0 \times ((a_{GaAs} / a_{GaAs:In})^5 - 1) \qquad (3\text{-}5)$$

where a_{GaAs} and $a_{GaAs:In}$ represent the lattice constants of GaAs and GaAs:In, respectively. E_0 represents the peak position of the Cr-V_{As} PL line observed in GaAs:Cr without In. As a result, it has been found that the calculated curve, which is denoted by a solid line in Fig. 3-23, quantitatively corresponds to the measured points for peak shift of all the Cr-related PL lines, which implies that their peak shifts are induced by the macroscopic variation in lattice constant in GaAs:In.

3-5-4. Estimation of local lattice strain in GaAs:In

Since the covalent bond of In is larger by 0.18 A than that of Ga[44], it is speculated that the Cr atom suffers stress induced by the existence of In atoms in the second-nearest neighbor of the Cr atom. Lines A and B are induced as due to a Cr-V_{As} pair influenced by the

existence of an In atom in the second-nearest neighbor of the Cr atom. In this case, the dominant stress which the Cr atom in a complex of Cr-V_{As}-In suffers is probably compressive uniaxial-stress along the [110] direction because the In atom in the complex is located in the [110] direction of the Cr atom. This is confirmed by the fact that the observed spectral pattern is in agreement with previously-reported [110] compressive uniaxial-stress data for the Cr-V_{As} PL line[16), these data showing that two stress-induced PL lines appear in the higher-energy side of the Cr-V_{As} PL line under compressive uniaxial-stress along the [110] direction and these PL lines can be attributed to lines A and B observed in GaAs:In,Cr. Therefore, based on previously-reported [110] uniaxial-stress data for the Cr-V_{As} PL line[16), the magnitude of lattice distortion around the Cr atom has been estimated from the relative peak positions of lines A and B with respect to the Cr-V_{As} PL line. In Fig. 3-24, solid lines represent the [110] compressive uniaxial-stress data reported by Barrou et al.[16) on the assumption that the pressure coefficient of each stress-induced PL line is independent of the magnitude in applied stress, because the previously-reported uniaxial-stress data were measured only under the stress below about 100 MPa. The relative peak positions of lines A and B are plotted by open circles together with those of the relative TA-phonon replicas to fit them to the solid lines. From this figure, it has been found that the Cr atom in the second-nearest neighbor of the In atom suffers stress of about 1.3 GPa. Furthermore, considering that the Young modulus along the [110] direction is about 120 GPa in GaAs[46), this result suggests that local lattice distortion of about 1 % exists in the second-nearest neighbor

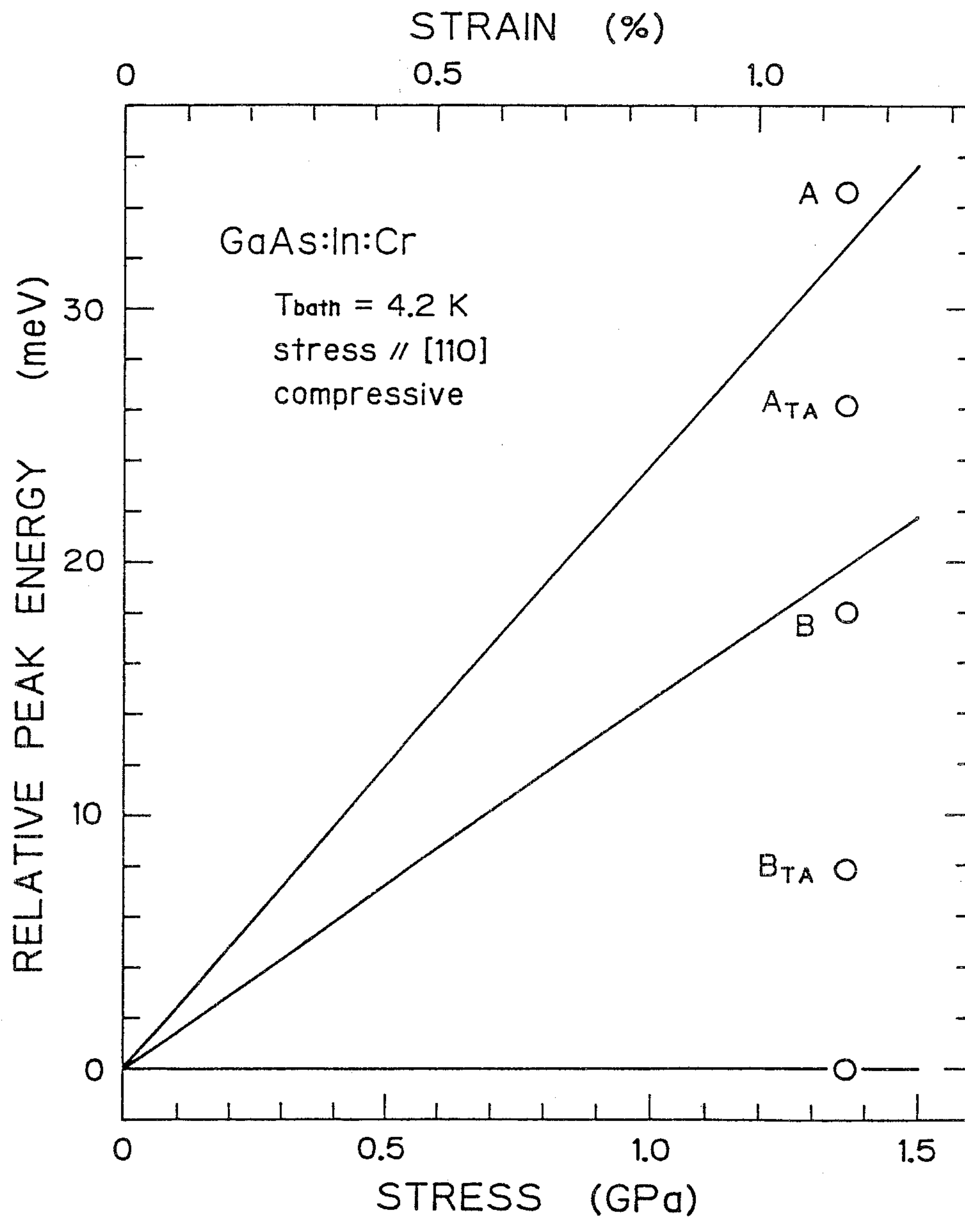

Fig. 3-24 Estimation of lattice strain induced by In-doping in GaAs. Solid lines represent the [110] compressive uniaxial-stress dependence of the Cr-V_{As} PL line.

of the In atom in GaAs. Here, it is interesting that this value is well comparable to the change in Ga-As and In-As bond lengths which were estimated by analysis of the extended X-ray absorption fine structure (EXAFS)[45].

3-6. Characterization of arsenic vacancy by Cr-related luminescence[37]

When GaAs crystals are annealed at high temperatures, a large concentration of lattice vacancies are created near the surface due to the evaporation of lattice atoms. As a result, the surface composition becomes nonstoichiometric, which plays an important role in the processing of GaAs materials and devices. Up to the present time only limited data relating to the nature, formation and diffusion of such defects have been available mainly through electrical measurements such as Hall-effect[47], since they form electrically-active centers. In this work, an optical characterization technique for arsenic vacancies has been developed by using the fact that the Cr deep acceptor forms various Cr-related PL centers in GaAs.

3-6-1. In-depth profiles of Cr-related luminescence intensities

The samples used here were prepared by the diffusion of Cr into boat-grown GaAs crystals doped with Te or Sn. The electron concentration of the GaAs crystals as starting materials was of the order of 10^{18} cm^{-3} at room temperature. The detailed Cr-diffusion conditions into GaAs substrate are shown in Table 3-2. In the case of

Table 3-2 Conditions for preparation of Cr-diffused GaAs samples.

sample	subtarate	diffusion time	remarks
HN-4	Sn-doped	24 h	under As pressure
HN-5	Te-doped	24 h	under As pressure
HN-6	Te-doped	48 h	face-to-face

sample HN-6, the Cr-evaporated surface was covered with another GaAs wafer during the diffusion.

The Cr-related PL spectrum obtained in this work is qualitatively the same in all the Cr-diffused GaAs samples doped with Te. The typical spectrum is displayed in Fig. 3-25, together with that observed in HB-grown Cr-doped GaAs. In commercially available melt-grown Cr-doped GaAs, a series of well-known sharp PL lines is observed only between 0.839 eV and 0.841 eV, as shown in the lower part of Fig. 3-25, the origin of which is attributed to internal transitions in a Cr-V_{As} complex in GaAs.[19-22] Following Lightowlers's nomenclature,[15] they correspond in order from the higher energy to line C, line E, line G which is called Cr-V_{As} PL line in this thesis, and line H, respectively, within experimental error. Moreover, the results of high-resolution luminescence measurements on this zero-phonon multiplet confirm that C line corresponds mainly to lines B_1 and B_2, line E to lines B_6 and B_7, line G to line A_3 and line H to lines A_6 and A_7, respectively, in Barrau's nomenclature.[16] In GaAs:Te diffused with Cr, a pair of sharp PL lines can be observed at 0.844 eV besides the above-mentioned PL lines around 0.839 eV, as shown in the upper part of Fig. 3-25. As mentioned before, they are

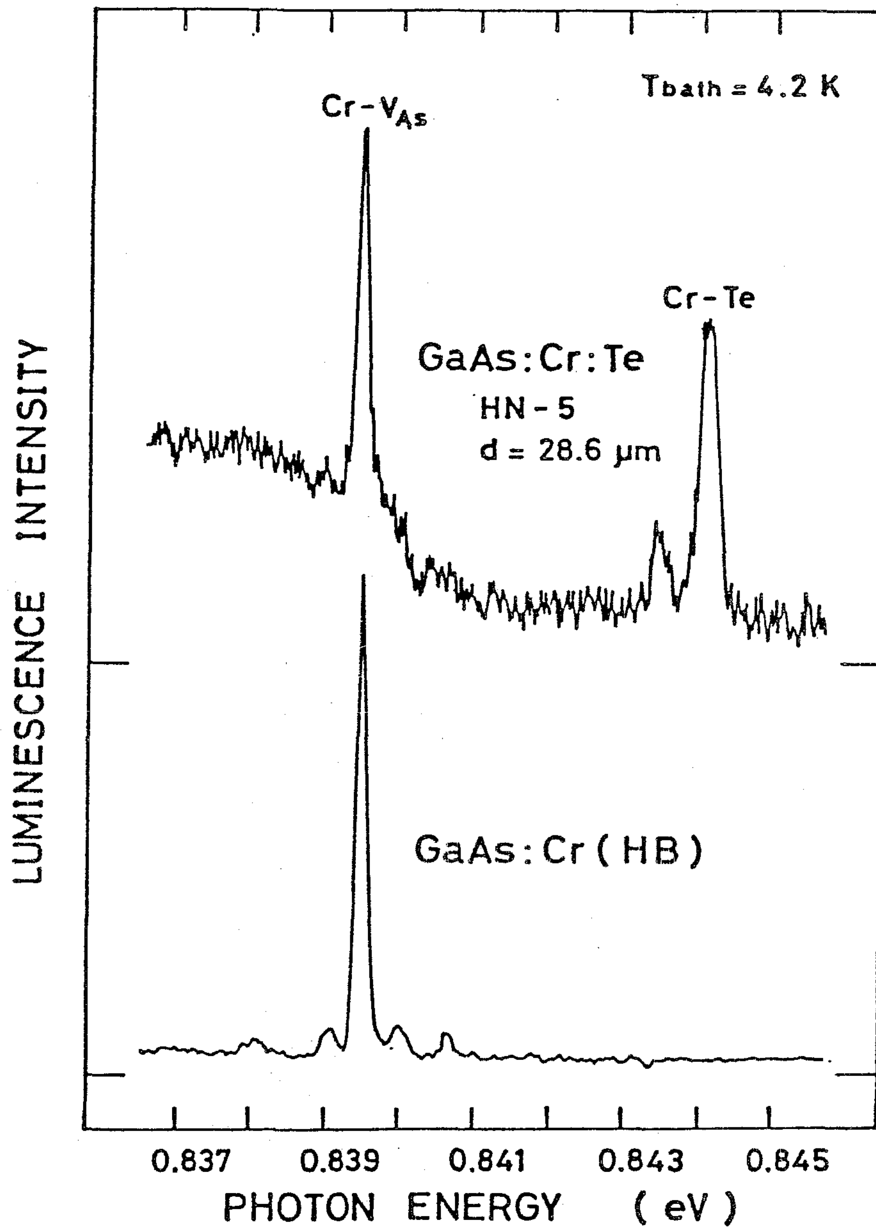

Fig. 3-25 Cr-related PL spectra in Cr-diffused GaAs doped with Te and commercially-available Cr-doped GaAs.

assigned to intra d-shell transitions of a Cr-Te center. In fact, we have never observed these PL lines in melt-grown Cr-doped GaAs and in GaAs:Sn diffused with Cr. The stronger PL line observed in GaAs diffused with Te corresponds to the Cr-Te PL line in section 3-4. Here, it is interesting to note that the PL intensity of the upper spectrum in Fig. 3-25 is weaker than that of the lower spectrum, which might be due to the effective decrease of the Cr-V_{As} center by the formation of another Cr-Te center in GaAs:Te diffused with Cr.

The in-depth profiles of intensities of the Cr-V_{As} and Cr-Te PL lines in Cr-diffused GaAs have been measured. Figure 3-26 shows the results for sample HN-5. As can be seen in the figure, the intensities of both PL lines gradually decrease with the increase of the distance from the surface, except in the region near the surface. However, their behaviors quite differ each other. That is, the intensity of the Cr-V_{As} PL line decreases more rapidly than that of the Cr-Te PL line in a deep region from the surface. These profiles can be well fitted by a complementary error function, assuming a constant supply of diffusion source at the surface:

$$N(d)/N(0) = 1 - \mathrm{erf}(d/2\sqrt{Dt}) \qquad (3\text{-}6)$$

where erf is the error function, d the distance from the surface, D the diffusion coefficient and t diffusion time. The solid lines in Fig. 3-26 show calculated curves fitted to the measured points, using the diffusion coefficient of 6×10^{-12} cm^2/s for the Cr-V_{As} PL center and 4×10^{-11} cm^2/s for the Cr-Te PL center, respectively. This result implies that the diffusion coefficient of the Cr-V_{As} PL center

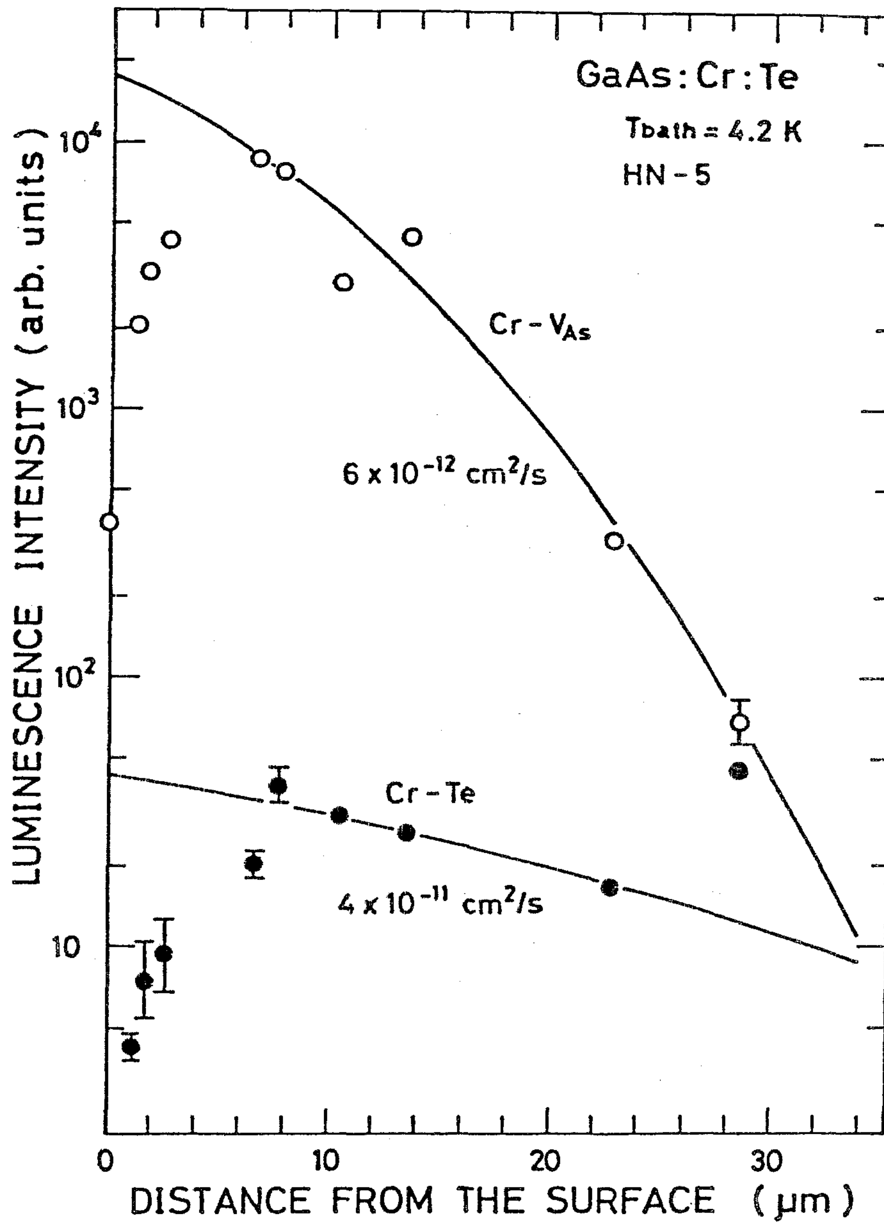

Fig. 3-26 In-depth profiles of the intensities of the Cr-V_{As} (open circles) and Cr-Te (closed circles) PL lines in sample HN-5.

is smaller than that for the Cr-Te PL center by about one order in magnitude.

Here it should be noted that the in-depth profile of the PL intensity cannot be directly expressed by eq. (3-6), since eq. (3-6) represents the in-depth profile of the diffused-center concentration. In general, the following three factors must be considered in order to accurately determine the in-depth profile of the luminescence-center through PL measurements: (1) absorption depth for excitation light, (2) diffusion depth of photoexcited carriers and (3) profile of non-radiative centers. However, the effects of factors (1) and (2) on the PL intensity can be neglected for the distance scale of Fig. 3-26, because the absorption depth is about 0.1 μm at 4.2 K for excitation light of 514.5 nm in GaAs crystals[48] and the diffusion length of photoexcited carriers is estimated to be about 0.5 μm by the Einstein relation, considering that the recombination time of the photoexcited carriers is shorter than 1 ns.[49] On the other hand, the effect of factor (3) can be also approximately neglected, since we consider only the deep region from the surface and eliminate data points measured in the region less than about five microns from the surface, which are remarkably influenced by non-radiative centers introduced during high-temperature heat-treatment. Therefore, it is thought that the in-depth profile of the PL intensity is approximately expressed by eq. (3-6) in the case of this work.

With particular emphasis on the Cr-V_{As} PL line, the effect of the donor type involved in GaAs substrate on the diffusion behavior of this line has been investigated. The results obtained with samples HN-4 and HN-5 are shown in Fig. 3-27, where the vertical scale is

normalized to coincide the data for these samples. It can be seen that the in-depth profile for the Cr-V_{As} PL line agrees between each other and follows relatively well a profile curve (solid line) calculated by eq. (3-6) using the diffusion coefficient of 6×10^{-12} cm^2/s. This result implies that the diffusion profile for the Cr-V_{As} PL line is independent of the donor type involved in the starting GaAs material.

The influence of the arsenic vapour pressure during high-temperature Cr-diffusion on the in-depth profiles of the Cr-V_{As} and Cr-Te PL intensities has been also investigated. Figure 3-28 shows the in-depth profiles for sample HN-6. As similarly as the case of sample HN-5 in Fig. 3-26, the intensities of both PL lines gradually decrease with the increase of the distance from the surface in the region far from the surface, and these profiles can be fitted to eq. (3-6) to estimate the diffusion coefficients for both the Cr-V_{As} and Cr-Te PL centers. However, the estimated diffusion coefficients in this sample HN-6 are 3×10^{-12} cm^2/s and 2×10^{-11} cm^2/s for the Cr-V_{As} and Cr-Te centers, respectively. Here, the difference in diffusion coefficients between sample HN-5 and HN-6 should be mentioned. The diffusion coefficients for the Cr-V_{As} and Cr-Te PL centers obtained with sample HN-6 are smaller than those in sample HN-5. This might reflect the difference of the arsenic vapour pressure during high-temperature Cr-diffusion into GaAs, considering that the As_2 vapour pressure in preparation of sample HN-6 was higher, since its surface was covered with another GaAs wafer. It is interesting to note here that the diffusion coefficient of an impurity becomes small with the increase of the vapour pressure of volatile

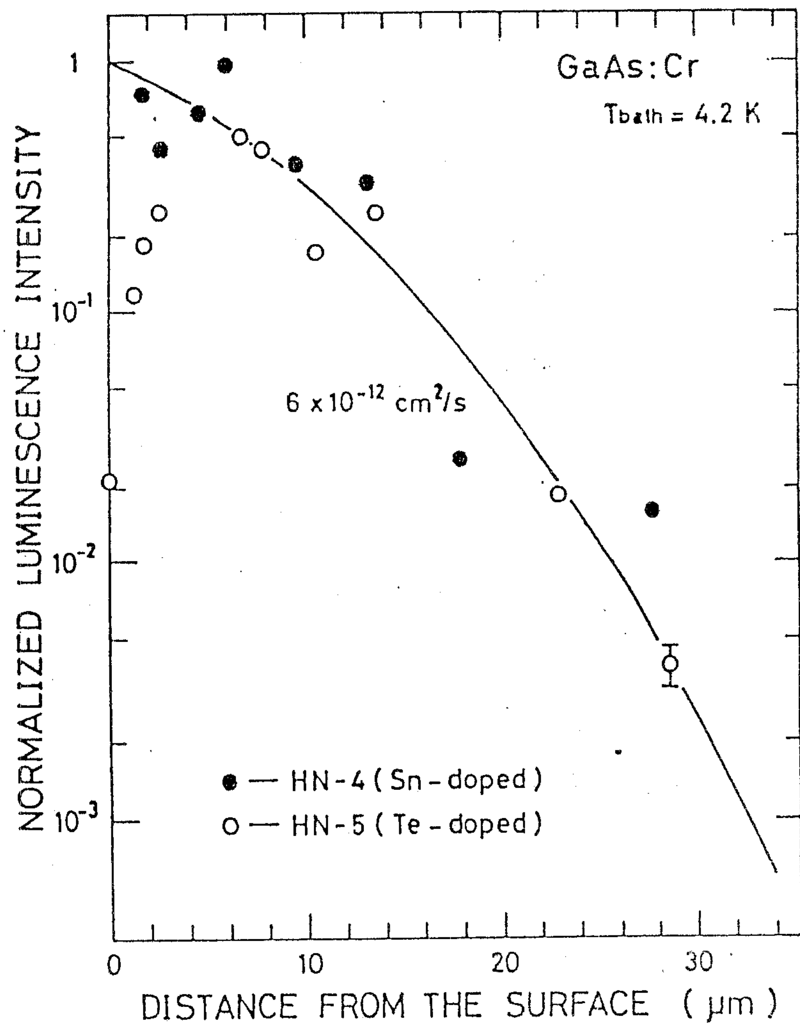

Fig. 3-27 In-depth profiles of the intensities of the Cr-V_{As} PL line in samples with different donor impurities.

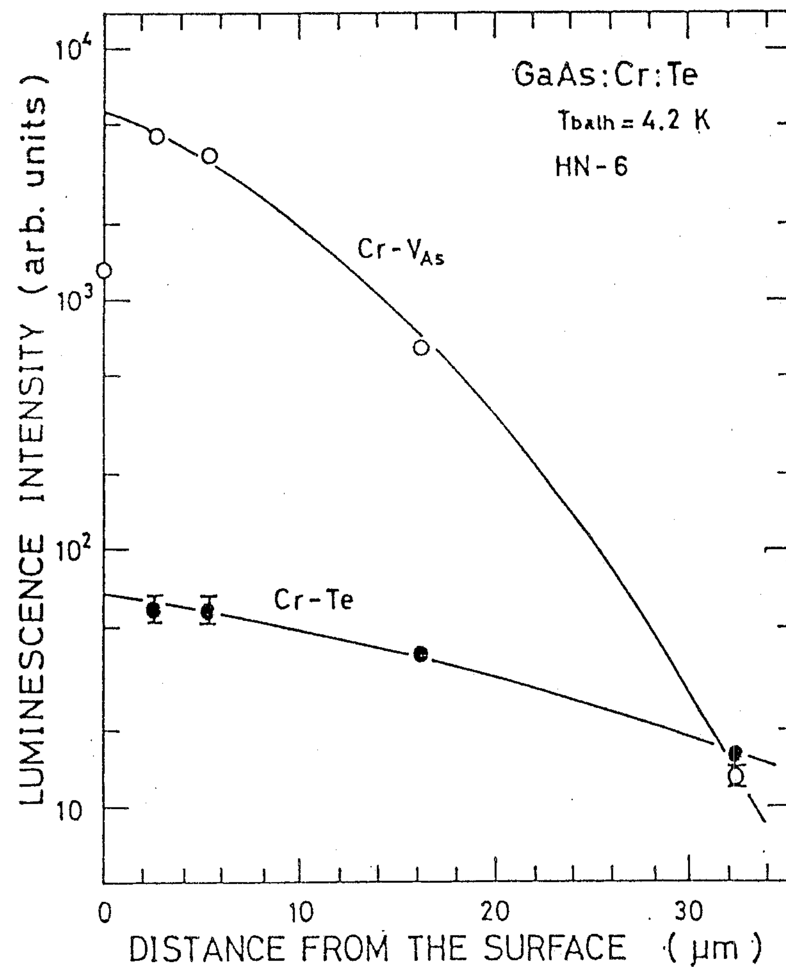

Fig. 3-28 In-depth profiles of the intensities of the Cr-V_{As} (open circles) and Cr-Te (closed circles) PL lines in sample HN-6.

atoms, as reported in the cases of Zn-diffusion into GaAs[50] and Cd-diffusion into InP[51].

3-6-2. Estimation of diffusion coefficient for arsenic vacancy

Based on these in-depth profile data mentioned above, the diffusion coefficient of the arsenic vacancy V_{As} in GaAs has been estimated. Here the following assumptions have been made. The first is that the diffusion coefficient of the Cr-Te center, D_{Cr-Te}, is equal to that of Cr impurity itself, D_{Cr}:

$$D_{Cr-Te} = D_{Cr}. \tag{3-7}$$

This implies that the redistribution of Te impurities is negligible during Cr-diffusion. The validity of this assumption is supported by the fact that the diffusion coefficient of Te in GaAs is small, 2×10^{-12} cm^2/s at 1100 °C[39] and that the diffusion coefficient of Cr determined using eq. (3-7) in this thesis work is in comparable to the value previously reported by Tuck et al.[38], 9×10^{-11} cm^2/s, considering the difference in the arsenic vapour pressure during Cr-diffusion. The second assumption is that the intensity of the Cr-V_{As} PL line at d, $I_{Cr-V}(d)$, is proportional to the product of the concentration of Cr, $N_{Cr}(d)$, and that of arsenic vacancy, $N_V(d)$:

$$I_{Cr-V}(d) \propto N_{Cr}(d) \cdot N_V(d). \tag{3-8}$$

Assuming that the in-depth profiles of Cr and V_{As} are presented by eq. (3-6) as mentioned above, eq. (3-8) is written as follows:

$$I_{Cr-V}(d) \propto N_{Cr}(0) \cdot N_V(0) \ (1 - \mathrm{erf}(d/2\sqrt{D_{Cr}t}\ ) \ (1 - \mathrm{erf}(d/2\sqrt{D_V t}\ ) \qquad (3\text{-}9)$$

where D_V is the diffusion coefficient of V_{As} in GaAs. Therefore, the diffusion coefficient of V_{As} can be estimated by fitting the above-mentioned in-depth profile of the Cr-V_{As} PL line with eq. (3-9).

Figure 3-29 shows the normalized in-depth profiles for the Cr-V_{As} and Cr-Te PL lines in sample HN-5, where all the measured points are normalized to coincide the extrapolated intensities at the surface. Two solid lines are the same as those in Fig. 3-26. The broken line indicates a profile curve calculated by eq. (3-9) to fit the in-depth profile of the normalized intensity of the Cr-V_{As} PL line. Then we have obtained the diffusion coefficient of V_{As} to be 8 x 10^{-12} cm^2/s. The dot-dashed line indicates the in-depth profile of V_{As} calculated by eq. (3-6) using this diffusion coefficient. The result for sample HN-6 can be also analyzed in the same way, which has enabled us to estimate 5 x 10^{-12} cm^2/s for the diffusion coefficient of V_{As} in this sample. The diffusion coefficient of V_{As} obtained with sample HN-5 is larger than that of sample HN-6, both of the values being comparable to the value, 1.6 x 10^{-11} cm^2/s, previously reported by Chiang and Pearson.[47)] As mentioned before, this difference in the diffusion coefficient of V_{As} probably reflects difference in the arsenic vapour pressure during Cr-diffusion.

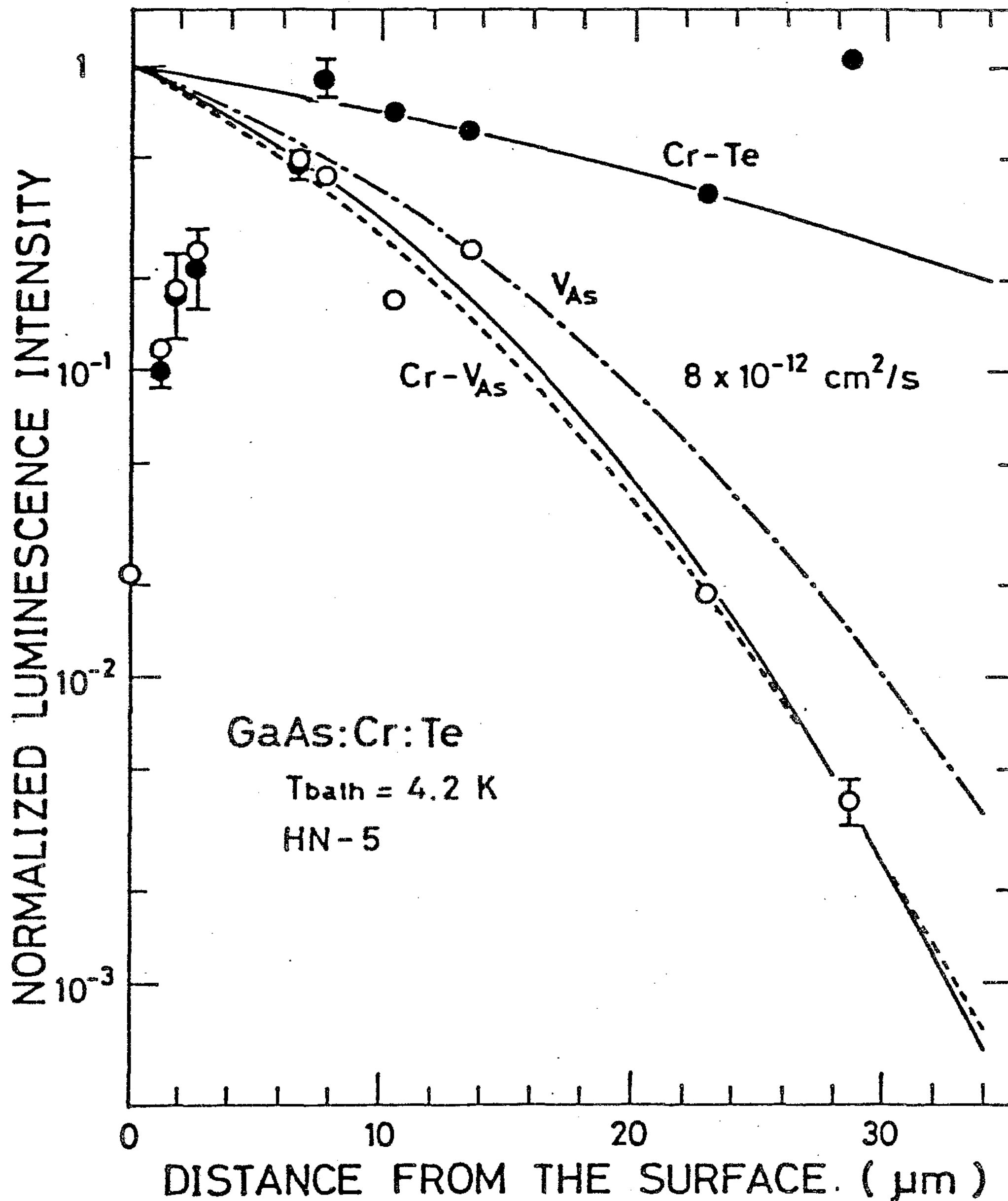

Fig. 3-29 Diffusion profile of arsenic vacancy estimated from analysis of in-depth profiles of Cr-V_{As} (open circles) and Cr-Te (closed circles) for sample HN-5.

3-7. Summary

Systematic studies on high-temperature thermal annealing of GaAs:Cr under various excess arsenic pressure have been performed. A series of behaviors of the 0.8395 eV Cr-related PL line have been analyzed based on mass-action equations for reactions involving several defects in GaAs, the result implying that an arsenic vacancy contributes to the Cr-related zero-phonon line at 0.8395 eV in GaAs:Cr and that the luminescence center is a complex involving a Cr at a Ga site and an arsenic vacancy in its nearest neighbor. Furthermore, by utilizing this luminescence center model , it has been shown that its annealing temperature and time dependences are well interpreted.

Effects of various donor impurities on the Cr-related PL spectra in GaAs have been investigated. For the first time, a series of new zero-phonon lines associated with the Cr-Se complex have been observed in Cr, Se-codoped GaAs. From the analysis of their peak positions together with those of previously-reported Cr-Te and Cr-V_{As} PL lines, it has been found that the trigonal field at the Cr-Se complex is about two times weaker than that at the Cr-Te complex and about four times than that at the Cr-V_{As} complex.

Effects of In-doping have been investigated by monitoring the Cr-related PL lines in In, Cr-codoped GaAs. New Cr-related zero-phonon lines have been, for the first time, observed in addition to the well-known Cr-V_{As} PL line. A series of results of luminescence measurements has indicated that these newly-observed Cr-related PL lines are originated from a complex involving a Cr-V_{As} pair influenced by the existence of an In atom in the second-nearest neighbor of the

Cr atom. Furthermore, their relative peak positions with respect to the Cr-V_{As} PL line have been analyzed by using uniaxial-stress data, the result suggesting that local lattice strain of about 1 % is induced by In-doping in GaAs.

The in-depth profiles of two kinds of Cr-related luminescence centers, Cr-V_{As} and Cr-Te, in Cr-diffused GaAs have been determined from luminescence measurements. Analysis of these in-depth profiles has enabled us to estimate the diffusion coefficient of the Cr impurity and the arsenic vacancy in GaAs. The values obtained are 2-4 x 10^{-11} cm^2/s for Cr and 5-8 x 10^{-12} cm^2/s for arsenic vacancy, comparable to the previously-reported values.

REFERENCES

1) H. Iwasaki and K. Sugibuchi: Appl. Phys. Lett. 18 (1971) 420.

2) F. H. Eisen and B. M. Welch: Ion-Implantation in Semiconductors (Plenum Press, New York, 1976) p. 97.

3) A. M. Huber, G. Morillt, N. T. Cinh, P. N. Favennec, B. Beveaud and B. Tonlous: Appl. Phys. Lett. 35 (1979) 853.

4) C. A. Evans, Jr. V. R. Deline, T. W. Sigmon and A. Lindow: Appl. Phys. Lett. 35 (1979) 291.

5) H. J. Stocker and M. Schmidt: J. Appl. Phys. 47 (1976) 2450.

6) W. H. Koschel, S. G. Bishop and B. D. McCombe: Proc. 13th Int. Conf. Physics of Semiconductors, Rome, 1976 (Tipografia Marves, Rome, 1976) p. 1065.

7) W. H. Koschel, S. G. Bishop and B. D. McCombe: Solid State Commun. 19 (1976) 521.

8) J. J. Krebs and G. H. Stauss: Phys. Rev. B15 (1977) 17.

9) J. J. Krebs and G. H. Stauss: Phys. Rev. B16 (1977) 971.

10) U. Kaufmann and J. Schneider: Solid State Commun. 20 (1976) 143.

11) G. H. Stauss and J. J. Krebs: Proc. Int. Symp. Gallium Arsenide & Related Compounds, Edinburgh, 1976 (Inst. of Phys., Bristol & London, 1977) p. 84.

12) U. Kaufmann and J. Schneider: Appl. Phys. Lett. 36 (1980) 747.

13) for example, G. M. Martin: Proc. Int. Conf. Semi-Insulating III-V Mater., Nottingham, 1980 (Shiva Publishing Limited, Orpington, 1980) p. 13.

14) E. C. Lightowlers and C. M. Penchina: J. Phys. C11 (1978) L405.

15) E. C. Lightowlers, M. O. Henry and C. M. Penchina: Proc. 14th

Int. Conf. Physics of Semiconductors, Edinburgh, 1978 (Inst. of Phys., Bristol & London, 1979) p. 307.

16) J. Barrou, Do Xuan Thanh, M. Brousseau, J. C. Brabant and F. Voillot: Solid State Commun. 44 (1982) 395.

17) Ch. Uihlein and L. Eaves: Phys. Rev. B26 (1982) 4473.

18) J. Barrou, F. Voillot, M. Brousseau, J. C. Brabant and G. Poilblaud: J. Phys. C: Solid State Phys. 14 (1982) 3447.

19) T. Nishino, Y. Fujiwara and Y. Hamakawa: Proc. Int. Symp. Gallium Arsenide & Related Compounds, New Mexico, 1982 (Inst. of Phys., London, 1983) p. 71.

20) Y. Fujiwara, T. Nishino and Y. Hamakawa: Jpn. J. Appl. Phys. 21 (1982) L727.

21) T. Nishino, Y. Fujiwara, A. Kojima and Y. Hamakawa: Proc. SPIE Symp. Spectroscopic Characterization Techniques for Semiconductor Technology, Massachusetts, 1983 (Soc. Photo-Optical Inst. Eng., Washington, 1984) p. 2.

22) Y. Fujiwara, A. Kojima, T. Nishino and Y. Hamakawa: J. Luminescence 31&32 (1984) 451.

23) M. Ozeki, K. Nakai, K. Dazai and O. Ryuzan: Jpn. J. Appl. Phys. 13 (1974) 1121.

24) D. J. Ashen, P. J. Dean, D. T. J. Hurle, J. B. Mullin, A. M. White and P. D. Greene: J. Phys. Chem. Solids 36 (1975) 1045.

25) M. S. Skolnick, M. R. Brozel and B. Tuck: Solid Satet Commun. 43 (1982) 379.

26) R. E. Honig: RCA Rev. 23 (1962) 567.

27) J. R. Arthur: J. Phys. Chem. Solids 28 (1967) 2257.

28) C. Y. Lou and G. A. Somorjai: J. Chem. Phys. 55 (1971) 4554.

29) T. Udagawa, M. Higashiura and T. Nakanishi: Proc. Int. Conf. Semi-Insulating III-V Mater., Nottingham, 1980 (Shiva Publishing Limited, Orpington, 1980) p. 108.

30) J. Kasahara and N. Watanabe: Proc. Int. Conf. Semi-Insulating III-V Mater., Nottingham, 1980 (Shiva Publishing Limited, Orpington, 1980) p. 108.

31) Y. Fujiwara, Y. Kita, Y. Tonami, T. Nishino and Y. Hamakawa: submitted to J. Phys. Soc. Jpn.

32) H. Ennen, U. Kaufmann and J. Schneider: Appl. Phys. Lett. 38 (1981) 355.

33) B. Deveaud, B. Lambart and G. Picoli: J. Appl. Phys. 55 (1984) 4356.

34) Y. Fujiwara, Y. Kita, Y. Tonami, T. Nishino and Y. Hamakawa: Jpn. J. Appl. Phys. 25 (1986) L232.

35) Y. Fujiwara, Y. Kita, Y. Tonami, T. Nishino and Y. Hamakawa: submitted to Appl. Phys. Lett.

36) Y. Fujiwara, Y. Kita, Y. Tonami, T. Nishino and Y. Hamakawa: to be published in Proc. Int. Conf. Semi-Insulating III-V Mater., Hakone, 1986.

37) Y. Fujiwara, A. Kojima, T. Nishino and Y. Hamakawa: Jpn. J. Appl. Phys. 24 (1985) 1479.

38) B. Tuck and G. A. Adegboyega: J. Phys. D 12 (1979) 1895.

39) H. C. Casey: Atomic Diffusion in Semiconductors (Prenum Press, New York & London, 1973) p. 417.

40) M. G. Mil'vidsky, V. B. Osvensky and S. S. Shifrin: J. Cryst. Growth 52 (1981) 396.

41) G. Jacob, M. Duseaux, J. P. Farges, M. M. B. Van den Boom and P.

J. Roksnoer: J. Cryst. Growth 61 (1983) 471.

42) H. Kimura, C. B. Afabel, H. M. Olsen, A. T. Hunter, K. T. Miller and H. V. Winston: Ext. Abst. 16th Int. Conf. Solid State Devices & Mater., Kobe, 1984 (Japan Business Center for Academic Societies, Tokyo, 1984) p. 59.

43) H. V. Winston, A. T. Hunter, H. M. Olsen, R. P. Bryan and R. E. Lee: Appl. Phys. Lett. 45 (1984) 447.

44) J. C. Phillips: Bonds and Bands in Semiconductors (Academic Press, New York & London, 1973) p. 21.

45) J. C. Mikkelsen, Jr. and J. B. Boyce: Phys. Rev. b28 (1983) 7130.

46) Yu. A. Burenkov, Yu. M. Burdukov, S. Yu. Davydov and S. P. Nikanorov: Sov. Phys. Solid State 15 (1973) 1175.

47) Y. S. Chiang and G. L. Pearson: J. Appl. Phys. 46 (1975) 2986.

48) M. D. Sturge: Phys. Rev. 127 (1962) 768.

49) R. H. Bube: Semiconductors and Semimetals (Academic Press, New York & London, 1967) Vol. 3, p. 475.

50) H. C. Casey: Atomic Diffusion in Semiconductors (Prenum Press, New York & London, 1973) p. 399.

51) K. Otsuka, T. Nishino and Y. Hamakawa: Jpn. J. Appl. Phys. 21 (1982) 1170.

IV. LUMINESCENCE IN GaAs DOPED WITH Ni OR V

4-1. Introduction

The 3d-transition metal impurities form deep acceptor centers in GaAs crystal and sometimes compensate the residual shallow donors, resulting in the increase in resistivity of the material. These deep acceptors can be observed as very sharp characteristic emission lines in low-temperature photoluminescence (PL) spectra in the near-infrared region. The sharpness of the PL lines comes from the fact that they are mainly originated from intracenter transitions between d-electron states in the metals, and the peak positions differ from each other. These results provide a spectroscopic characterization method for the identification of these 3d-transition metal impurities in GaAs. However, the origin of their characteristic PL lines is not completely understood, though the Cr-related PL lines have become well-known by recent extensive studies. This is, in part, due to the fact that these 3d-transition metal impurities form various kinds of complexes including another impurity or defect in GaAs and that the complexes become the luminescence centers.

In this chapter, following the brief description of the luminescence associated with Ni deep acceptors in GaAs, results of the in-depth profile measurements on the Ni-related PL intensities for Ni-diffused GaAs are presented. Secondly, the identification of charge state of a V ion responsible for the 0.7388-eV luminescence center in GaAs:V is given through the time-resolved PL measurements.

4-2. Ni-related luminescence

Since Ni is a persistent inadvertent impurity in as-grown GaP, even in device-grade materials[1], its detailed electronic states in GaP have been intensively studied by optical and ESR measurements[1-9]. Ni plays an essential role in GaAs contact technology, but it is also known that Ni traces disadvantageously affect minority carrier properties in n-type GaAs.[10,11] However, the Ni deep acceptor in GaAs has been hardly investigated except for only a few absorption and luminescence measurements. In this section, deep-level PL spectra of Ni-diffused GaAs have been investigated, with emphasis on the in-depth profiles of their PL intensities.[12]

4-2-1. Donor-species dependence

Figure 4-1 shows typical PL spectra associated with Ni in the 0.5 eV region in GaAs at 4.2 K. All the samples were prepared by Ni-diffusion into the starting GaAs crystals doped with a variety of majority donor impurities and the surface region of some dozens of microns were etched off after the diffusion. In accordance with the chemical species of donor impurity in GaAs substrate, some specific sharp PL lines accompanying with satellites in their lower-energy side are observed. This behavior is quite different from that of the well-known 0.839 eV Cr-related PL lines, which are originated from a complex involving a Cr at a Ga site and an arsenic vacancy in its nearest-neighbor[13]. Similar sharply-structured PL bands were previously observed by Ennen et al.[9] Based on the relation to the donor type involved in GaAs substrate, they were assigned to intra

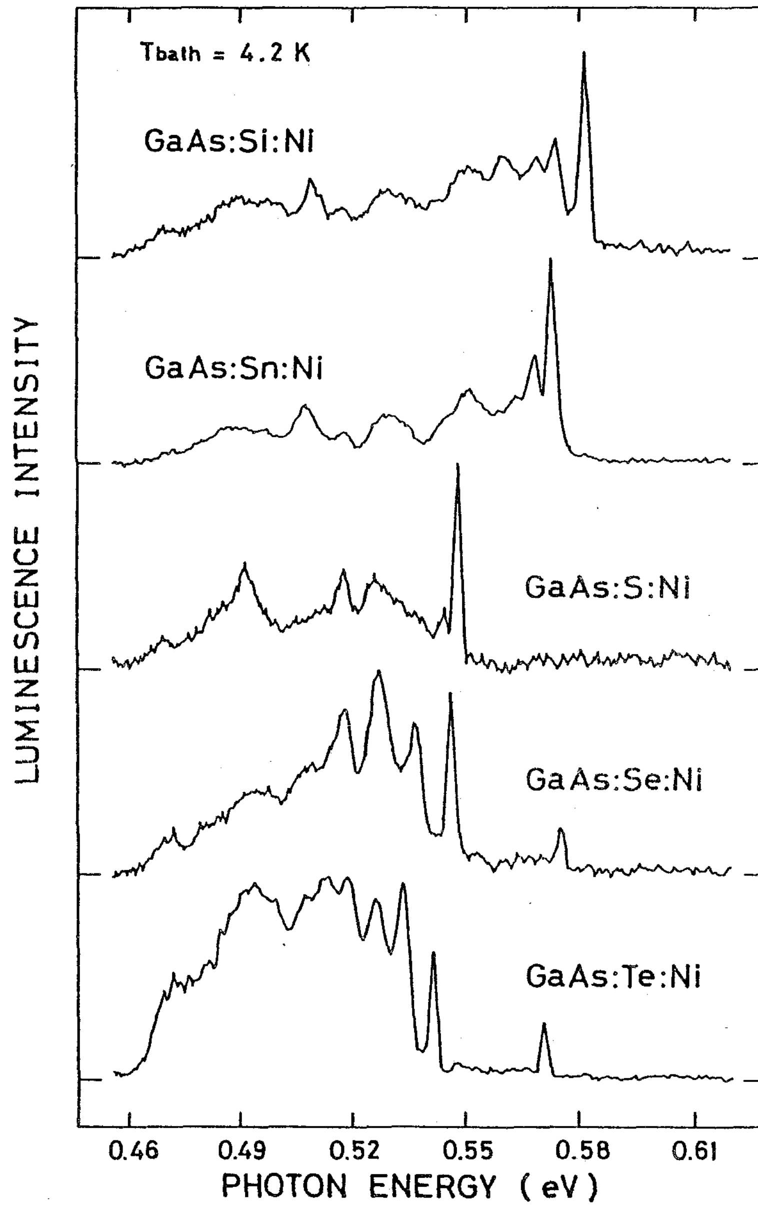

Fig. 4-1 PL spectra associated with the Ni deep acceptor in various kinds of Ni-diffused GaAs.

d-shell transitions of Ni acceptor-shallow donor near-neighbor associates in GaAs. Following their nomenclature, the dominant sharp luminescence lines observed in this work correspond, in order from the upper part of Fig. 4-1, to Ni-Si, Ni-Sn, Ni-S, Ni-Se and Ni-Te pairs, respectively, within the experimental error. Moreover, in samples of GaAs:Se and GaAs:Te, a new PL line has been observed close to the sharp absorption line recently identified as an internal transition in the double acceptor state, $Ni^{+}(3d^{9})$, of an isolated Ni_{Ga} [14]. However, it is not clear whether the same luminescence center is responsible for them or not, since their energy positions are slightly different from each other.

4-2-2. In-depth profiles of donor impurities

The in-depth profiles of the deep-level PL intensities have been measured in Ni-diffused GaAs. In Fig. 4-2, the typical result of the Ni-related PL spectra is shown for a variety of thickness, d, of the surface layer successively etched off. In the region near the surface, the observed PL spectrum is dominated by the same lines as that measured in GaAs:S:Ni, as shown in Fig. 4-1. However, with the increase of the distance from the surface, the intracenter luminescence associated with Ni-S pairs gradually decreases and the luminescence associated with Ni-Te pairs becomes to appear. Ultimately, the former luminescence vanishes completely and the latter becomes dominant in the region far from the surface. Figure 4-3 shows the depth dependence of the intensities of the Ni-related intracenter luminescence associated with Ni-S and Ni-Te pairs in GaAs:Te diffused with Ni. As can be seen in the figure, the PL intensity due to Ni-S

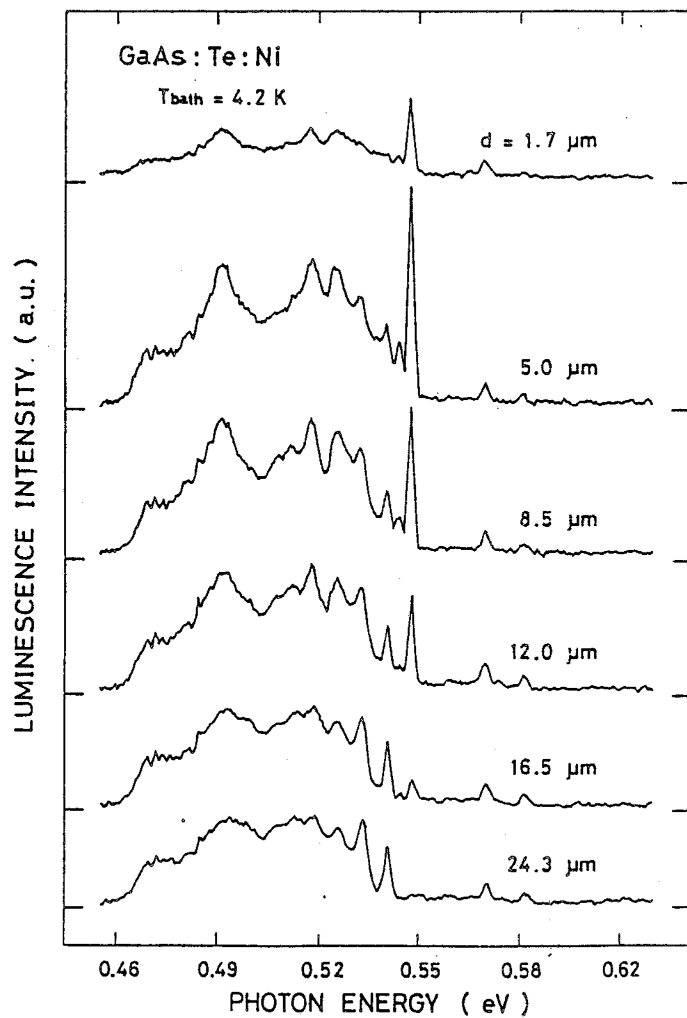

Fig. 4-2 Spectral change of the Ni-related luminescence with the depth from the sample surface.

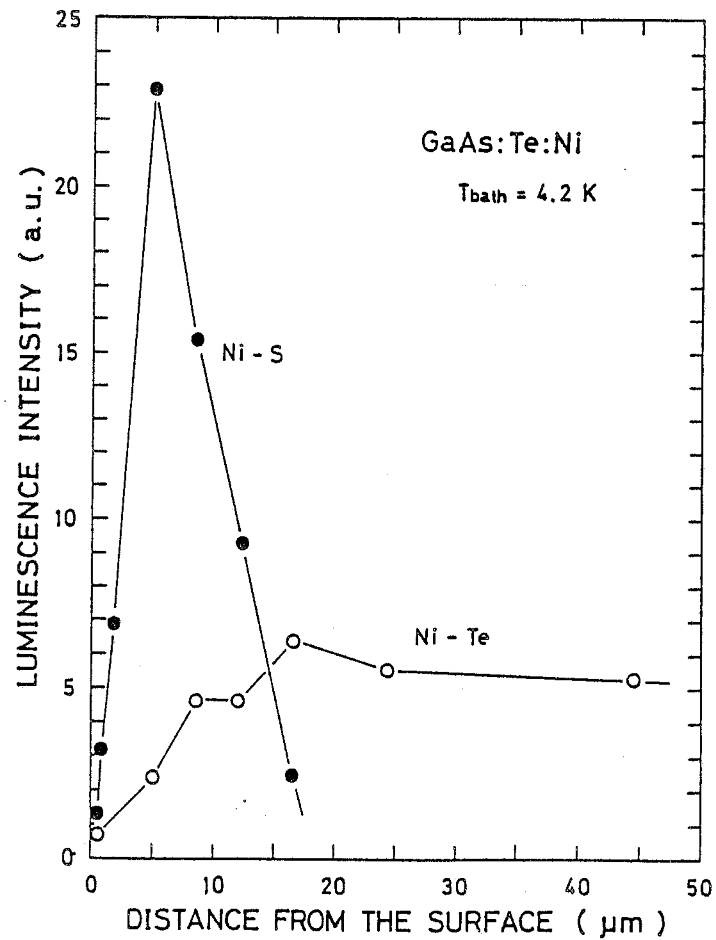

Fig. 4-3 In-depth profiles of the intensities of the Ni-related luminescence lines in GaAs:Te diffused with Ni.

associates rapidly decreases in the deeper region from the surface but the PL intensity due to Ni-Te associates changes only slightly in the surface region, which is probably due to surface effects. Assuming the diffusion coefficient of Ni in GaAs to be 5 x 10^{-8} cm^2/s at 500 °C as reported by Partin et al.[10,11], it can be easily estimated that Ni atoms distribute almost flatly in GaAs over several tens microns from the surface. Therefore, it seems reasonable to consider that the in-depth profiles of Fig. 4-3 reflect the distribution of donor impurities involved in GaAs, in particular, the builtup of S donors in the vicinity of the surface region. Similar tendency has been observed in all the GaAs samples studied here. Figure 4-4 shows the result on GaAs:S diffused with Ni. In this sample, only the intracenter luminescence associated with Ni-S pairs is observed, and the intensity rapidly decreases with the distance from the surface and remains nearly constant in the region far from the surface, as can be seen in the figure. The observation of the Ni-S pair luminescence in the deep region from the surface is probably due to the background S donors involved in the substrate. It is likely that the builtup of S in the vicinity of the surface comes from the out-diffusion of the S residual impurities involved in the substrate during the high-temperature diffusion, since recent data by secondary ion mass spectroscopy (SIMS) indicate that S is the main persistent background impurity in GaAs bulk crystals[15]. However, there remains the possibility that the S builtup comes from the starting Ni metal used for diffusion into GaAs, since the analysis of the Ni metal by spark source mass spectroscopy (SSMS) indicates the existence of S in the

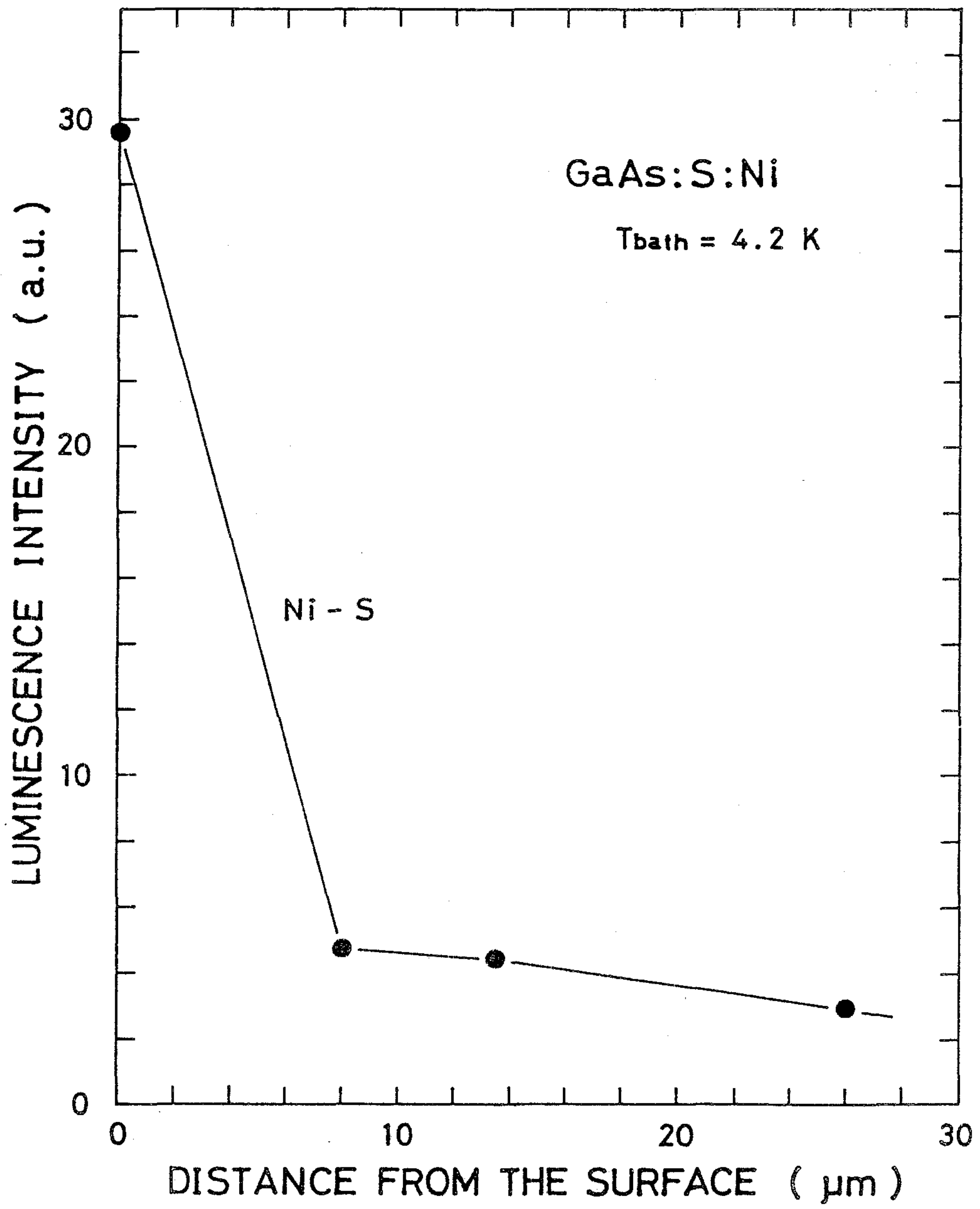

Fig. 4-4 In-depth profile of the intensity of the Ni-related luminescence line in GaAs:S diffused with Ni.

range of several ppms which is of the same order as the background S impurity in GaAs.

4-3. V-related luminescence

3d-transition metal impurities in III-V compound semiconductors form deep levels in the forbidden band. Therefore, for the last decade, their behaviors and states in various semiconductors have been the subject of intensive investigations. Interest in semi-insulating V-doped III-V materials is growing on account of their potential as easily grown and thermally stable[16], high-resistivity materials. However, the role played by V is far from clear and its characterization is not straightforward. In this section, the charge state of the V ion as the luminescence center is identified by analyzing results of time-resolved PL measurements on the 0.7388 eV V-related sharp zero-phonon line in GaAs:V based on a configuration interaction model.

4-3-1. Time-resolved PL measurements

In GaAs doped with V, a characteristic PL spectrum can be observed at 4.2 K, which is dominated by a sharp zero-phonon line at 0.7388 eV. Recent Zeeman spectroscopic data on the 0.7388 eV V-related PL line have shown that it is originated from an isolated V ion in T_d symmetry.[17] However, there has been controversial discussion on the charge state of the V ion as the 0.7388 eV PL center. Vasil'ev et al.[18], Ushakov et al.[19] and Kaufmann et al.[17] have proposed that the PL center is a divalent V ion. As for the

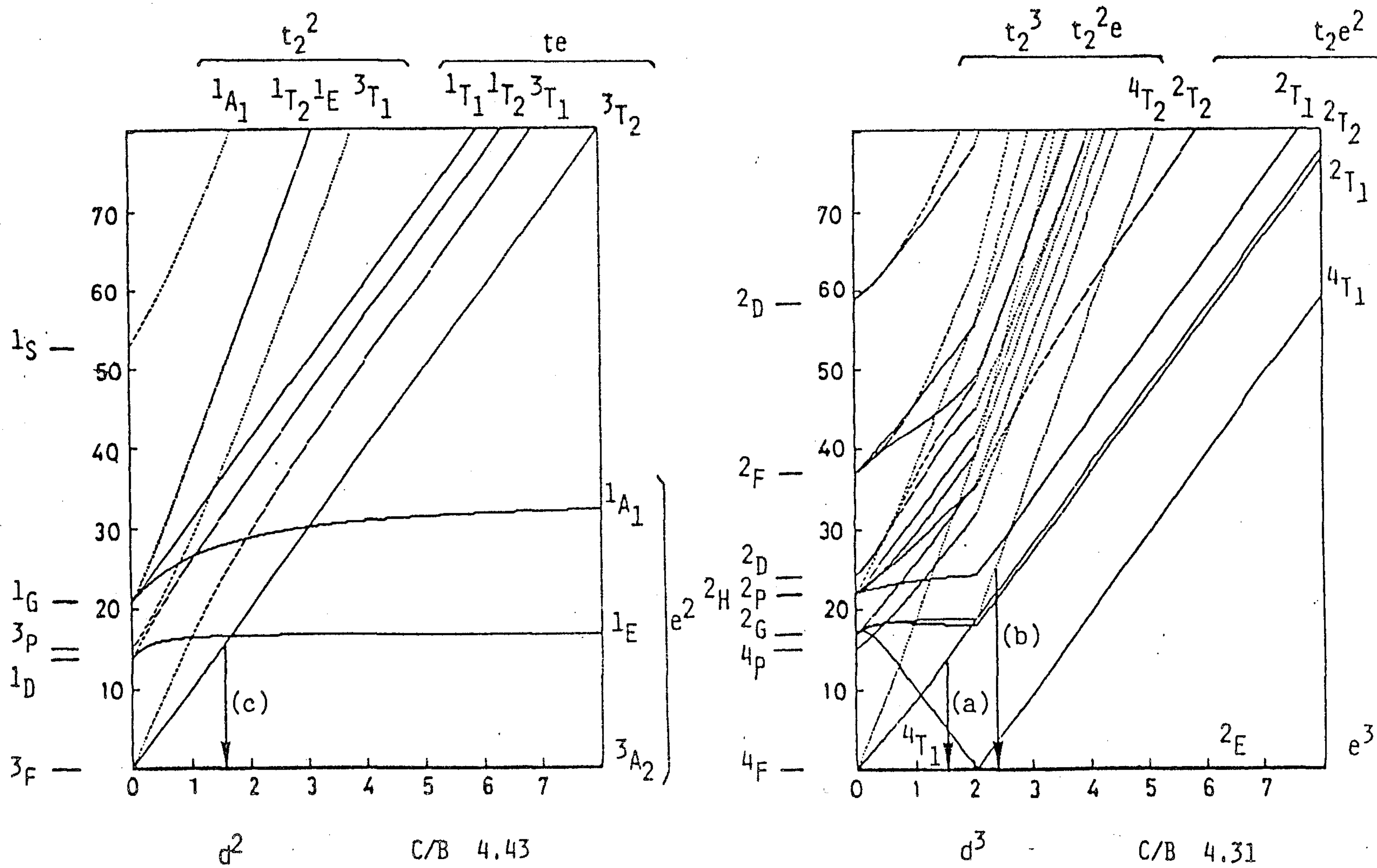

Fig. 4-5 Energy splitting of V^{2+} and V^{3+} in T_d symmetry. Transitions (a), (b) and (c) indicate the proposed origins for the V-related sharp zero-phonon line at 0.7388 eV in GaAs:V.

responsible transitions, the former two groups have assigned to $^4T_2(F)$ - $^4T_1(F)$ transitions in the high-spin region (transition (a) in Fig. 4-5), and the latter group to $^4T_2(F)$ - $^2E(G)$ transitions in the low-spin region (transition (b) in Fig. 4-5). On the other hand, Skolnick et al.[20] have reported that a V-related sharp zero-phonon line observed in InP:V is attributed to $^3T_2(F)$ - $^3A_2(F)$ transitions of an isolated V^{3+} (transition (c) in Fig. 4-5). Therefore, to clarify the PL center, the 0.7388 eV V-related zero-phonon line has been investigated by a time-resolved PL technique.

Time-resolved PL measurements were performed using the system shown in Fig. 4-6. The luminescence was measured by the conventional Ar^+ laser excitation and lock-in detection technique. The time-resolved PL spectra were taken by the use of an acousto-optical modulator (Coherent 305) and a boxcar averager (PAR 162).

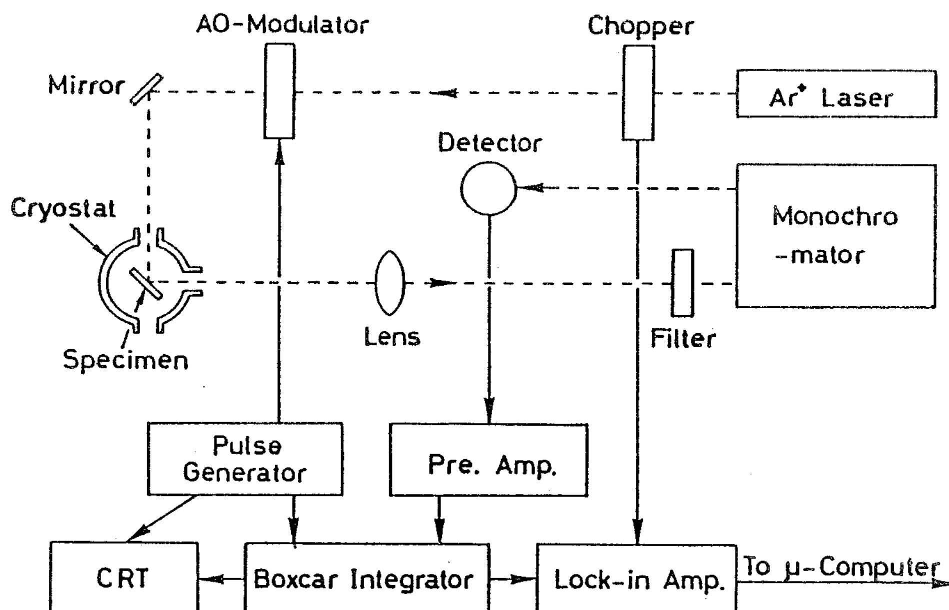

Fig. 4-6 Diagram of time-resolved PL measurement system.

Time-resolved PL spectra associated with V have been measured in GaAs:V at 4.2 K. Figure 4-7 shows the time-resolved PL spectra in the 0.74 eV region. No remarkable deformations are observed with the lapse of time in the PL spectra. From an analysis of the decay characteristics, one can estimate the lifetime of the excited states for the V-related luminescence center in GaAs. In Fig. 4-8, the result for the 0.7388 eV V-related zero-phonon line in GaAs:V is shown. In this case, the lifetime of the excited states is 119 μs. This value is much larger than the decay time of the edge emission such as radiative recombination of bound excitons. Similar result has been previously reported by Guillot et al.[21], their data showing that the lifetime is 125 μs.

Cr-related time-resolved PL spectra have been also measured in GaAs:Cr at 4.2 K for comparison. Figure 4-9 shows the typical result of time decay of the well-known 0.8395 eV Cr-related zero-phonon line. As can be seen in the figure, it has been found that the lifetime of the excited states is 0.77 μs and of two orders smaller than that in the case of the V-related zero-phonon line at 0.7388 eV. It is interesting to note that the decay characteristics are similar between the Cr-related zero-phonon line and a broad band in its lower-energy side.

4-3-2. Identification of charge state

The optical absorption and luminescence spectra associated with 3d-transition metal impurities in semiconductors are mainly attributed to electric-dipole transitions.[22] However, pure d-d transitions are parity-forbidden by Laporte's rule. Therefore, to obtain matrix

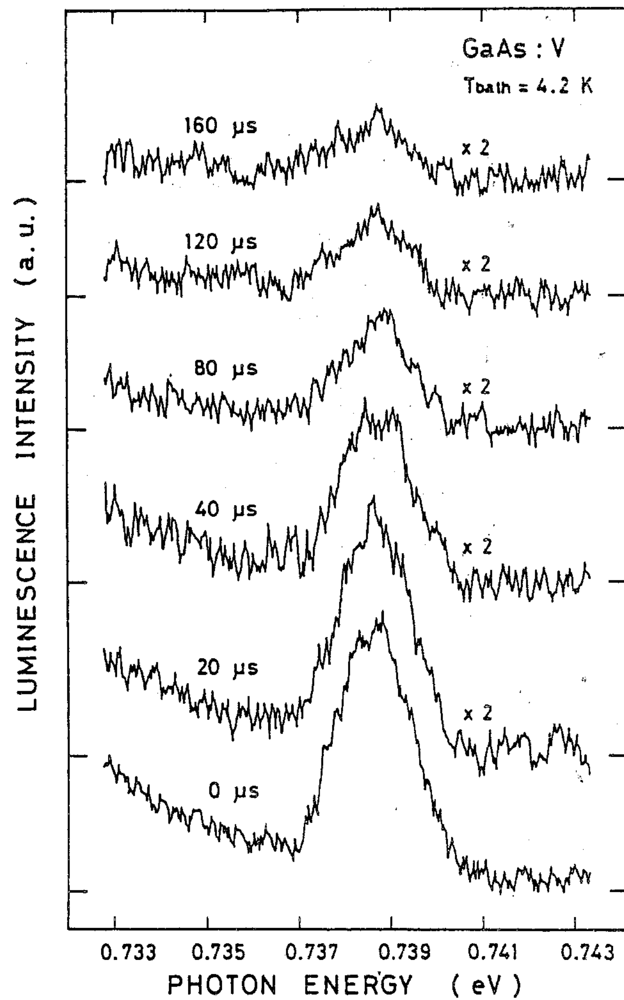

Fig. 4-7 Time-resolved PL spectra associated with V at 4.2 K.

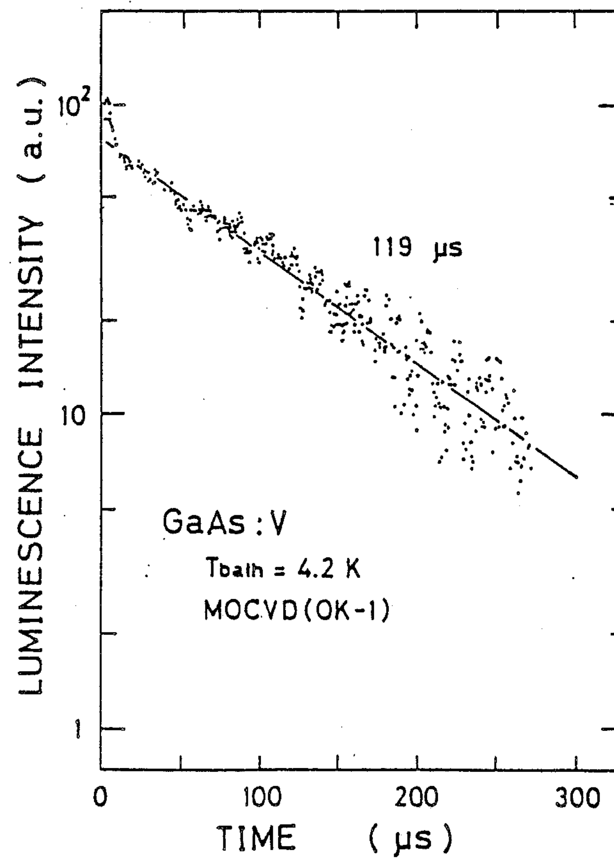

Fig. 4-8 Decay characteristic of the V-related zero-phonon line in GaAs:V.

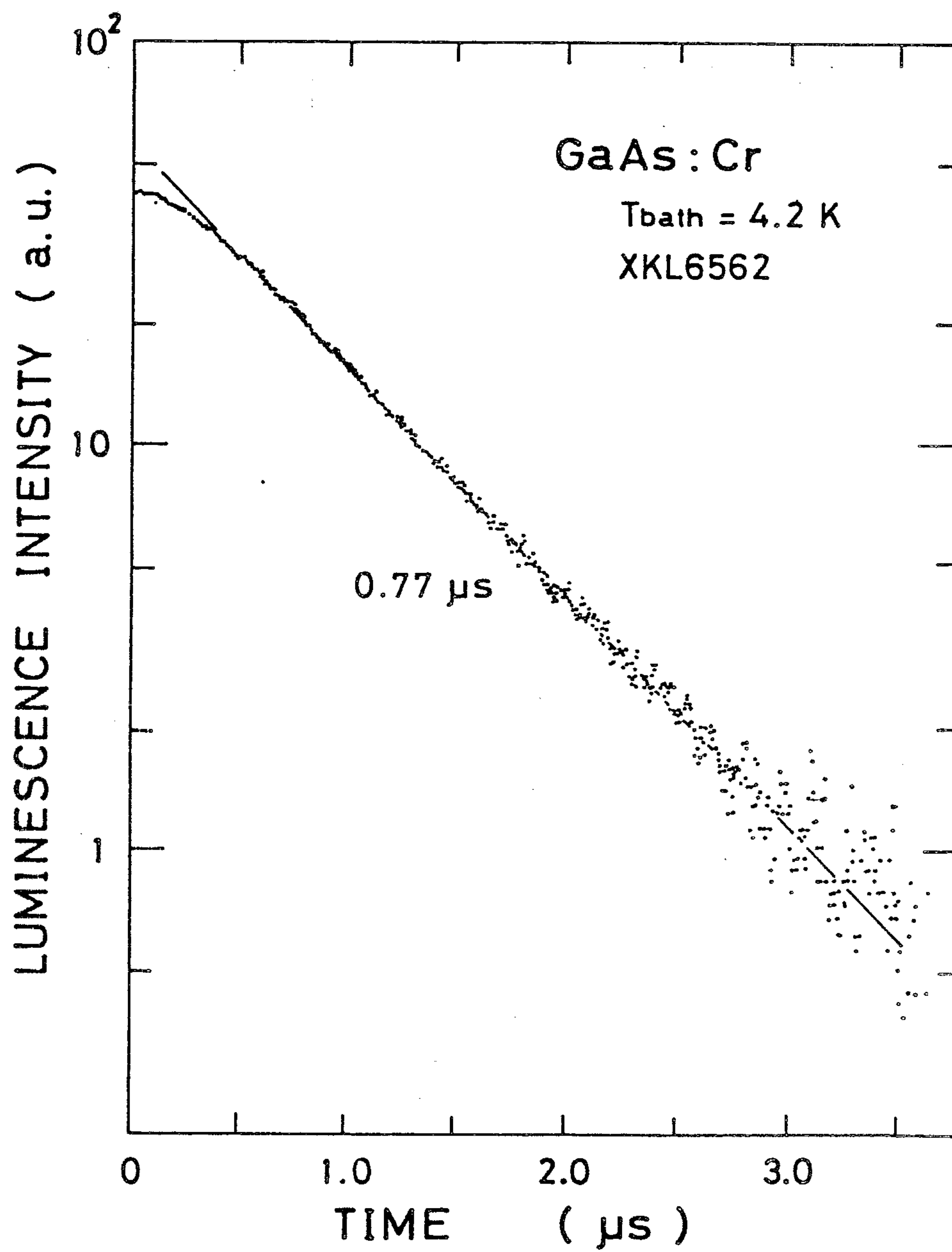

Fig. 4-9 Decay characteristic of the Cr-related zero-phonon line in GaAs:Cr.

elements unequal to zero, an odd-parity mixing mechanism consisting of a mixture of d- and p- like states should be considered. In the configuration interaction model introduced in II-VI compound semiconductors by Rentz et al.[23], the contribution of the 4p states of the impurity to the transition probability is considered in addition to the 3d states, which is due to symmetry distortions by lattice vibration. If the initial state is characterized by a ket symbol $|i\rangle$, the final state by $|f\rangle$ and the position operation by r, the matrix element in this model is as follows;

$$\langle f\ |r|\ i\rangle = k \langle \Phi_{3d}\ |r|\ \Phi_{4p}\rangle \qquad (4\text{-}1)$$

where k is a mixing parameter. From the normalization condition, the following relation is obtained;

$$0 \leq k \leq 1 \qquad (4\text{-}2)$$

The probability p_{fi} of a spontaneous electric-dipole transition which occurs in a dispersive medium with a real part n of the refractive index is given as

$$P_{fi} = (2\ e_0^{\ 2}\ n\ (n^2 + 2)\ \omega^3\ /\ 27\ \varepsilon_0\ h\ c^3\ g_i)\ \sum \langle f\ |r|\ i\rangle^{\ 2}. \qquad (4\text{-}3)$$

Here, e_0 is the elementary charge, ε_0 the vacuum permittivity, h Planck's constant, g_i the degeneracy of the initial state and ω the angular frequency. In this equation, the effective electrical field

at the site of the emitting oscillator is approximated by the Lorentz local-field expression which accounts for dipole-dipole interactions and is assumed to hold for intracenter transitions involving ions with incomplete shells[24]. Furthermore, in one-electron approximation usually applied, eq. (4-3) is simplified by $g_i = 1$ and by omission of the sum.

The decay time of the luminescence corresponds to the mean radiative lifetime of an excited state, which is inversely equal to p_{fi}, provided that both non-radiative and vibronic processes are negligible. In Table 4-1, the decay times obtained in this study and the resulting mixing parameters are summarized together with those previously reported in various III-V compound semiconductors. Here, it is assumed that the 0.7388 eV V-related sharp zero-phonon line in GaAs:V is attributed to $^3T_2(F)$ - $^3A_2(F)$ transitions of a trivalent V ion, which corresponds to transition (c) in Fig. 4-5 and its validity is briefly described below. As can be seen in the table, the mixing parameter is dependent upon the contributed transition type in T_d symmetry. The results are presented in Table 4-2 with the corresponding mixing parameters in II-VI compound semiconductors[23]. The ordering is easily interpreted by considering that the mixing is due to lattice vibration in the configuration interaction model, i.e., the average lattice displacement due to zero-point vibrations decreases with the increase in symmetry of the charge distribution.

The above-mentioned identification of the PL center from which the V-related sharp zero-phonon line is originated in GaAs:V is justified by the following reason. Temporarily, it is assumed that the charge state of the V ion contributing to the luminescence is

Table 4-1 Decay times obtained in this work and the resulting mixing parameters together with those previously reported in various III-V compound semiconductors.

Material	Transition type	Transition energy (eV)	Decay time (μs)	Mixing parameter
*GaAs:Cr	$^5E - ^5T_2$ (Cr^{2+})	0.839	0.77[a)]	(0.43)
GaAs:V	$^3T_2 - ^3A_2$ (V^{3+})	0.739	119[a)]	0.15
			125[b)]	0.14
GaP:V	$^3T_2 - ^3A_2$ (V^{3+})	0.791	110[b)]	0.14
InP:V	$^3T_2 - ^3A_2$ (V^{3+})	0.706	80[b)]	0.20
GaAs:Fe	$^5T_2 - ^5E$ (Fe^{2+})	0.37	10[b)]	0.39
InP:Fe	$^5T_2 - ^5E$ (Fe^{2+})	0.35	11[b,c)]	0.42
InP:Co	$^4T_2 - ^4A_2$ (Co^{2+})	0.47	120[b)]	0.09

*) In this case, the luminescence is originated from the complex consisting of a Cr and an As vacancy.

a) this work, b) G. Guillot et al.[21)], c) P. L. Klein et al.[25)]

divalent. In this case, the resulting mixing parameters are 0.07, 0.07, and 0.09 in GaAs, GaP and InP, respectively. However, considering that the previously-proposed transitions for V^{2+} in GaAs:V are $^4T_2(F)$ - $^4T_1(F)$ and $^4T_2(F)$ - $^2E(G)$ transitions, these mixing parameters violate the rule shown in Table 4-2, this result implying that the most probable candidate as the origin of the V-related PL line at 0.7388 eV in GaAs:V is V^{3+}.

Table 4-2 Relation between the contributed transition types and the mixing parameters in III-V compound semiconductors. For comparison, results for II-VI compound semiconductors are shown together.

Transition type	III - V semicond.	II - VI semicond.*
A - T	0.15	0.3
E - T	0.4	0.6
T - T		0.8

* R.Renz and H-J.Schulz[23)]

4-4. Summary

The luminescence associated with Ni deep acceptors has been investigated in various kinds of Ni-diffused GaAs. It has been found that the Ni-related luminescence drastically changes from the surface

to the deep region of Ni-diffused GaAs. In particular, the Ni-S pair luminescence is strongly observed near the surface of all the GaAs samples doped with a variety of donor impurities. The in-depth profile measurements on the Ni-related PL intensities have shown the builtup of S in the vicinity of the surface region of Ni-diffused GaAs, which is probably due to the redistribution of the background S donors involved in GaAs during the high-temperature diffusion of Ni into GaAs.

Time-resolved PL spectra associated with V- and Cr-related deep centers in GaAs at 4.2 K have been measured and the electronic lifetime of the excited states of these deep centers has been estimated. In both cases, no remarkable deformation has been observed in the PL spectra, and the PL intensity has decreased exponentially with the lapse of time, which indicates that a monomolecular recombination is effective. From an analysis of the decay characteristics, it has been found that the electronic lifetime of the excited state is 119 μs for the V-related deep center and 0.77 μs for the Cr-related center. On the premises of the configuration interaction model introduced in II-VI compound semiconductors, the mixing parameters from the above results have been calculated. It has been found that the resulting mixing parameters reflect the symmetry of the crystal-field levels involved in the transition and are satisfied with the assumption of configuration interaction, the result suggesting that the V-related sharp zero-phonon line at 0.7388 eV in GaAs:V is attributed to ${}^3T_2(F) - {}^3A_2(F)$ transitions of an isolated V^{3+}.

References

1) P. J. Dean, A. M. White, B. Hamilton, A. R. Peaker and R. M. Gibb: J. Phys. D 10 (1977) 2545.

2) J. M. Baranowski, J. W. Allen and G. L. Pearson: Phys. Rev. 167 (1968) 758.

3) S. A. Abagyan, G. A. Ivanov and K. A. Koroleva: Sov. Phys. Semicond. 10 (1976) 1056.

4) U. Kaufmann and J. Schneider: Solid State Commun. 25I (1978) 1113.

5) U. Kaufmann, W. H. Koschel, J. Schneider and J. Weber: Phys. Rev. B19 (1979) 3343.

6) W. Hayes, J. F. Ryan, C. L. West and P. J. Dean: J. Phys. C 12 (1979) L815.

7) H. Ennen and U. Kaufmann: J. Appl. Phys. 51I (1980) 1615.

8) S. G. Bishop, P. J. Dean, P. Porteous and D. J. Robbins: J. Phys. C 13 (1980) 1331.

9) H. Ennen, U. Kaufmann and J. Schneider: Appl. Phys. Lett. 38 (1981) 355.

10) D. L. Partin, A. G. Milnes and L. F. Vassamillet: J. Electron. Mater. 7 (1978) 279.

11) D. L. Partin, A. G. Milnes and L. F. Vassamillet: J. Electrochem. Soc. 126 (1979) 1584.

12) Y. Fujiwara, A. Kojima, T. Nishino and Y. Hamakawa: Jpn. J. Appl. Phys. 22 (1983) L476.

13) for example, Y. Fujiwara, A. Kojima, T. Nishino and Y. Hamakawa: J. Luminescence 31&32 (1984) 451.

14) W. Drozdzewicz, A. M. Hennel and Z. Wasilewski: Proc. Int. Conf. Semi-Insulating III-V Mater., Evian, 1982 (Shiva Publishing Limited, Orpington, 1982) p. 220.

15) V. Swaminathan, A. R. Von Neida, R. Caruso and M. S. Young: J. Appl. Phys. 53 (1982) 6471.

16) W. Kutt, D. Bimberg, M. Maier, H. Krautle, F. Kohl and E. Bauser: Appl. Phys. Lett. 44 (1984) 1078.

17) U. Kaufmann, H. Ennen, J. Schneider, R. Worner, J. Weber and F. Kohl: Phys. Rev. 25 (1982) 5598.

18) A. V. Vasil'ev, G. K. Ippolitova, E. M. Omel'yanovskii and A. I. Ryskin: Sov. Phys. Semicond. 10 (1976) 341.

19) V. V. Ushakov and A. A. Gippius: Sov. Phys. Semicond. 14 (1980) 197.

20) M. S. Skolnick, P. J. Dean, M. J. Kane, Ch. Uihlein, D. J. Robbins, W. Haynes, B. Cockayane and W. R. MacEwan: J. Phys. C 16 (1983) L767.

21) G. Guillot, C. Benjeddou, P. Leyral and A. Nouailhat: J. Luminescence 31&32 (1984) 439.

22) J. S. Griffith: The theory of Transition-Metal Ions (Cambridge University Press, Cambridge, 1961)

23) R. Renz and H-j. Schulz: J. Phys. C 16 (1983) 4917.

24) D. L. Dexter: Solid State Physics (Academic Press, New York, 1958) vol. 6 p. 353.

25) P. L. Klein, J. E. Furneaux and R. L. Henry: Phys. Rev. 29 (1984) 1947.

V. CHARACTERIZATION OF RESIDUAL STRESS IN GaAs

5-1. Introduction

It is important to obtain information about stress in GaAs wafers, since the residual stress greatly affects the performance and reliability of GaAs large-scale integrated circuits. The residual stress is introduced into GaAs wafers mainly during two processes; the crystal-growth and device-fabrication process. The residual stress introduced during the crystal-growth process is caused by temperature gradient in the crystal-growth environment[1,2], which leads to nonuniformity in the wafer. The stress introduced during the device-fabrication process is caused by direct ion implantation into the wafer and subsequent various thermal treatments using a conventional encapsulation technique, which induces the redistribution of the residual impurities and compensators and leads to thermal-conversion in conduction type of the wafer surface[3]. On the other hand, the interface stress is induced by lattice mismatch in GaAs-based heterostructures such as a semiconductor laser operating at room temperature. Such stress greatly influences the material parameters (band gap and lattice constant etc.) of the epitaxial layer (epi-layer) and induces misfit dislocation such as dark-line-defect (DLD)[4], which degrades the device performance.

Up till now, stress in GaAs crystals has been measured mainly by X-ray diffraction, photoelasticity and Raman scattering spectroscopy. Recently, Takano et al. made precise lattice parameter measurements

for semi-insulating (SI) GaAs by the two-beam double crystal method of X-ray diffraction and showed the lattice parameter varies greatly (order of 10^{-4} A) among GaAs wafers and in each wafer.[5] However, such a method is not suitable for the measurement of residual stress in a local area. Photoelasticity is sensitive to stress, but not essentially suitable to the analysis of stress with multi-axes because it utilizes an anisotropy of refractive index. In recent years, Raman scattering spectroscopy has come to be successfully used to estimate the interface stress at the heterostructures such as silicon-on-sapphire (SOI)[6] and InGaAs/GaAs[7]. Raman spectra are, however, not sensitive to such stress. The detection limit is about 100 MPa (10^9 dyne/cm^2) and therefore it is only restricted to heterostructures with extremely large stress. From these points of view, a new powerful characterization technique for residual stress is strongly desired.

In this chapter, the results of systematic measurements on the dominant Cr-related zero-phonon line at 0.8395 eV in a series of SI GaAs:Cr wafers plastically bent along the three principal crystallographic [001], [110] and [111] axes are described. The author considers the use of these PL results for characterizing the residual stress in GaAs:Cr wafers and demonstrates that the type, axis and magnitude of the residual stress in GaAs:Cr wafers can be sensitively estimated by this PL method. In the final section of this chapter, this PL method is applied to the characterization of the interface stress of OMVPE-grown ZnSe/GaAs:Cr heterostructure, which is important for blue light emitting devices, and its effectiveness is confirmed.

5-2. Residual stress in plastically-bent GaAs:Cr[8,9)]

5-2-1. Sample preparation

Mirror-polished specimens used in this thesis work with the [110], [111] or [001] bending axis were cut from Cr-doped GaAs wafers with (100) or (110) crystal orientation, which were grown by a gradient freeze (GF) technique. In order to produce homogeneous deformation, one surface of the specimen was abraded with #3000 silicon-carbide powder before the deformation. The specimen was bent at 350 °C or 400 °C by a four- point bending apparatus previously described[10)] with a bending rate of 100 μm/min or 200 μm/min. As shown in Fig. 5-1, compressive stress was introduced by bending with the mirror-polished surface up and tensile stress with the mirror-polished surface down. The magnitude of the stress was controlled by a load-point deflection, that is, a crosshead

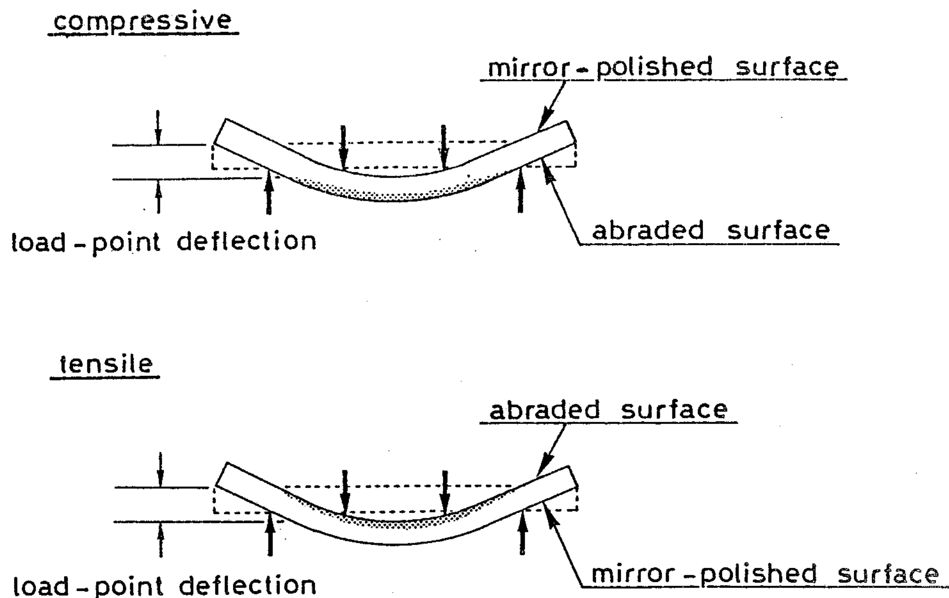

Fig. 5-1 Sample preparation by four-point bending.

displacement. The deformation was stopped at a crosshead displacement and the specimen was rapidly dropped into water to quench the distribution of dislocations introduced from the abraded side of the specimen during bending. The mirror-polished side of the specimens obtained in this way remains to be stressed along the bending axis.

5-2-2. Cr-related luminescence spectra in bent specimens

The Cr-related PL spectra in the 0.839 eV region for the mirror-polished side of plastically-bent SI GaAs:Cr specimens with compressive or tensile stress along various bending axes have been systematically measured. Figure 5-2 (a) and (b) show typical Cr-related PL spectra in bent specimens, together with that of an as-received wafer. In commercially-available melt-grown Cr-doped GaAs, a familiar series of sharp PL lines[11,12] is observed only between 0.839 eV and 0.841 eV. The origin of these lines is attributed to internal transitions in a Cr-V_{As} complex in GaAs.[13-15] Following Lightowlers's nomenclature[11], the lines correspond in order from high energy to line C, line E, line F, line G and line H (H'), respectively, within the experimental error. In the bent specimens, it is clearly seen that the Cr-related lines observed with the as-received wafer shift accompanying the appearance of new PL lines. In Fig. 5-2 (a), for simplicity, only new stress-induced lines related to line G are denoted in Barrau's nomenclature[16]. Furthermore, in accordance with the type of introduced stress and the direction of bending axis, the observed Cr-related spectra are quite different between each other.

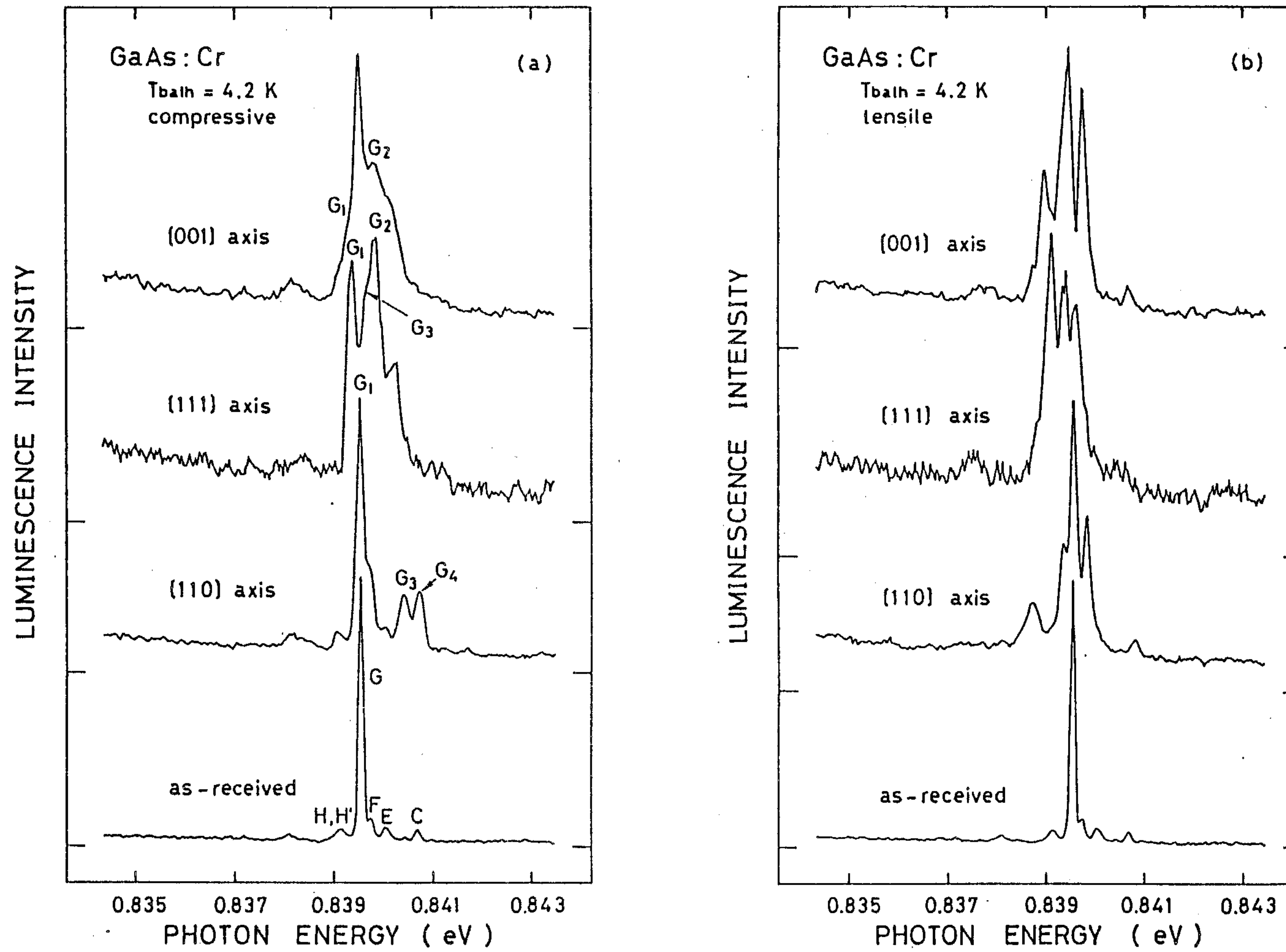

Fig. 5-2 Cr-related PL spectra of as-received and plastically-bent GaAs:Cr wafers with compressive (a) and tensile (b) stress along various bending axes.

The above observation can be well explained by the splitting of degenerate Cr levels in GaAs under the residual stress involved in specimens. Figure 5-3 shows the theoretically expected splitting of Cr-related levels versus stress intensity, and the energy level scheme in the high stress regime for the [111] axis, which were predicted by Barrau et al[16]. Here, for simplicity, the stress dependence of the lowest level in the excited states is only shown. On the other hand, in the ground states, the effect of the trigonal perturbation is neglected because it is expected to be sufficiently quenched by a stronger Jahn-Teller coupling. The vertical lines represent optical transitions under stress, restricted to those which come from the splitting of zero-stress lines in order to make the representation clearer. From this figure, it is expected that the dominant line G

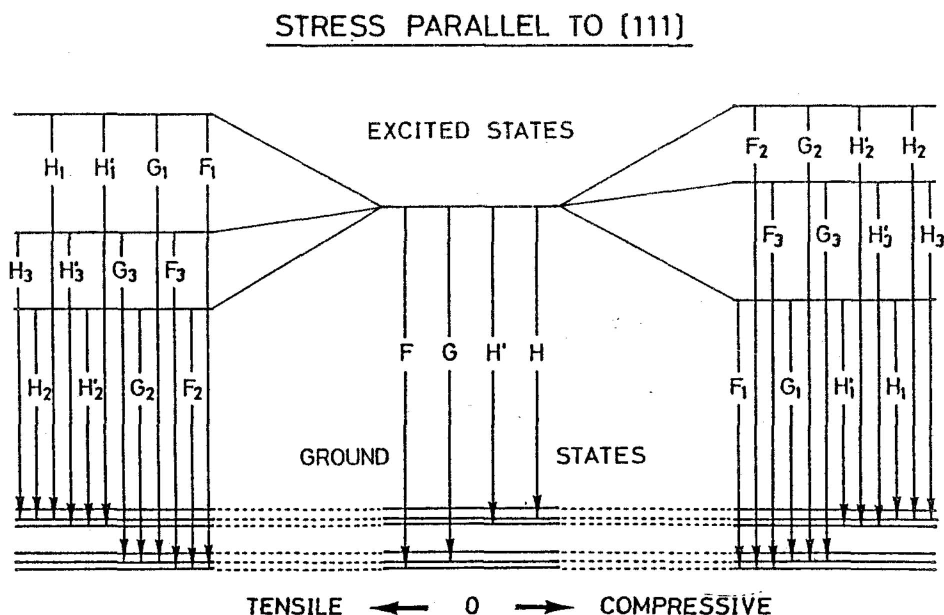

Fig. 5-3 Splitting of Cr-related levels versus stress and schematic energy level scheme under high stress for [111] axis.

observed in the as-received wafer is split into three lines G_1, G_2 and G_3 under stress for the [111] axis. In fact, in the specimen bent along the [111] axis, three lines expected to be originated from line G can be seen independent of stress-type, as shown in Fig. 5-2, which implies that the residual stress in the mirror-polished side of specimens prepared by the four-point bending method is almost uniaxial. The stress-type dependence of the Cr-related spectra in the bent specimens can be explained by considering that the polarity of the pressure coefficient of each excited state changes in accordance with stress-type, which is shown in Fig. 5-3. Furthermore, the bending-axis dependence of the Cr-related spectra reflects the symmetry of the luminescence center and is concerned with the difference of splitting in the degenerate Cr levels in accordance with the direction of applied stress. Therefore, based on the above observations, information about the type and axis of the residual stress in Cr-doped SI GaAs wafers can be easily obtained by this PL method.

5-2-3. Effects of stress along [111] bending axis

Based on uniaxial-stress data for the Cr-related PL lines in the 0.839 eV region, the magnitude of the residual stress in a bent specimen can be estimated from the energy shift of new stress-induced PL lines. Figure 5-4 (a) and (b) show Cr-related PL spectra for plastically-bent specimens with compressive or tensile stress along the [111] bending axis as a parameter of load-point deflection, together with that of the as-received wafer. The specimens were deformed at 350 °C by a bending rate of 100 μm/min. In the specimens

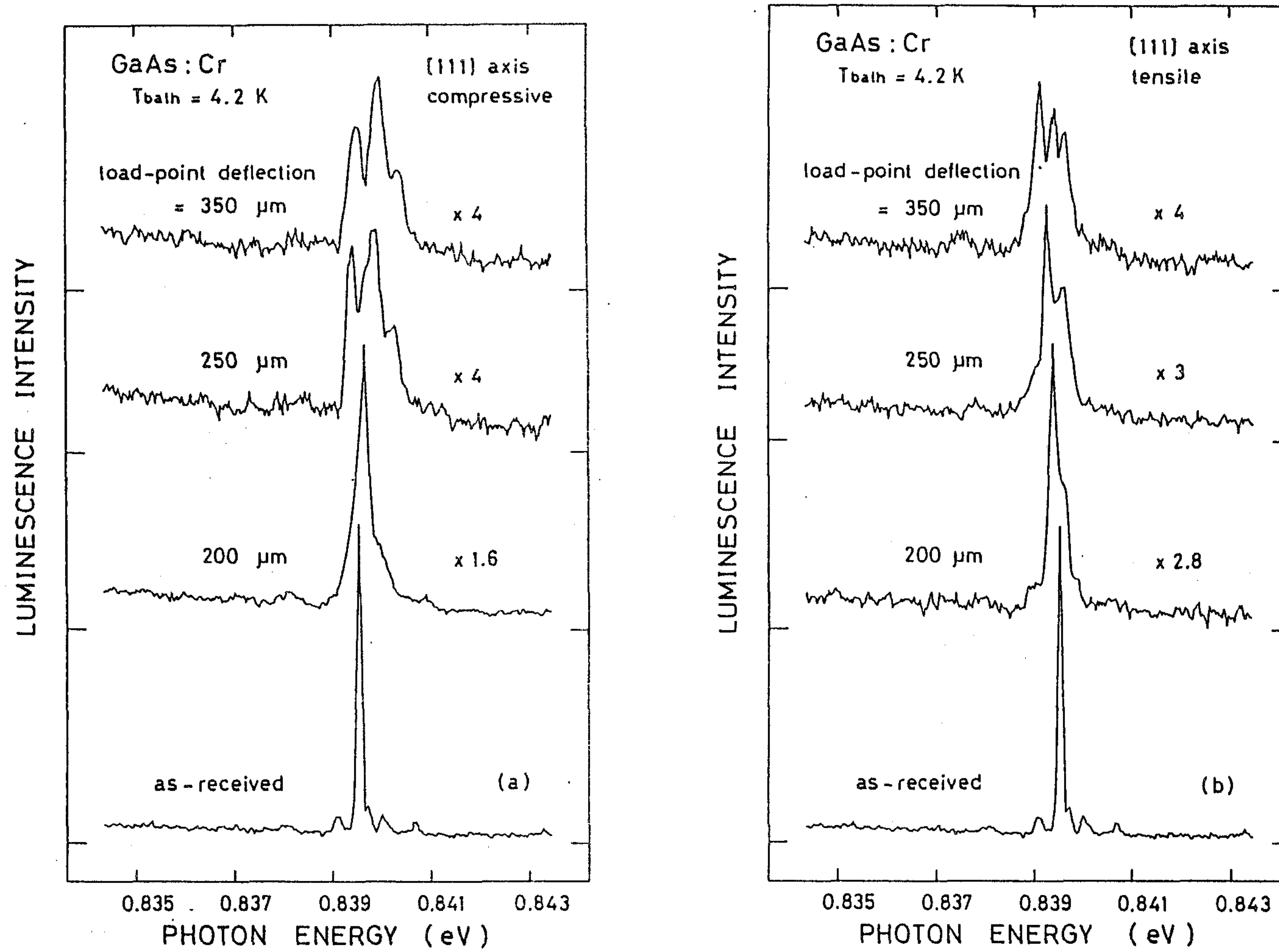

Fig. 5-4 Cr-related PL spectra of as-received and plastically-bent GaAs:Cr wafers with compressive (a) and tensile (b) stress along [111] bending axis.

with stress along the [111] bending axis, the intensity of the main Cr-related PL line (line G in Fig. 5-2) decreases and three new PL lines can be observed at the larger load-point deflection, as mentioned before. With the increase of the load-point deflection, the stress-induced higher-energy line G_2 clearly shifts toward the higher-energy side for compressive stress and the stress-induced lower-energy line G_2 clearly shifts toward the opposite side for tensile stress. In the specimens deformed at larger load-point deflection, the half-width of each line becomes broad. This broadening can be interpreted by the existence of the stress distribution over the excited area on the specimen surface due to the introduction of dislocations from the rear side abraded with silicon-carbide powder, which was confirmed by observation of such dislocation distribution on the cleaved plane by the etch pit method using AB etching[17).

By comparing the energy shift of these stress-induced PL lines with previously-reported uniaxial-stress data, the magnitude of residual stress in bent specimens can be estimated. The [111] uniaxial-stress dependence of the energy shift of three stress-induced PL lines was experimentally obtained by Barrau et al.[16), as follows;

line G_1: $E_1 = -0.0051 \times P$ (meV)

line G_2: $E_2 = 0.018 \times P$ (meV)

line G_3: $E_3 = 0.0051 \times P$ (meV)

where E_1, E_2 and E_3 are, respectively, the energy shift of lines G_1, G_2 and G_3 under the [111] uniaxial-stress whose magnitude is P in MPa.

In Fig. 5-5, the solid lines represent the above-mentioned uniaxial-stress dependence of the dominant Cr-related G lines in GaAs. Here, they are extrapolated to the tensile stress region. The peak positions of the stress-induced lines observed in the specimens with stress along the [111] bending axis are plotted, in this figure, to fit them to the solid and dotted lines. For comparison, the peak positions of the stress-induced lines observed in the specimen which was deformed with the load-point deflection of 400 μm at 400 °C are similarly plotted by closed circles. It should be noticed that this PL method is very sensitive to stress and the detection limit is a few MPa.

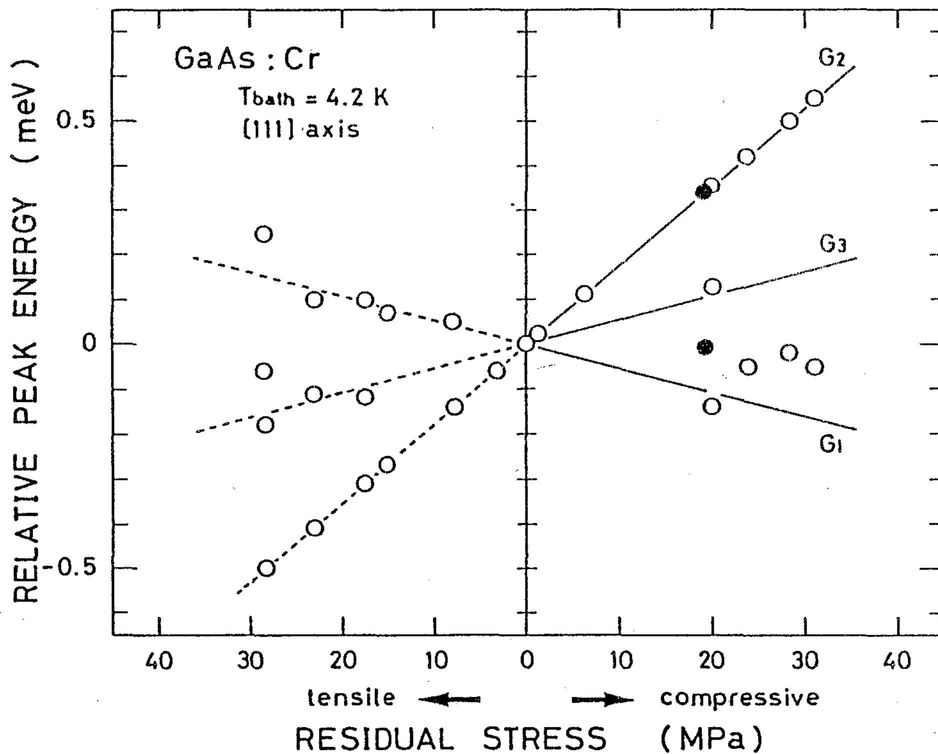

Fig. 5-5 Peak positions of stress-induced Cr-related PL lines observed for plastical deformation along [111] bending axis as a function of stress intensity.

Figure 5-6 shows the residual stress obtained by this PL method in the specimens compressively deformed along the [111] bending axis as a parameter of load-point deflection. The inset represents the load-point deflection dependence of the load applied to the specimens for deformation. As can be seen in the figure, the residual stress suddenly increases at the load-point deflection over 200 μm and after then gradually saturates. This result corresponds to the load-point deflection dependence of the applied load, which is shown in the inset, and implies that plastic deformation begins at the load-point deflection around 200 μm due to the introduction of dislocations from the abraded side. Furthermore, in spite of the same load-point deflection of 400 μm, the residual stress in the specimen deformed at 350 °C is larger than that in the specimen deformed at 400 °C, which can be well explained by the fact that the dislocation velocity is higher at 400 °C[18] and the residual stress is more easily relaxed at high temperature.

5-2-4. Effects of compressive stress along [110] and [001] bending axes

The residual stress in the specimens plastically deformed along the [110] and [001] bending axes has been also characterized by monitoring the Cr-related PL lines. Figure 5-7 (a) and (b) show the Cr-related PL spectra for plastically-bent specimens with compressive stress along the [110] and [001] bending axes as a parameter of load-point deflection, together with that of the as-received wafer. The specimens with the [110] bending axis were deformed at 400 °C by a bending rate of 100 μm/min. And the specimens with the [001] bending

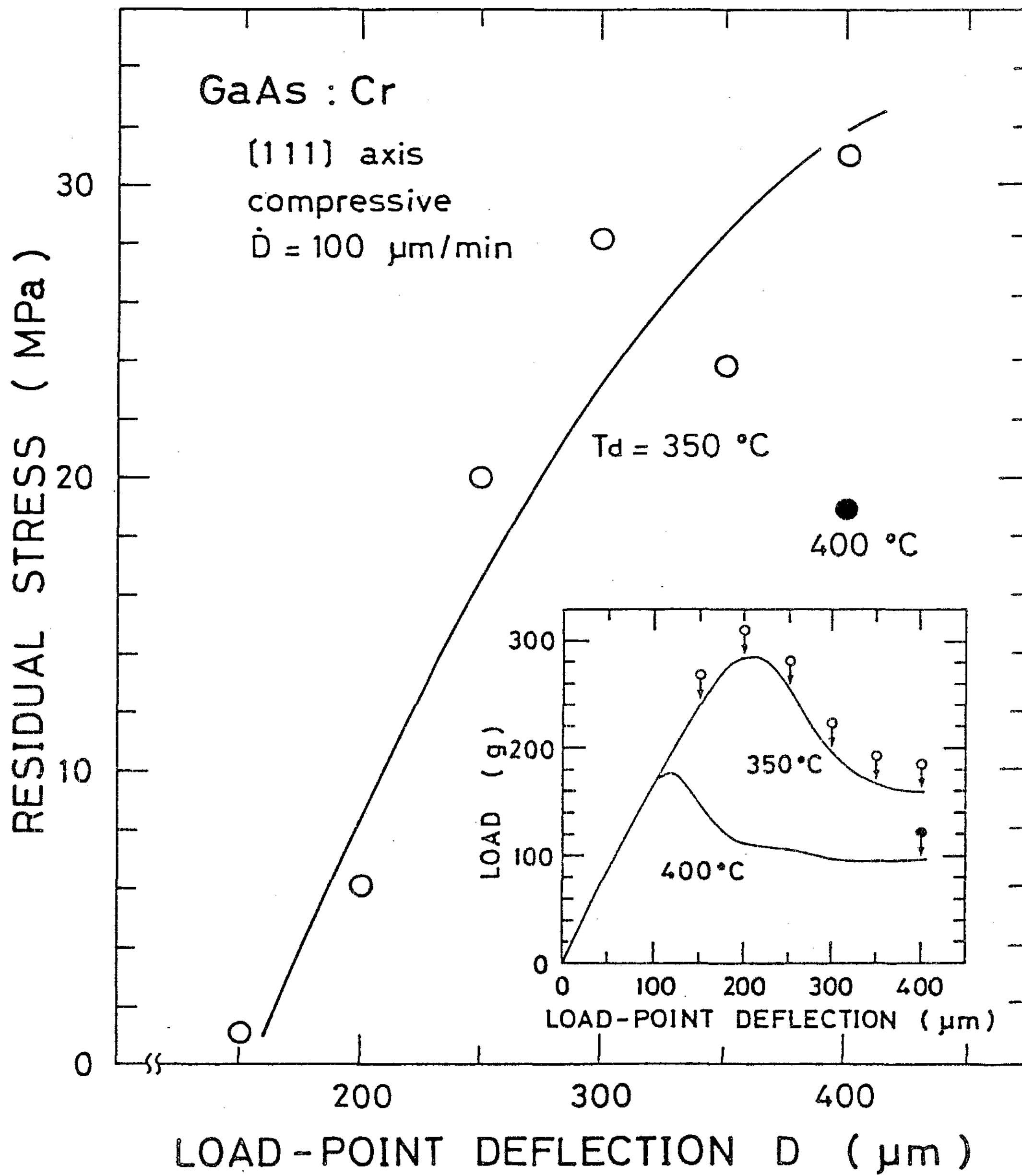

Fig. 5-6 Load-point deflection dependence of stress intensity for plastical deformation along [111] bending axis.

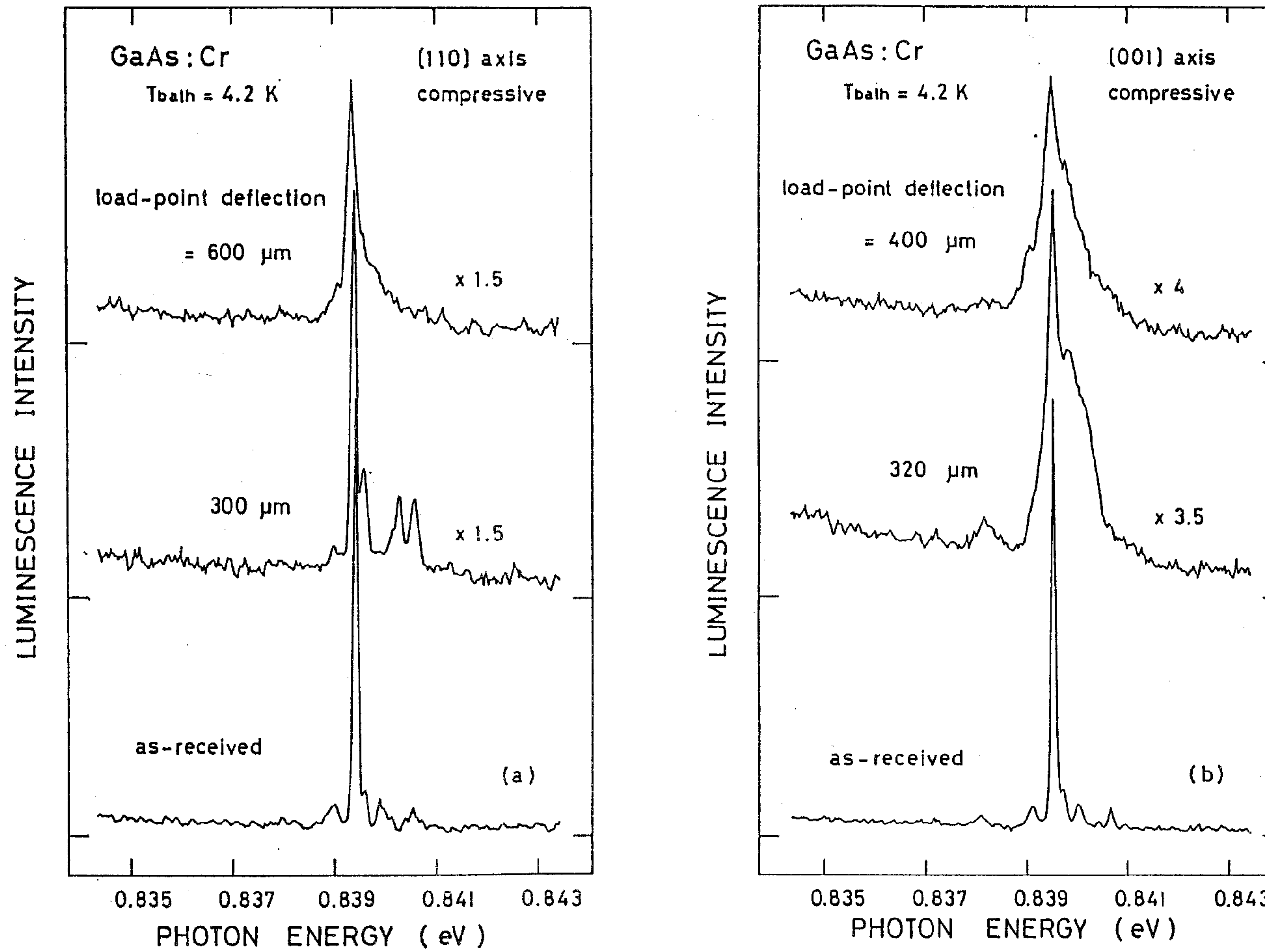

Fig. 5-7 Cr-related PL spectra of as-received and plastically-bent GaAs:Cr wafers with compressive stress along [110] (a) and [001] (b) bending axes.

axis were deformed at 350 °C by a rate of 200 μm/min. In these specimens with the [110] bending axis, the intensity of the main Cr-related PL line G (= G_1) decreases and a pair of new lines appears in the higher-energy side, which are respectively denoted by line G_3 and G_4 in Barrau's nomenclature[16]. The peak positions of these stress-induced lines shift toward the higher-energy side with increasing the load-point deflection, though the peak position of the main PL line G is almost unchanged[9]. When the load-point deflection increases up to 600 μm, a pair of stress-induced lines disappear and the main PL line G becomes broad with the peak position almost unchanged. This broadening can be also explained by inhomogeneous distribution of stress due to the introduction of dislocations from the abraded surface, as mentioned above. In the specimens with the [001] bending axis, line G can be still observed accompanying a shoulder and a new line on both sides, which are respectively denoted by line G_1 and G_2 in Barrau's nomenclature[16], though the intensity of line G similarly decreases. This observation is inconsistent with Barrau's data, reporting that line G was completely split into lines G_1 and G_2 and not observed under the [001] uniaxial stress. However, considering that our specimens were prepared by the four-point bending method, it might be related to local relaxation of residual stress due to the introduction of dislocations from the abraded side on the early stage of deformation. This is supported by the fact that slip systems are much more in the deformation along the [001] bending axis than along the other bending axes. The peak position of line G_2 clearly shifts toward the higher-energy side with increasing the load-point deflection. In this case, when the load-point deflection increases up

to 400 μm, line G_2 becomes obscure and the main line G becomes broad with the peak position almost unchanged.

By the same procedure, the magnitude of residual stress can be estimated from the energy shift of stress-induced PL lines. The [110] and [001] uniaxial-stress dependences of the energy shift of these lines were experimentally obtained as follows[16];

for the [110] uniaxial-stress

line G_1: $E_1 = 0$ (meV)

line G_3: $E_3 = 0.016 \times P$ (meV)

line G_4: $E_4 = 0.025 \times P$ (meV)

for the [001] uniaxial-stress

line G_1: $E_1 = -0.012 \times P$ (meV)

line G_2: $E_2 = 0.028 \times P$ (meV)

where E_1, E_2, E_3 and E_4 are defined similarly to the previous section. In Fig. 5-8, for example, the solid lines represent the [110] compressive uniaxial-stress dependences of the dominant Cr-related line G in GaAs. The peak positions of the stress-induced lines observed in the specimens with compressive stress along the [110] bending axis are plotted in the above-mentioned way. The closed circles correspond to them for the specimen plastically deformed at the load-point deflection of 300 μm shown in Fig. 5-7 (a). From this figure, the magnitude of the residual stress for this specimen can be easily estimated to be about 50 MPa. The residual stress in the

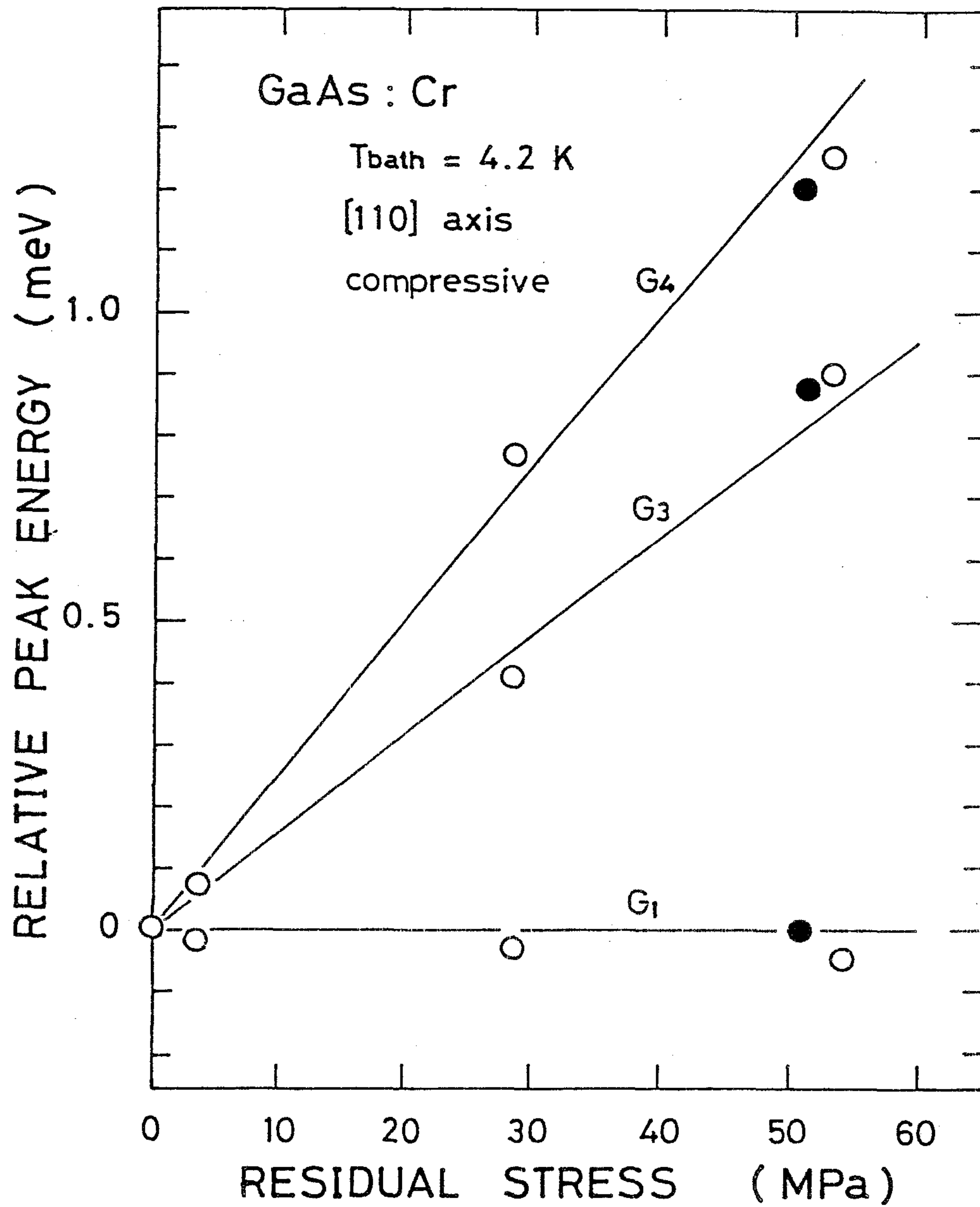

Fig. 5-8 Peak positions of stress-induced Cr-related PL lines observed for the plastically-bent specimens with compressive stress along [110] bending axis as a function of stress intensity.

specimens with tensile stress can be also characterized by the same procedure.

5-3. Application to ZnSe/GaAs heterostructure[19]

5-3-1. Sample preparation

The substrates used in the present thesis work were cut from (100), (110) and (111) oriented SI GaAs:Cr wafers which were grown by a GF technique. Prior to the growth of ZnSe, the GaAs substrates were etched for 2 min by a solution of $H_2SO_4:H_2O_2:H_2O$ = 5:1:1, and followed by a thorough rinse in pure methanol. ZnSe epitaxial layers were grown on the GaAs substrates by two techniques, i.e., OMVPE and MBE.

The OMVPE growth of ZnSe on GaAs has been made by the system described in ref. 20. After being loaded into a reactor, the substrate was heated in pure hydrogen stream at 550 °C for about 10 min for heat cleaning, and then the substrate temperature was maintained at 400 °C. ZnSe epi-layers were grown using dimethylzinc [$(CH_3)_2Zn$, DMZ] and 5%-H_2Se as source materials which were transported into a reactor with Pd-purified hydrogen carrier gas. Source flow rates into the reactor were 37.6 x 10^{-5} mol/min for H_2Se and 9.6 x 10^{-5} mol/min for DMZ, the flow-rate ratio [H_2Se] / [DMZ] therefore being equal to 3.9. The reactor pressure was controlled by a throttle valve placed between the reactor tube and a rotary pump (850 l/min), and the growth of ZnSe on GaAs was carried out at the reactor pressure of 0.28 Torr. The ZnSe epi-layers with various thickness were obtained by changing the growth time.

The MBE growth of ZnSe on GaAs has been performed in a conventional MBE machine equipped with a load lock system. After the mount of the GaAs substrate on a Mo heat sink, the substrate was thermally cleaned in ultra high vacuum at 600 °C for about 10 min and then the substrate temperature was maintained at 350 °C. 6-nine Zn and Se metals were employed as source materials. The molecular-beam flux ratio of Zn to Se was about 1.

5-3-2. Interface stress due to lattice mismatch

Firstly, what kind of stress exists in the GaAs substrate surface of the ZnSe/GaAs heterostructures has been considered. In the ZnSe/GaAs heterostructure, the lattice mismatch is about 0.26 % between the epi-layer and the substrate at room temperature, i.e., the unstrained lattice parameter of ZnSe is larger by 0.015 A than that of GaAs. On the assumption of the coherent growth of ZnSe on GaAs, the lattice of the ZnSe epi-layer is tetragonally deformed due to compressive biaxial stress on a plane parallel to the heterointerface. Therefore, the GaAs substrate suffers tensile biaxial stress to satisfy the balance of force and moment. This tensile biaxial stress can be decomposed into a tensile hydrostatic stress component and a compressive uniaxial stress component along the direction perpendicular to the heterointerface plane, which have the same magnitude, considering the stress tensor.[21)]

Secondly, the interface stress effects on the well-known Cr-related PL lines at 0.839 eV in GaAs have been considered. These Cr-related PL lines are thought to be due to intracenter transitions between excited and ground states of a divalent substitutional Cr ion

in the GaAs lattice. The tensile hydrostatic stress enlarges uniformly the GaAs lattice without symmetry change of the crystal-field around the Cr ion. Based on the crystal-field theory, the magnitude of the crystal-field splitting between excited and ground states is inversely proportional to the fifth power of the lattice parameter of a host material. Therefore, it is expected, under the application of the tensile hydrostatic stress, that the Cr-related PL lines shift toward the lower-energy side with the spectral shape unchanged, and that the magnitude of the energy shift is dependent on the hydrostatic-stress intensity. On the other hand, the application of the uniaxial stress changes the symmetry of the luminescence center, different from the case of the hydrostatic stress, and induces an energy-level splitting in the degenerate ground and excited states of the Cr ion. Therefore, it is expected that new stress-induced Cr-related PL lines appear depending on the direction of the uniaxial stress. The change in the Cr-related PL lines induced by the application of the tensile biaxial stress, which is seen in the case of ZnSe/GaAs heterointerface, can be analyzed by the stress effects mentioned above. This type of stress characterization has been already performed for LPE-grown InGaAsP/GaAs:Cr heterostructures.[21)]

5-3-3. Cr-related luminescence spectra from GaAs substrates

For this ZnSe/GaAs heterostructure the GaAs substrate was directly photo-excited through the ZnSe epi-layer by the 514.5 nm Ar^+ laser. Figure 5-9 shows Cr-related PL spectra in the 0.839 eV region from the GaAs substrates for (100) and (111) OMVPE-grown ZnSe/GaAs:Cr

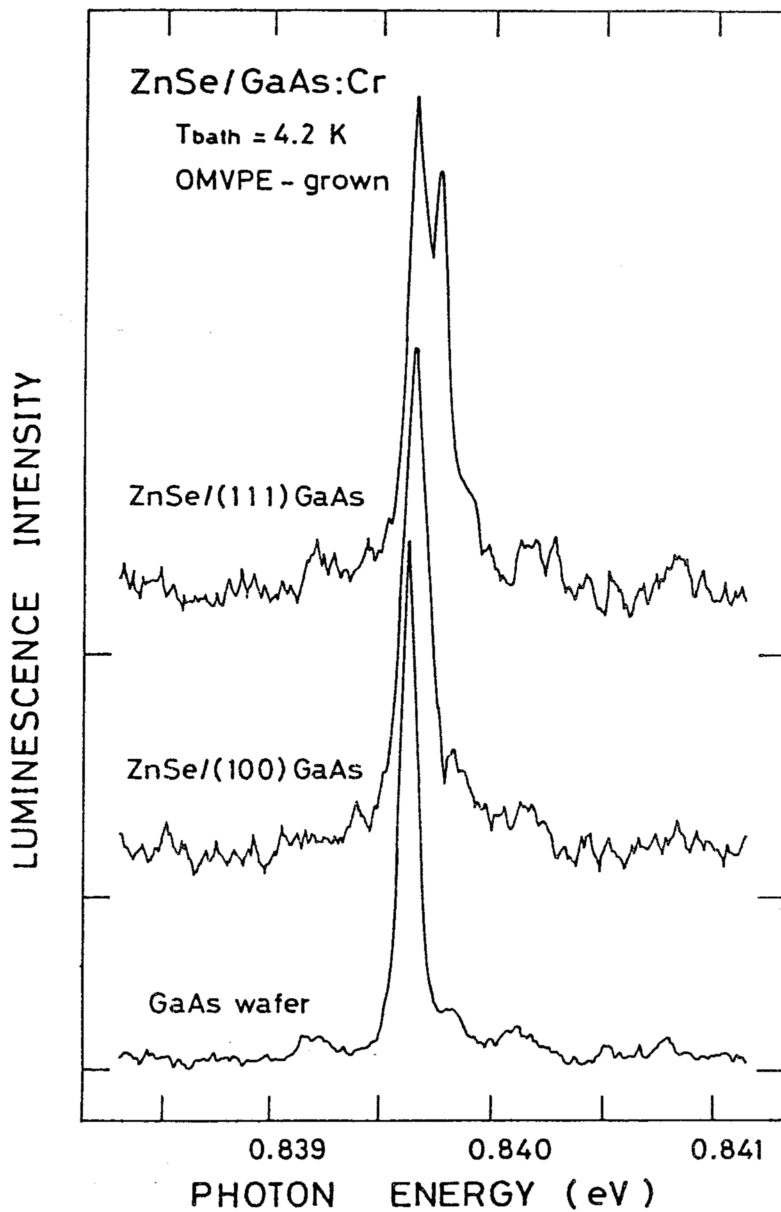

Fig. 5-9 Cr-related PL spectra from GaAs substrates for (100) and (111) OMVPE-grown ZnSe/GaAs:Cr heterostructures, together with that of as-received GaAs:Cr wafer.

heterostructures whose epi-layer thickness is 7.7 μm, together with that of a commercially-available SI GaAs:Cr wafer. In an as-received wafer, a dominant sharp PL line can be observed at 0.8395 eV, which is thought to be originated from a Cr_{Ga}-V_{As} complex[13-15] and referred to line G by Lightowlers et al.[11] It can be seen in the figure that the peak position of line G observed in these ZnSe/GaAs:Cr heterostructures slightly shifts toward the higher-energy side and its half-width becomes larger, compared with line G observed in the GaAs:Cr wafer. These changes in Cr-related PL lines can be explained by the existence of the hydrostatic stress and the uniaxial stress perpendicular to the interface in the GaAs substrates of ZnSe/GaAs:Cr heterostructures; the positive peak shift is caused by the compressive hydrostatic stress and its half-width broadening by the uniaxial stress.[21] The type of the uniaxial stress is considered to be tensile, because the spectral shape observed in (111) ZnSe/GaAs:Cr heterostructure is similar to that in plastically-bent specimen with a tensile stress along the [111] bending axis. The magnitude of the tensile uniaxial stress can be estimated to be about 4 MPa from the peak separation of 0.1 meV using the previously-described pressure coefficients of stress-induced PL lines, which corresponds to the lattice strain of about 0.003 %. This stress is not consistent with stress induced by the lattice mismatch between ZnSe epi-layer and GaAs substrate as mentioned before.

The ZnSe epi-layer thickness dependence of the Cr-related PL lines from the GaAs substrates for OMVPE-grown ZnSe/GaAs:Cr heterostructures has been investigated. In Fig. 5-10 (a) and (b), the relative peak position of line G with respect to that of an

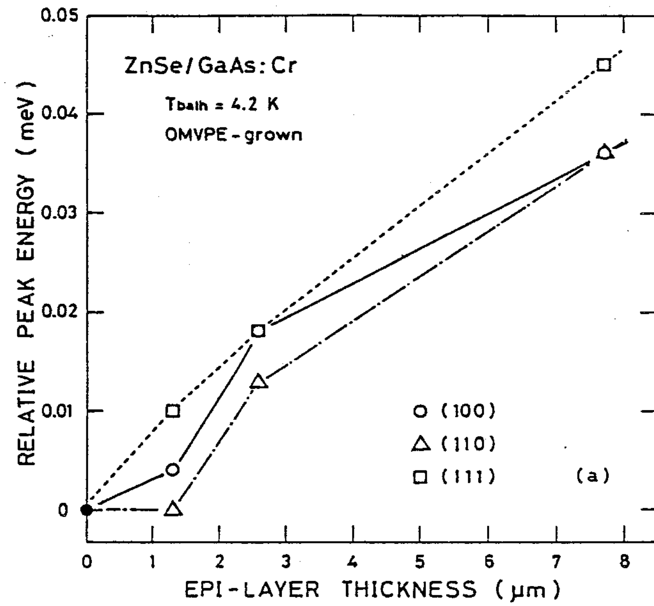

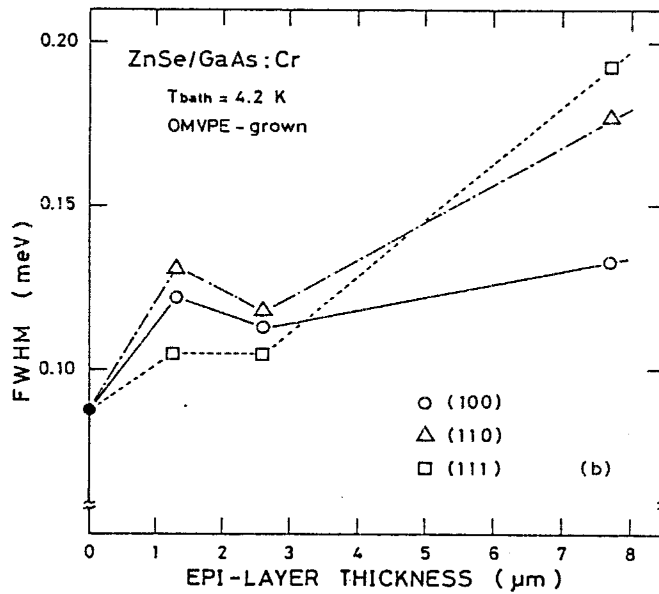

Fig. 5-10 ZnSe epi-layer thickness dependence of relative peak positions (a) of line G in respect to that of as-received wafer and its half-widths (b) for (100) (circle), (110) (triangle) and (111) (square) OMVPE-grown ZnSe/GaAs:Cr heterostructures.

as-received GaAs:Cr wafer and its half-width are shown as a parameter of the ZnSe epi-layer thickness for (100), (110) and (111) ZnSe/GaAs:Cr heterostructures. As can be seen in the figures, the peak shift of line G and its half-width become larger with the increase of the epi-layer thickness, which is independent of the crystallographic orientation. This observation indicates that both the compressive hydrostatic and tensile uniaxial stresses in the GaAs substrate increase with the ZnSe epi-layer thickness, suggesting that such stress is induced by the existence of the ZnSe epi-layer on the substrate, not by effects like thermal damage.

The substrate-thickness dependence of the Cr-related PL lines for OMVPE-grown ZnSe/GaAs:Cr heterostructures has been also investigated. Figure 5-11 shows the substrate thickness dependence of the Cr-related PL spectra from the GaAs substrate for (111) ZnSe/GaAs:Cr heterostructure whose epi-layer thickness is 7.7 μm, together with that of an as-received GaAs:Cr wafer. It can be seen that the peak position of line G gradually shifts toward the higher-energy side with decreasing the substrate thickness. In addition, the stress-induced PL line observed in the higher-energy side shifts similarly, as indicated by arrows in the figure. Furthermore, it has been found that the relative peak positions of these lines with respect to line G are inversely proportional to the GaAs substrate thickness d, the results being shown in Fig. 5-12. Here, open circles represent the relative peak positions for line G, closed circles for the stress-induced PL line, and an open square for line G, which was observed in an MBE-grown ZnSe/GaAs:Cr heterostructure. Similar results have been also obtained for (100) ZnSe/GaAs:Cr

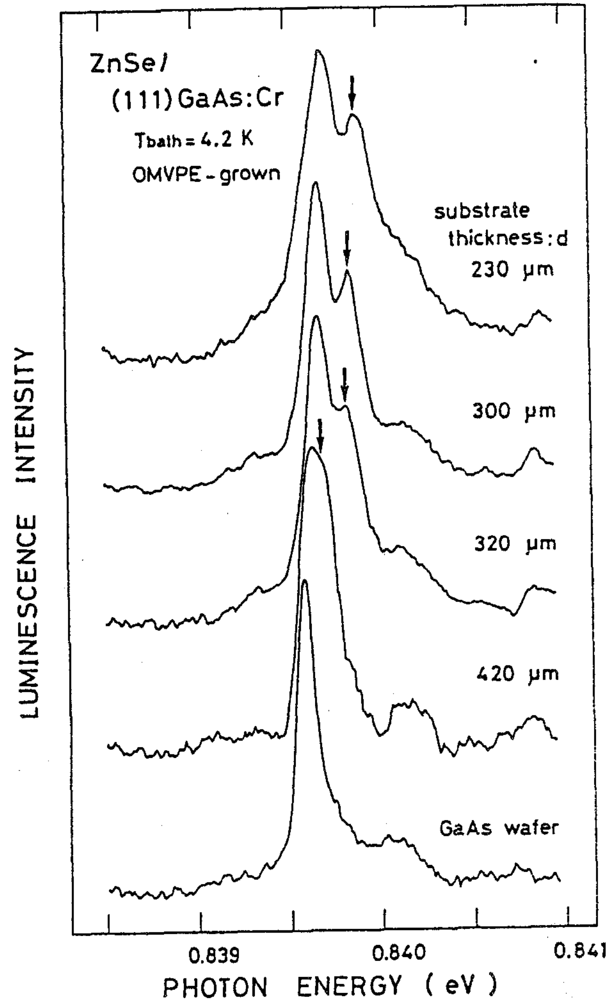

Fig. 5-11 GaAs substrate thickness dependence of Cr-related PL spectra from GaAs substrates for (111) OMVPE-grown ZnSe/GaAs:Cr heterostructures, together with that of as-received GaAs:Cr wafer. Arrows indicate stress-induced PL lines.

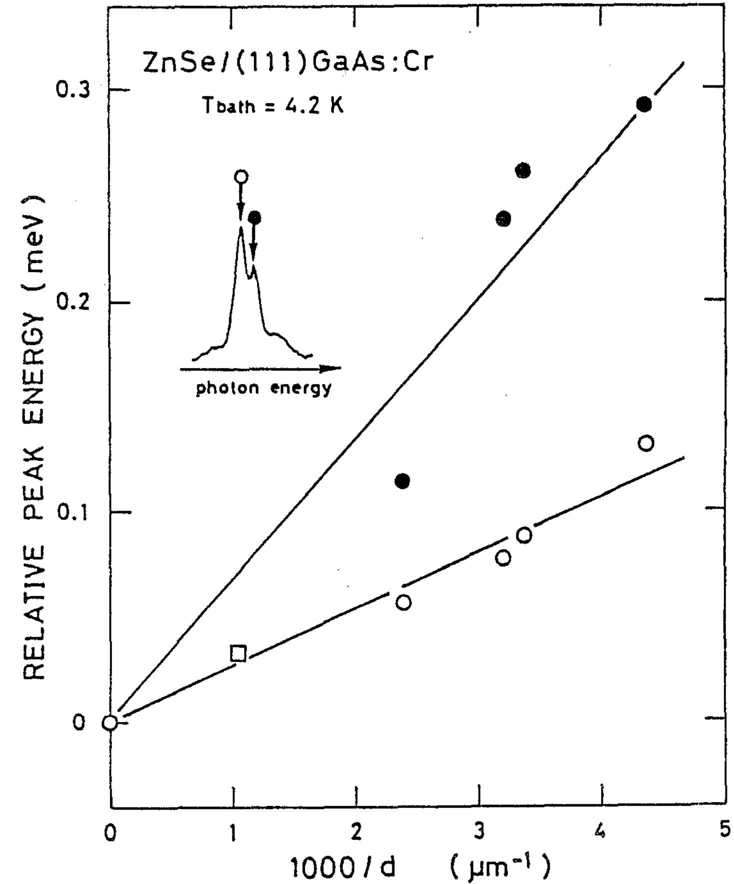

Fig. 5-12 GaAs substrate thickness dependence of relative peak positions of line G (open circle) and stress-induced line (closed circle) with respect to line G of as-received GaAs:Cr wafer for (111) OMVPE-grown ZnSe/GaAs:Cr heterostructures. Open square indicates that for (111) MBE-grown ZnSe/GaAs:Cr heterostructure.

heterostructure, though the stress-induced PL line could not be clearly separated. The above observations imply that both the compressive hydrostatic and tensile uniaxial stresses increase with reducing the substrate thickness, suggesting that this stress induced by the existence of the ZnSe epi-layer extends over the whole GaAs substrate.

The Cr-related PL spectra for MBE-grown ZnSe/GaAs:Cr heterostructures have been also measured in order to examine whether the above-mentioned results are dependent on the growth technique of ZnSe or not. Figure 5-13 shows the Cr-related PL spectra from the GaAs substrates for the MBE-grown (100) and (111) ZnSe/GaAs:Cr heterostructures, together with that of an as-received GaAs:Cr wafer. The peak shift of line G toward the higher-energy side as well as the half-width broadening have been observed in these ZnSe/GaAs:Cr heterostructures independent of the crystallographic orientation, though a stress-induced PL line can not be observed because of the thin ZnSe epi-layer of 3.4 μm. The relative peak position of line G observed for (111) ZnSe/GaAs:Cr heterostructure is plotted by an open square in Fig. 5-12, where the position for the MBE-grown epi-layer was estimated on the assumption that the effective substrate thickness increases by 2.3 times, i.e., the ratio of 7.7 μm (OMVPE-grown epi-layer) to 3.4 μm (MBE-grown epi-layer). As seen in this figure, the result obtained for the MBE-grown sample is consistent with the data obtained for OMVPE samples, which indicates that the stress subjected to the GaAs substrate for the MBE-grown heterostructure is similar to that for the sample grown by OMVPE.

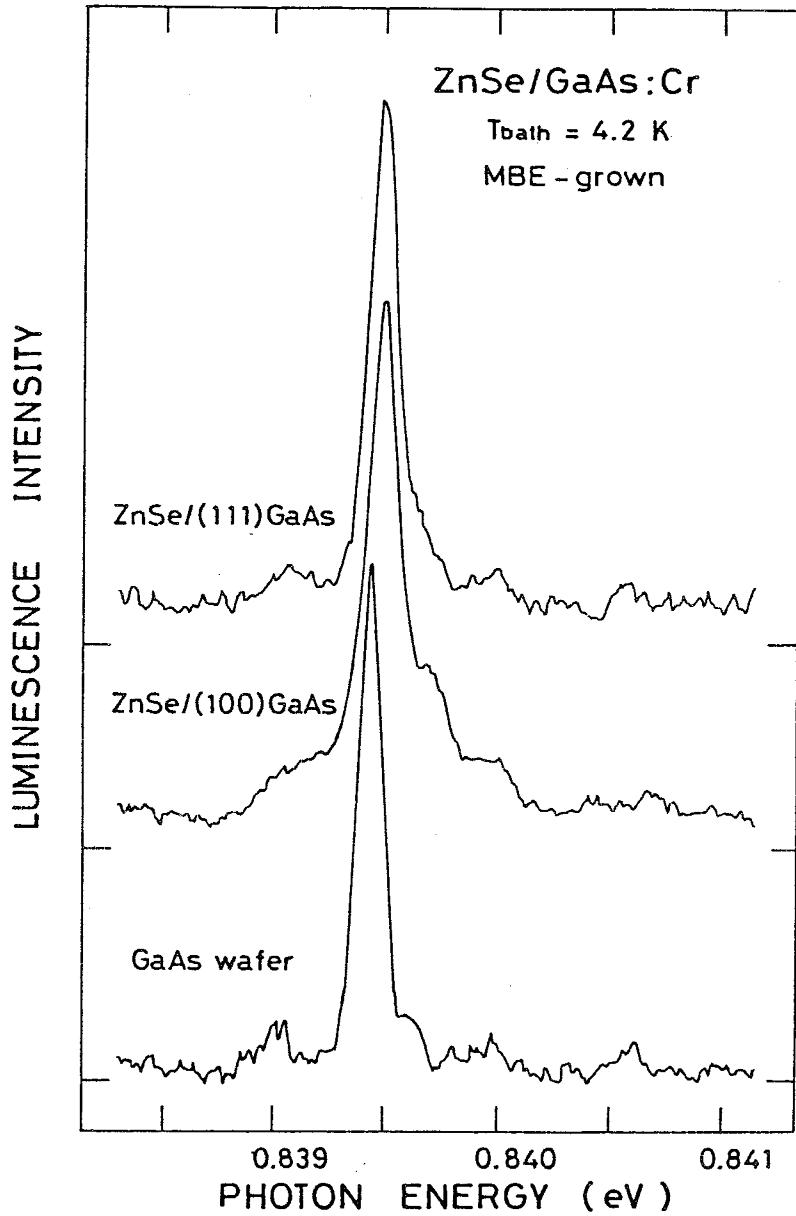

Fig. 5-13 Cr-related PL spectra from GaAs substrates for (100) and (111) MBE-grown ZnSe/GaAs:Cr heterostructures, together with that of as-received wafer.

5-3-4. Model for anomalous stress at ZnSe/GaAs interface

Firstly, it is important to consider the thermal expansion coefficients of ZnSe and GaAs, because a series of PL measurements were carried out at a low temperature of 4.2 K. At room temperature, the thermal expansion coefficients are 6.84×10^{-6} K^{-1} and 6.86×10^{-6} K^{-1} for ZnSe and GaAs, respectively.[22] Although the precise temperature dependences of these thermal expansion coefficients in the low-temperature region have not been available, the thermal expansion coefficient of a semiconductor becomes, in general, smaller as temperature is lowered, which implies that the lattice parameter varies largely at high temperatures, while that is almost invariable at low temperatures. Therefore, even though the thermal expansion coefficients for ZnSe and GaAs are independent of temperature as a first approximation, in which the unstrained lattice parameter of ZnSe

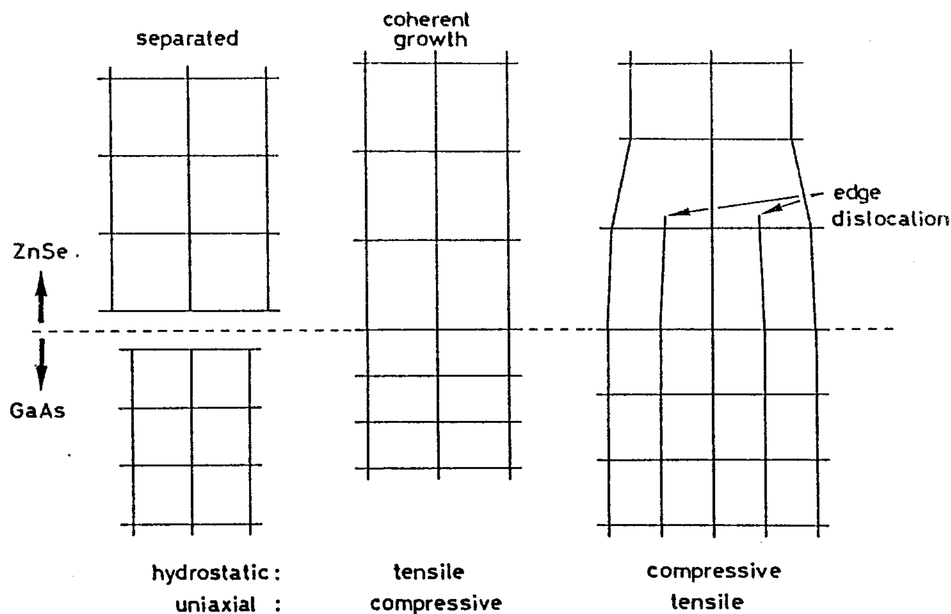

Fig. 5-14 Models for interface stress at ZnSe/GaAs heterostructure.

is much underestimated in comparison with the actual one, the lattice parameter of the ZnSe epi-layer is unlikely to become smaller than that of the GaAs substrate at 4.2 K. Based on the above discussion, the origin of the anomalous interface stress in the GaAs substrates for ZnSe/GaAs:Cr heterostructures can not be explained by using the difference in thermal expansion coefficients of ZnSe and GaAs.

A model for the anomalous interface stress between ZnSe and GaAs is tentatively proposed, which is illustrated in the right side of Fig. 5-14, compared with the interface for the normal coherent growth. Here it is assumed that lattice disordering and crystal deterioration (edge dislocations are considered as an example in the figure) occur in the ZnSe epitaxial growth for thicker ZnSe epi-layers than a critical value, though strain due to lattice mismatch between ZnSe epi-layer and GaAs substrate sustains the heterostructure up to the critical epi-layer thickness. This assumption is supported from the results of X-ray diffraction analysis of OMVPE-grown ZnSe epi-layers, reported by Kamata et al.[23)] who showed that the critical ZnSe epi-layer thickness is about 2000 A. It is expected that the GaAs substrate suffers compressive biaxial stress parallel to the ZnSe/GaAs heterointerface, if these edge dislocations exist in the ZnSe epi-layer with high density. This compressive biaxial stress can be decomposed into compressive hydrostatic stress and tensile uniaxial stress perpendicular to the heterointerface plane, which is consistent with the results obtained in this study.

5-4. Summary

The Cr-related PL lines in the 0.839 eV region in a series of plastically-bent SI GaAs:Cr with compressive or tensile stress along various bending axes have been systematically investigated. As a result, is has been found that the residual stress in SI GaAs:Cr wafers can be characterized by the low-temperature PL method, since the specific Cr-related PL lines in the bent specimens are observed in a different way depending upon the type of stress, compressive or tensile, and also the direction and magnitude of the stress.

This PL method measuring the Cr-related PL lines has been applied to the characterization of the interface stress at OMVPE-grown ZnSe/GaAs:Cr heterostructures. Based on the analyses of the peak shift and splitting of the PL lines, it has been found that both compressive hydrostatic stress and tensile uniaxial stress coexist in the GaAs substrate, and that such the interface stress is not consistent with that predicted for lattice mismatch between a ZnSe epi-layer and a GaAs substrate. The interface stress at ZnSe/GaAs:Cr heterostructure grown by MBE has been also investigated and the results were similar to those for the OMVPE-grown heterostructure. Finally, a model for interpreting the results obtained in this thesis work has been tentatively proposed.

References

1) A. S. Jordan, R. Caruso and A. R. Von Neida: Bell Syst. Tech. J. 59 (1980) 593.

2) M. G. Milvidsky and E. P. Bochkarev: J. Cryst. Growth 44 (1978) 61.

3) C. A. Evans, Jr. V. R. Deline, T. W. Sigmon and A. Lidow: Appl. Phys. Lett. 35 (1979) 291.

4) S. Kishino, N. Chinone, Hisao Nakashima and R. Ito: Appl. Phys. Lett. 29 (1976) 488.

5) Y. Takano, T. Ishiba, N. Matsunaga and N. Hashimoto: Jpn. J. Appl. Phys. 24 (1985) L239.

6) K. Yamazaki, M. Yamada, K. Yamamoto and K. Abe: Jpn. J. Appl. Phys. 23 (1984) 681.

7) K. Kakimoto and T. Katoda: Appl. Phys. Lett. 40 (1982) 826.

8) Y. Fujiwara, T. Nishino and Y. Hamakawa: submitted to Appl. Phys. A.

9) Y. Fujiwara, A. Kojima, T. Nishino, Y. Hamakawa, K. Yasutake, M. Umeno and H. Kawabe: Ext. Abst. 16th Int. Conf. Solid State Devices & Mater., Kobe, 1984 (Japan Business Center for Academic Societies, Tokyo, 1984) p. 177.

10) K. Yasutake, J. Murakami, M. Umeno and H. Kawabe: Jpn. J. Appl. Phys. 21 (1982) L288.

11) E. C. Lightowlers, M. O. Henry and C. M. Penchina: Proc. 14th Int. Conf. Phys. Semiconductors, Edinburgh, 1978 (Inst. of Phys., Bristol & London, 1979) p. 307.

12) J. Barrau, Do Xuan Thanh, M. Brousseau, J. C. Brabant and F.

Voillot: Solid State Commun. 44 (1982) 395.

13) M. S. Skolnick, M. R. Brozel and B. Tuck: Solid State Commun. 43 (1982) 379.

14) Y. Fujiwara, T. Nishino and Y. Hamakawa: Jpn. J. Appl. Phys. 21 (1982) L727.

15) Y. Fujiwara, A. Kojima, T. Nishino and Y. Hamakawa: J. Luminescence 31&32 (1984) 451.

16) J. Barrau, F. Voillot, M. Brousseau, J. C. Brabant and G. Poiblaud: J. Phys. C: Solid State Phys. 14 (1982) 3447.

17) M. S. Abrahams and C. J. Buiocchi: J. Appl. Phys. 36 (1965) 2855.

18) S. K. Choi, M. Mihara and T. Ninomiya: Jpn. J. Appl. Phys. 16 (1977) 737.

19) Y. Fujiwara, S. Shirakata, T. Nishino, Y. Hamakawa and S. Fujita: submitted to Jpn. J. Appl. Phys.

20) S. Fujita, Y. Matsuda and A. Sasaki: Jpn. J. Appl. Phys. 23 (1984) L360.

21) S. Shirakata, Y. Fujiwara, M. Kondo, T. Nishino and Y. Hamakawa: Ext. Abst. 17th Conf. Solid State Devices & Mater., Tokyo, 1985 (Japan Business Center for Academic Societies, Tokyo, 1985) p. 205.

22) K. -H. Hellwege: Landolt-Bornstein Numerical Data and Functional Relationships in Science and Technology, Vol. 17 (Springer-Verlag, Berlin-Heidelberg-New York, 1982).

23) A. Kamata, K. Hirahara, M. Kawachi and T. Beppu: Ext. Abst. 17th Conf. Solid State Devices & Mater., Tokyo, 1985 (Business Center for Academic Societies Japan, Tokyo, 1985) p. 233.

VI. CONCLUSIONS

The conclusions obtained in this thesis work on the photoluminescence study of 3d-transition metal impurities in GaAs are summarized as follows;

(1) We have performed systematic photoluminescence studies for high-temperature thermally annealed GaAs:Cr under various excess arsenic pressure. A series of behaviors of the well-known Cr-related sharp zero-phonon line at 0.8395 eV have been analyzed based on mass-action equations for reactions involving several defects in GaAs, the result suggesting an arsenic vacancy (V_{As}) contributes to the luminescence line and that the luminescence center is a complex consisting of a Cr at a Ga site and an arsenic vacancy in its nearest-neighbor. Furthermore, it has been found that the annealing temperature and time dependences of in-depth profiles of the luminescence intensity in annealed GaAs:Cr can be well interpreted by considering the dissociation of this luminescence center and the redistribution of its constitutional elements.

(2) Effects of various donor impurities on the Cr-related luminescence in GaAs have been investigated. A series of new Cr-related zero-phonon lines associated with a Cr-Se complex have been observed, for the first time, in the 0.837 eV region in Cr, Se-codoped GaAs. From an analysis of their peak positions

together with those of previously-reported luminescence lines due to Cr-Te and Cr-V_{As} complexes, the magnitude of the trigonal field at each complex has been estimated. It has been found that the trigonal field at the Cr-Se complex is about two times weaker than that at the Cr-Te complex and four times weaker than that at the Cr-V_{As} complex.

(3) Effects of In-doping on the Cr-related luminescence have been also investigated in In, Cr-codoped GaAs. New Cr-related zero-phonon lines have been observed, for the first time, in addition to the well-known Cr-V_{As} luminescence line. A series of photoluminescence measurements has led us to the conclusion that these newly-observed Cr-related luminescence lines are originated from a complex involving a Cr-V_{As} pair influenced by the existence of an In atom in the second-nearest neighbor of the Cr atom. Furthermore, by comparing their relative peak positions of the Cr-V_{As} luminescence line with previously-reported uniaxial-stress data, it has been found that local lattice strain of about 1 % exists around an In atom in GaAs:In.

(4) The in-depth profiles of the intensities of the Cr-V_{As} and Cr-Te luminescence lines have been measured in Cr-diffused GaAs. It has been found that these in-depth profiles can be fitted by the usual complementary error function. The analysis of the profiles for both the Cr-V_{As} and Cr-Te luminescence lines has enabled us to estimate the diffusion coefficients of Cr and V_{As} in GaAs. The obtained values are 2-4 x 10^{-11} cm^2/s for Cr and

$5\text{-}8 \times 10^{-12}$ cm^2/s for V_{As}, respectively, which are comparable to the previously-reported data, though the values vary a little bit depending upon the arsenic vapour pressure during the high-temperature Cr-diffusion in preparation of Cr-diffused GaAs samples.

(5) The deep-level photoluminescence associated with Ni acceptors has been investigated in various kinds of Ni-diffused GaAs. It has been found that the luminescence drastically changes from the surface to the deep region. In particular, the luminescence previously attributed to Ni-S pairs is strongly observed near the surface of all the GaAs samples doped with a variety of donor impurities. The in-depth profile measurements on these Ni-related luminescence intensities have revealed the builtup of S atoms in the vicinity of the surface region of Ni-diffused GaAs, which is probably due to the redistribution of the background S donors in GaAs bulk crystals during the high-temperature diffusion of Ni into GaAs.

(6) Based upon time-resolved photoluminescence spectra associated with Cr- and V-related deep centers in GaAs at 4.2 K, the electronic lifetimes of the excited states of these deep centers have been estimated. In both cases, no remarkable deformation has been observed in the luminescence spectra, and the luminescence intensity has decreased exponentially with the lapse of time, which indicates that monomolecular recombination is effective. From an analysis of the decay characteristics, it

has been found that the electronic lifetime of the excited state is 0.77 μs for the Cr-related deep center and 119 μs for the V-related center. On the premises of the configuration interaction model introduced in II-VI compound semiconductors, we have calculated a mixing parameter from the above results for each deep center. It has been found that the obtained mixing parameter is 0.43 for the Cr center and 0.15 for the V center, these values implying that the most probable origin for the V-related sharp zero-phonon line at 0.7388 eV in GaAs:V is $^3T_2(F)$ - $^3A_2(F)$ transitions of an isolated V^{3+}.

(7) A new characterization technique for the residual stress in GaAs has been demonstrated. The Cr-related luminescence lines in the 0.839 eV region for a series of plastically-bent GaAs:Cr with compressive or tensile stress along various bending axes have been systematically measured. It has been found that the residual stress in GaAs:Cr wafers can be sensitively characterized from a splitting and energy shift of the 0.8395 eV Cr-related luminescence lines in the low-temperature photoluminescence spectra, since the specific Cr-related luminescence lines in the bent specimens are observed in a different way depending upon the type of stress, compressive or tensile, and also the direction and magnitude of the stress.

(8) This photoluminescence technique has been applied to the characterization of the interface stress at OMVPE-grown ZnSe/GaAs:Cr heterostructures. Based on the analyses of the peak

shift and splitting of the C-related luminescence lines, it has been found that both compressive hydrostatic stress and tensile uniaxial stress coexist in the GaAs substrate, and that such interface stress is not consistent with that predicted for lattice mismatch between a ZnSe epi-layer and a GaAs substrate. In addition, it has been found that this anomalous stress is induced by the existence of the ZnSe epi-layer and extends over the whole GaAs substrate, based on the results obtained by the thickness dependences of the Cr-related luminescence lines for both ZnSe epi-layer and GaAs substrate. Furthermore, MBE-grown ZnSe/GaAs:Cr heterostructures have been also investigated. As a result, it has been found that this anomalous stress exists in the GaAs substrates independent of the growth technique of ZnSe on GaAs. Finally, we have tentatively proposed a model for interpreting the results obtained in this work.

VITA

Yasufumi FUJIWARA was born in Kashihara, Nara, Japan on February 14, 1959. He graduated from Unebi Senior High School, Nara in March 1977 and entered Osaka University, Toyonaka, Osaka in April 1977. He graduated from Osaka University in March 1981 and entered the Graduate School in April of that year. He received his master of Engineering degree in Electrical Engineering in March 1983 from Osaka University. He is a member of the Japan Society of Applied Physics.